INFORMATION TO USERS

This manuscript has been reproduced from the microfilm master. UMI films the text directly from the original or copy submitted. Thus, some thesis and dissertation copies are in typewriter face, while others may be from any type of computer printer.

The quality of this reproduction is dependent upon the quality of the copy submitted. Broken or indistinct print, colored or poor quality illustrations and photographs, print bleedthrough, substandard margins, and improper alignment can adversely affect reproduction.

In the unlikely event that the author did not send UMI a complete manuscript and there are missing pages, these will be noted. Also, if unauthorized copyright material had to be removed, a note will indicate the deletion.

Oversize materials (e.g., maps, drawings, charts) are reproduced by sectioning the original, beginning at the upper left-hand corner and continuing from left to right in equal sections with small overlaps. Each original is also photographed in one exposure and is included in reduced form at the back of the book.

Photographs included in the original manuscript have been reproduced xerographically in this copy. Higher quality 6" x 9" black and white photographic prints are available for any photographs or illustrations appearing in this copy for an additional charge. Contact UMI directly to order.

UMI

A Bell & Howell Information Company
300 North Zeeb Road, Ann Arbor MI 48106-1346 USA
313/761-4700 800/521-0600

Downloaded from SHAREOK. Persistent Handle URL: https://hdl.handle.net/11244/5709

UNIVERSITY OF OKLAHOMA

GRADUATE COLLEGE

" 'TIS SOMETHING, NOTHING",
A SEARCH FOR RADIO SUPERNOVAE

A DISSERTATION

SUBMITTED TO THE GRADUATE FACULTY

in partial fulfillment of the requirements for the

degree of

DOCTOR OF PHILOSOPHY

By

CHRISTOPHER R. ECK

Norman, Oklahoma

1998

UMI Number: 9905625

UMI Microform 9905625
Copyright 1998, by UMI Company. All rights reserved.

This microform edition is protected against unauthorized copying under Title 17, United States Code.

UMI
300 North Zeeb Road
Ann Arbor, MI 48103

©Copyright by Christopher Eck 1998
All Rights Reserved.

" 'TIS SOMETHING, NOTHING",

A SEARCH FOR RADIO SUPERNOVAE

A DISSERTATION APPROVED FOR THE DEPARTMENT OF PHYSICS AND ASTRONOMY

BY

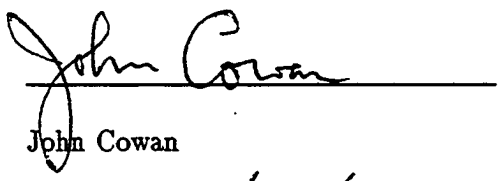

John Cowan

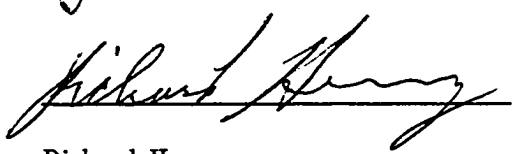

Richard Henry

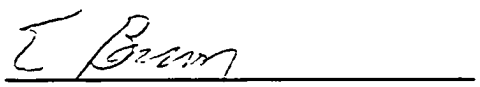

Edward Baron

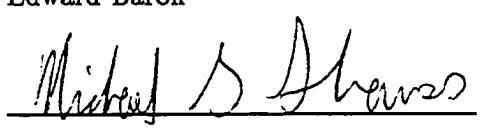

Michael Strauss

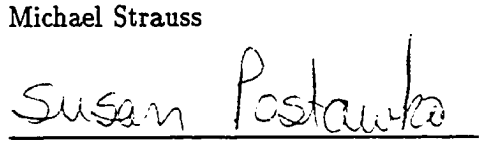

Susan Postawko

Acknowledgments

There are so many people who have helped bring me to this point in my life, I could fill up an entire thesis just thanking all of them. For the sake of brevity and anyone who ventures into this largish tome, I will try to keep my acknowledgements to a (relative) minimum. I've strived for this since before high school, so that is a good place to start.

Fr. O'Neill: Math first "clicked" for me while in your high school Calculus class. Thank you for showing me that difficult things can eventually make sense. I've always learned the most from the hardest teachers—thank you for pushing so hard.

Dr. Lee: You made physics "click" for me.

Dr. Federman: Your guidance in the last 2 years of my undergraduate training showed me how to apply this training to solve real problems.

I would like to acknowledge the help from W. Miller Goss, Rick Perley, Bill Romanishin, Schyler Van Dyk, Paul Hodge, Doug Roberts, Francesca Boffi, and Kurt Weiler, all of whom have contributed to this work.

To my dear friends: Don, Erin, Dan, and Sharon

Don and Erin. Since high school, you have been the one I measure myself up against as an analyst, Don. Thank you for being there. Erin, thank you being a part of our circle of friends and accepting me even when things get a little out of hand. I value our friendship more than even I realize sometimes. Lastly, Don (again) thank you for being a part of my stress relief efforts. Without our games, I think I would have been in Bellevue long since.

Dan and Sharon. I first met you in high school, Dan, and I'm still amazed at

how alike we think sometimes. To both of you—without your friendship, life since meeting you would have been much harder. You have always been a reminder to me that theres so much in the world to see and explore.

Bob, Carol, Teresa, Brad, Barbara, Rick: Thank you for accepting me into your family. Your care and generosity are a model for the world.

To the faculty at OU: You have shown me the way, the truth, and the light to critical thinking.

Dr. Cowan: You have been the cornerstone of my academic career. Without your guidance I would never have achieved such a difficult goal. Thank you for pushing so hard and keeping me on track. 20-20 hindsight is a wonderful thing, and now I think I see the hows and whys of getting to this point in my career. You have been a mentor and a friend.

To my sister, Laura: Thank you for being one of the supports in my life. Without you to anchor our family together, life would be much harder.

To my parents: You have always been there for me, encouraging, guiding, and believing in me. You gave me what I needed to grow as a person in all aspects of my life. Thank you for giving me the confidence that I have and use every day of my life. Thank you.

Debra: I've known you through thick and thin (and even been the cause of "thin" at times), and I will be forever grateful for having known you. You are more important than you sometimes realize to those around you. You are the model of what a good person should be, and I want to thank you for being here during these years and for being such a good friend. I am a better person for having known you.

Michelle, Marie, and Samantha: Words cannot describe how much you all mean

to me. Michelle, sometimes I cannot believe the fortune that brought you to me. My life is so blessed by what you have taught me about it and by what you have done for me. This accomplishment means so much more to me because you are here to share it. Marie and Samantha, you cannot know the joy you have brought to me. The worst day can become nothing just by coming home to you and interacting with you and watching you play, grow, and learn. Thank you my precious family, you have made life beautiful just by being in it. You have been there with me and for me through it all.

Contents

1 Introduction 1
- 1.1 Supernova Classification . . . 2
  - 1.1.1 SN Type II . . . 2
  - 1.1.2 SN Type I . . . 3
- 1.2 Observations of Radio Supernovae . . . 4
  - 1.2.1 Younger Supernovae ($\sim$ 1–15 years old) . . . 4
  - 1.2.2 Intermediate Age Supernovae ($\sim$ 15—300 years old) . . . 11
  - 1.2.3 Non-detections . . . 15
  - 1.2.4 Supernova Remnants (SNRs) . . . 15
- 1.3 Theoretical Models for Radio Emission . . . 17
  - 1.3.1 Chevalier Model for Radio Emission from Supernovae . . . 17
  - 1.3.2 Gull Model for Radio Emission from SNRs . . . 20

2 SN 1923A: The Oldest Radio Supernova? 26
- 2.1 Introduction . . . 26
- 2.2 Observations and Data Reduction . . . 27
- 2.3 Discussion and Conclusions . . . 34

3 SNe 1984E and 1986E 39
- 3.1 Introduction . . . 39
- 3.2 Observations and Data Reduction . . . 40
- 3.3 Results and Discussion . . . 47
  - 3.3.1 SN 1984E . . . 50
  - 3.3.2 SN 1986E . . . 52

4 Radio Observations of SN 1986G 53
- 4.1 Introduction . . . 53
- 4.2 Observations and Data Reduction . . . 54
- 4.3 Discussion . . . 55

5 Observations of Radio SNe up to 90 Yrs Old **61**
5.1 Introduction 61
5.2 Observations 62
5.3 Discussion 71
5.3.1 The Model 71
5.3.2 Comparisons 80
5.3.3 Luminosity-Age Plots 84
5.4 Conclusions 91

6 Summary **94**

Bibliography **99**

A Derivation of the Chevalier Model Luminosity **109**

B Description of Radio Analyses **113**

List of Tables

1.1 Data on young Galactic SNRs 16
1.2 Mass-loss rates for well-observed RSNe 21
1.3 Well studied RSNe (20 cm) 22
1.4 Well studied RSNe (6 cm) 24

2.1 Parameters for Radio Observations of SN 1923A (M 83) 28
2.2 Observations of the site of SN 1923A 30

3.1 Calibrator positions and fluxes for observations of SNe 1984E and 1986E 41
3.2 Observations of SNe 1984E and 1986E 46

5.1 Observational parameters for the SNe in this survey 63
5.2 Distances assumed for SNe in this survey 65
5.3 Summary of data on intermediate-age SNe and younger SNe in this survey. 66
5.4 Derived mass-loss rates for the SNe I in this survey 75
5.5 Derived mass-loss rates for the SNe II in this survey 76
5.6 Derived mass-loss rates for the unknown Type SNe in this survey . . 77

B.1 Summary of observational data on non-SN radio sources 157

List of Figures

2.1 A 20 cm map of half of M 83 31
2.2 A 20 cm map of the region near SN 1923A 32
2.3 A 6 cm map of the region near SN 1923A 33
2.4 A plot of 20 cm luminosity versus age for select RSNe, including SN 1923A 38

3.1 A 20 cm map of the region surrounding SN 1984E 43
3.2 A 20 cm map of the region surrounding SN 1986E 44
3.3 A 6 cm map of the region surrounding SN 1986E 45
3.4 Light curves at 6 cm for different mass-loss rates 48
3.5 Light curves at 20 cm for different mass-loss rates 49

4.1 A 6 cm map of the region near SN 1986G 56
4.2 A 2 cm map of the region near SN 1986G 57
4.3 A graph of flux versus mass-loss rate based on Chevalier model applied to SN 1986G 60

5.1 A plot of 20 cm luminosity versus age for the SNe II in this survey . . 85
5.2 A plot of 6 cm luminosity versus age for the SNe II in this survey . . 86
5.3 A plot of 20 cm luminosity versus age for the SNe I in this survey . . 87
5.4 A plot of 6 cm luminosity versus age for the SNe I in this survey . . . 88
5.5 A plot of 3.6 cm luminosity versus age for the SNe I in this survey . . 89

B.1 A 6 cm contour map of the region surrounding the site of SN 1909A . 116
B.2 A 20 cm contour map of the region surrounding the site of SN 1937C 119
B.3 A 20 cm contour map of the region surrounding the site of SN 1951H 123
B.4 A contour map of the eastern region of NGC 5457 (M 101) 124
B.5 A 20 cm contour map of the region surrounding the site of SN 1954A 126
B.6 A contour map of NGC 4214 127
B.7 A 20 cm contour map of the region surrounding the site of SN 1954J 131
B.8 A contour map of NGC 2403 132

B.9 A 20 cm contour map of the region surrounding the site of SN 1959D at the first epoch 134
B.10 A 20 cm contour map of the region surrounding the site of SN 1959D at the second epoch 135
B.11 A 6 cm contour map of the region surrounding the site of SN 1959D . 136
B.12 A 20 cm contour map of the region surrounding the site of SN 1966B 141
B.13 A 6 cm contour map of the region surrounding the site of SN 1969L at the second epoch 143
B.14 A contour map of the southern region of NGC 5457 (M 101) 145
B.15 A 20 cm contour map of the region surrounding the site of SN 1973R 149
B.16 A 20 cm contour map of the region surrounding the site of SN 1980D 151
B.17 A 6 cm contour map of the region surrounding the site of SN 1983K . 152
B.18 A 6 cm contour map of the region surrounding the site of SN 1989B . 155
B.19 A 3.6 cm contour map of the region surrounding the site of SN 1989B 156

Chapter 1

Introduction

Supernovae (SNe) have been observed visually and recorded for at least the last 1000 years (Clark & Stephenson 1982), but only in this century have we been able to observe these bright, energetic events in a waveband other than the optical. The first confirmation of radio emission from supernovae came from Supernova (SN) 1970G (Gottesman et al. 1972) and only enabled a very rough determination of a radio light curve (Allen et al. 1976). It wasn't until the Very Large Array (VLA) radio telescope was established, and it detected the strong radio source SN 1979C that the search for radio SNe (RSNe) began to have more success. There have been 9 other well-observed radio SNe as well as detections of radio emission from SNe with ages between 15 – 70 years and from supernova remnants (SNRs) more than 300 years old.

Observations of these RSNe and of some SNRs will now be presented. Examination of these observations will allow us to gain knowledge of some of the general properties of RSNe and their remnants. Also of interest is the relationship *between* SNe and their remnants and the fact that there have been no radio observations of SNe or SNRs

of known age between about 70 and 300 years. Does the answer lie in the intrinsic evolution of the SNe themselves, the environment around them or a mix of each? In addition to the observations presented, the Chevalier (RSNe) and Gull (SNR) model for radio emission are briefly investigated to help understand how the emission arises and to help understand the relationship between the two models.

1.1 Supernova Classification

There are two main classifications of SNe, distinguished from one another by features in the optical spectrum. This section will explain the differences between the SN types and their sub-classifications and the implications of the SN type on the pre-SN progenitor masses. While a basic understanding of the pre-SN progenitor stars has been achieved (e.g., Branch, Nomoto, & Filippenko 1991, Branch et al. 1995), the specifics are still a matter of some debate (e.g., Nomoto et al. 1996).

1.1.1 SN Type II

SNe Type II are distinguished by the presence of optical hydrogen lines in the spectra. The absolute magnitude, M_B, for these SNe has an average value of $< -18^m$ (assuming $H_o = 50$ km/s/Mpc) with a large scatter about this value. They are generally found in late-type galaxies near H II regions. The progenitor is believed to be a young, high mass ($\sim 7 - 30$ $M_\odot$) star that undergoes a core-collapse after exhausting its nuclear fuel. Knowledge of the pre-SN progenitor will enable models for the radio emission to be proposed in section 1.3.

SNe Type II-L, II-P

Following convention, the sub-classifications using a capitol letter designate classifications based on features in the light curve. The Type II-L SN shows the presence of an approximately linearly sloping decline of brightness after optical maximum and the Type II-P SN shows a "plateau" or slower rate of decline during the first few months after optical maximum and then a decline that occurs more quickly.

1.1.2 SN Type I

The Type I SN is characterized by the absence of hydrogen in its optical spectra. The average absolute magnitudes and pre-SN progenitor masses vary with SN type.

SN Type Ia

In addition to the absence of optical hydrogen, the Type Ia SN contains optical silicon lines in its spectra. These SNe have a characteristic absolute magnitude $M_B \sim -20\overset{m}{.}0$ (based on $H_o = 50$ km/s/Mpc), with very little dispersion about this value. One proposed progenitor is the explosion of a white dwarf that has exceeded its Chandrasekhar Mass limit via mass transfer in a binary system (e.g., Munari & Renzini 1992, Branch et al. 1995). The progenitor mass for this type of SN is estimated to be $\sim 5 - 8\ M_\odot$.

SN Type Ib

The SN Type Ib is characterized by the presence of helium, but no hydrogen or silicon in its optical spectra. The average brightness is $M_B \sim -18\overset{m}{.}0$ ($H_o = 50$ km/s/Mpc)

with some scatter about this value. The proposed progenitors are the highest mass stars ($>\sim 16$ $M_\odot$) that die as core-collapse SNe when nuclear burning can no longer support the star (e.g., Nomoto et al. 1996).

SN Type Ic

The SN Type Ic is similar to the SN Type Ib except for the absence of helium in the optical spectra. They share the other properties of the SNe Type Ib as well as the same proposed progenitor—the highest mass stars' demise (core-collapse SN) (e.g., Nomoto et al. 1996).

1.2 Observations of Radio Supernovae

Radio data on the well-studied RSNe at or near peak are presented in Tables 1.3 and 1.4. The following sections review observations of each SN in more detail.

1.2.1 Younger Supernovae ($\sim$ 1–15 years old)

This section reports radio observations of SNe beginning with the first one detected at radio wavelengths, SN 1970G, and ending with the most recent radio SN with more than one or two data points, SN 1993J (Ripero 1993).

SN 1970G

SN 1970G is an SN Type II located in M 101 with a nearby H II region, NGC 5455. Due to the close proximity of the H II region, determination of the radio light curve for this SN was difficult. To correct for the H II region, the pre- and post-SN

flux measurements of NGC 5455 were averaged and subtracted from the total flux obtained from both the H II region and the SN. Data at 49, 20, and 6 cm (Allen et al. 1976, Weiler et al. 1986) show that it had fallen below the limits of detectability by 1630 days after the date of optical maximum. Examination of the data reveals that the emission began at smaller wavelengths first and has a spectral index characteristic of thermal emission, $\alpha > 0$ between 49 and 20 cm (see the next footnote for a definition of α). This may indicate a contribution to the radio emission from the thermal H II region.

SN 1978K

Originally identified as a nova in NGC 1313 (Dopita & Ryder 1990), Ryder et al. (1993) suggest that this object is an SN, based on the object's optical light curve, optical spectra, and radio and x-ray data. From these observations Ryder et al. (1993) also determine that this SN is a very unusual Type II, sharing many of the above characteristics with SN 1961V and SN 1986J (see relevant sections in this chapter).

The radio data indicate a very powerful, non-thermal radio source, with a peak 0.843 GHz flux density of about 230 mJy (1 Jy = 10^{-23} Watts / m^2) on the date ~1984.5. Assuming a distance of 3.7 Mpc (distance to host galaxy NGC 1313 from Tully 1988), this corresponds to a luminosity of 3.77 $\times 10^{27}$ erg/s Hz. (To provide a reference for comparison with the other RSNe, the 20 cm luminosity observations are presented next.) The earliest attempts to detect the SN at 20 cm occurred in 1992 with a luminosity measured to be $\sim$ 140 times that of Cas A, a 300 year old SNR whose SN is believed to have exploded in $\sim$ 1670. The radio emission from SN 1978K

is comparable to that of SN 1979C, a strong well-studied radio SN (see next section).

SN 1979C

SN 1979C has an extensive data set taken with more than 10 years of data compiled by Weiler et al. (1986, 1991) and Montes et al. (1998). This SN Type II-L, discovered by Johnson (1979), is one of the strongest observed and occurred in NGC 4321. Inspection of a plot of the data from Montes et al. (1998) shows the same phenomena (radio emission beginning first at smaller wavelengths), first observed in SN 1970G, observed here (this could be explained as a change in optical depth with wavelength as in section 1.3). The data allows a better determination of the evolution of the spectral index [1], α_6^{20} between 20 cm (1.5 GHz) and 6 cm (5 GHz) (Weiler et al. 1991) than was possible with data from SN 1970G. While initially indicative of thermal emission (positive spectral index), α declines rapidly to a more or less constant negative value, $\alpha_6^{20} \sim -0.75$, indicative of non-thermal emission. One source of non-thermal emission is synchrotron radiation which arises when relativistic electrons spiral around strong magnetic field lines. One explanation for the evolution of the spectral index (from a positive value to a negative value) could be that a change in optical depth is occurring, due to a decrease in absorption (see section 1.3). The extent of the data makes SN 1979C an ideal candidate to test models for radio emission. Weiler et al. (1986, 1991, 1998) have fit the data to a model whose origin will be discussed in section 1.3. Finally, it is clear from the data that the radio emission from SN 1979C is now increasing again and this will be explained using a model for the emission (see section

[1] The spectral index, α, is defined by $S \propto \nu^{\alpha}$, where S is the flux density and ν is the frequency of radiation.

1.3).

SN 1980K

This SN, discovered in NGC 6946 by Wild (1980), had a flux density about 5 times weaker than SN 1979C, and the flux determination was further complicated by disk emission from the galaxy. This is an SN Type II, and examination of the plot of radio data (Weiler et al. 1986, Weiler et al. 1992a) reveals the same shorter wavelength "turn-on" as the others. The plot of spectral index evolution with time (Weiler et al. 1986, Weiler et al. 1992a) repeats the general behavior of the previous SN—initial thermal spectrum evolving to a non-thermal spectrum α_6^{20} averaging to ~ -0.5. Recent data (Montes et al. 1998) indicate that the radio emission from SN 1980K has dropped off more sharply than initially, but it is still visible.

SN 1981K

Discovery of this SN in NGC 4258 occurred first in the radio (van der Hulst et al. 1983) and was later confirmed in the optical (Wild 1983, van der Hulst et al. 1983). A plot of about 8 years of data has been compiled by Van Dyk et al. (1992). They compute the spectral index to be relatively constant with time at $\alpha_6^{20} =\sim -0.74$ starting with day 627 after optical maximum. It is clear from the data that the emission at this time is past the peak radio fluxes at both wavelengths with the data available. Although the SN type was never determined from the optical spectrum, Van Dyk et al. (1992) suggest that SN 1981K was probably a Type II by comparing its radio properties to the other SN Type II and contrasting to a different SN 1983N, a Type Ib SN. (Perhaps radio data in the future could provide an additional method

for identifying SN type).

SN 1983N

SN 1983N was discovered by Evans (1983) in NGC 5236 (M 83), and is classified as a Type Ib. A plot of the data from Chevalier (1984) shows a short rise time and that emission was detected days *before* optical maximum light. Weiler et al. (1986) report a very steep spectral index, α_6^{20}, clustering around -1 at later times. There are obvious differences between the radio properties of SNe Types Ib and II (shorter rise times and steeper spectral indices for Type Ib SNe).

SN 1984L

This SN, discovered by Evans (1984) in NGC 991, was also determined to be a Type Ib, but the number of observations is very small. Nevertheless Panagia et al. (1986) have constructed a radio light curve with a spectral index, $\alpha_6^{20} \sim -1.2$ for the one simultaneous measurement at both wavelengths (at 92 days after optical maximum). Looking at the data shows that the peak emission occurred before any of the measurements shown were taken (approximately 33 days after optical maximum for the first 6 cm data point). This is consistent with the observations of SN 1983N, for the radio emission beginning early and for the steep non-thermal spectral index. Panagia et al. (1986) speculate that perhaps SNe Type Ib may be used as standard candles based on this and other model fit parameters' similarities (see Tables 1.3 and 1.4). This makes a total of two Type Ibs observed. Unfortunately no other RSNe of this type have been observed.

SN 1986J

This Type II SN, discovered as a new radio source in NGC 891 by van Gorkom et al. (1986), has been observed extensively and has a radio luminosity about 3 times brighter than SN 1979C. Inspection of the radio light curves at 5 wavelengths (Weiler et al. 1990) reveal that the light curves "turn-on" relatively slowly with time in comparison with the other SNe Type II. Another unusual feature is at the shortest wavelength, 1.3 cm, where the flux is observed to be roughly constant with time. Weiler et al. (1990) plot the evolution of the spectral index between several different wavelengths and several things are noticed. Examination of the evolution of α_{20}^{90} shows that it is still in its optically thick phase ($\alpha > 0$) at an age of about 3 years. The evolution of α_6^{20} is a bit unusual in form, but at late times seems to approach a constant value (~ -0.7) typical of the other SNe Type II. The spectral index between 6 and 2 cm has already reached the optically thin phase as we are seeing non-thermal emission with a constant value of $\alpha_2^6 \sim -0.7$. The spectral index between 2 and 1.3 cm remains relatively flat (~ -0.2), although with large errors. SN 1986J is unusual in many ways (peculiar radio light curves, spectral evolution, and slow turn-on).

SN 1987A

The discovery of this nearby SN Type II in the Magellanic Clouds by Turtle et al. (1987) enabled detection of radio emission only 2 days after discovery. Unfortunately, the radio emission was already fading quickly by the next day. In fact, this SN was only detected due to its close proximity. It is fortunate that pre-SN observations of the star were available and so we have knowledge of the progenitor—SN 1987A was

the explosion of a B3 I blue supergiant (Sonneborn, Altner, & Kirshner 1987). This seems to support the suggested progenitor for SNe Type II.

Recent observations of SN 1987A (Gaensler et al. 1997) reveal that the radio emission is rising again at an age of about 10 years. This can be interpreted using the Chevalier model presented in section 1.3.

SN 1988Z

Discovered independently by Candeo (Cappellaro & Turatto 1988) and Pollas (Pollas 1988) in MCG +03-28-022, this is the most distant radio SN observed (z=0.022). It is a very strong radio source (~2 times brighter than SN 1986J), and optical observations classified this as an SN Type II (Stathakis & Sadler 1991), but displayed some unusual optical characteristics. Examination of the radio light curve (Van Dyk et al. 1993b) reveals that the emission turned on relatively slowly and seems to follow the general trend that smaller wavelengths turn-on first. The data indicate that the 20 cm emission has not peaked, and therefore the SN is likely still in the optically thick phase at an age of about 3 years.

SN 1990B

Discovered optically by Perlmutter & Pennypacker (1990) in NGC 4568, SN 1990B represents another subset of SNe Type I, the Type Ic.

This particular SN seems to be similar to the Type Ib SNe 1983N and 1984L. Van Dyk et al. (1993a) plot the radio light curve and the spectral index evolution for several pairs of wavelengths. The initial observations at relatively early time (about 20 days after optical maximum) imply, from their shape, that the emission peaked

at an even earlier time. The steep non-thermal spectral index measurements cluster around $\alpha_6^{20} \sim -1$. Both of these properties are very similar to the corresponding properties of the SNe Type Ib.

SN 1993J

After discovery by Ripero (1993), radio observations of this Type II began early (Van Dyk et al. 1994) and data indicate that this SN has not yet reached the optically thin phase of emission (i.e., the data is near-peak or pre-peak and characterized by thermal emission). We must wait to determine the asymptotic approach value for the spectral index for comparison with other SNe.

1.2.2 Intermediate Age Supernovae ($\sim$ 15—300 years old)

This section describes recent radio observations of SNe older than (and including) SN 1970G, but younger than the radio source Cassiopeia A (Cas A), a Galactic SNR from a SN that exploded $\sim$ 1670. The oldest "modern" SN for which we have radio data is the probable detection of SN 1923A (Eck et al. 1998a), and there are no detections of historical SNe older than this until the age of the SNR Cas A. This is an interesting problem—why have we not seen radio emission from SNRs for almost 250 years prior to SN 1923A? No one seems to know at present, but perhaps observations of the SNe and SNRs that we can monitor continually will help explain the absence of intermediate-age radio SNe in that age range.

SN 1923A

The probable radio detection of this SN at an age of about 70 years is discussed in detail in Chapter 2.

SN 1950B

This SN posed a different problem to observers—it lacks an accurate positional reference to measure emission from. Cowan & Branch (1985) and Cowan, Roberts, & Branch (1994a) (hereafter CRB) adopted an optical position (based on offsets to the galaxy center) and an uncertainty of 10″ for SN 1950B. They reported detection of a non-thermal source within the errors of the position for SN 1950B at 20 and 6 cm with spectral index $\alpha_6^{20} \sim -0.57$. They suggested that both the positional coincidence and the non-thermal emission make it likely this source is SN 1950B. Because of its position in the spiral arm (birthplace of young, massive stars) of the parent galaxy (M 83), this SN is suggested as an SN Type II. Interestingly, CRB report that the radio emission from measurements taken in 1990-1992 has not changed significantly from measurements taken in 1983-1984. If this is emission from the site of SN 1950B, why has it not decreased as expected?

SN 1957D

An accurate position for this SN was determined in 1983 (Pennington & Dufour 1983). Cowan & Branch (1985) and CRB detected a source at the SN position in 1983-1984 and in 1990-1992, but whose flux was decreasing rapidly with time ($\sim$ 20% drop in 6 cm flux and $\sim$ 40% drop in 20 cm flux). This drop is sharper than that for SN 1970G, at 20 cm, over the 16 years prior to 1994, and may indicate that SN 1957D

has used up and/or overrun the material producing the radio emission (see section 1.3). When fit to a power-law decay rate with time, $S_\nu \propto t^\beta$, β was found to have a very steep value of about -3.0 at 20 cm. When compared to the 300 yr old SNR Cas A, SN 1957D is found to have a comparable luminosity, at an age of only $\sim$ 35 yrs. Spectral index studies (α_6^{20}) show that the emission has changed from a non-thermal spectral index of ~ -0.23 in 1984 to a slightly inverted value in 1992. CRB report that while the radio emission may still be dropping, a simpler explanation may be that the SN emission has fallen below that of a nearby H II region, resulting in the inverted spectrum. If this is so, then the emission from the SN may be lower than that of the H II region, and consequently, the power-law decay index, β, is only a lower limit. They suggest that the short term emission will remain constant from this site unless it brightens enough to rise above the H II emission. Due to its position in the spiral arm, SN 1957D has also been suggested as an SN Type II.

SN 1961V

Branch & Cowan (1985) and Cowan et al. (1988) reported observations of two non-thermal sources in NGC 1058. One of the sources was determined to be coincident with the precise astrometric position (Klemola 1986) of SN 1961V. The spectral index was calculated to be $\alpha_6^{20} = -0.60$ and the radio luminosity at 20 cm is very similar to that of Cas A (Cowan et al. 1988). It was fortunate that the pre-SN star had been observed for decades — the explosion being one of Zwicky's prototypical Type V SN. Today it would have been classified as a peculiar Type II based on this. Of interest is the other non-thermal source detected at a spectral index of $\alpha_6^{20} = -0.3$. Cowan et al. (1988) suggest that it is probably an SN that was not observed or identified

optically. But it is not clear whether the outburst associated with SN 1961V was an SN explosion or something else. It is suggested (Goodrich et al. 1989, Filippenko et al. 1995) that SN 1961V was a result of the superoutburst of a luminous blue variable based on optical observations and the form of its optical light curve. The similarities of their observations of the site of SN 1961V to those of other luminous blue variables undergoing large eruptions led them to this conclusion.

SN 1968D

Recovered 26 years after explosion (Hyman et al. 1995), this Type II SN is found in the same galaxy as SN 1980K. They identify the radio emission as coming from SN 1968D based on the non-thermal, $\alpha_6^{21} \sim -0.92$, nature of the emission detected, along with the excellent agreement with the reported position of SN 1968D.

SN 1970G

This SN is mentioned again, now as an intermediate age SN, because of the radio recovery in 1990 by Cowan et al. (1991). The SN was determined to have the usual non-thermal spectrum, $\alpha_{3.5}^{20} \sim -0.56$, and a very low flux density of 0.20 mJy at 20 cm and 0.08 mJy at 3.6 cm. This puts the 20 cm luminosity at a level somewhere between that of SNRs Cas A and the Crab Nebula (see section 2.5). When fit to a power-law decay rate in time, the index is found to be $\beta \simeq -2$, a steep decay index but certainly not the steepest (see SNe 1923A and 1957D).

1.2.3 Non-detections

To date, no one has detected radio emission from SNe Type Ia, but many have tried to do so. Attempts were made by Sramek et al. (1993) to detect radio emission from 14 SNe that occurred between 1983 and 1987 (6 of which are Type Ia) resulting in upper limits (i.e., non-detections). Weiler et al. (1989) report radio observations of all SNe optically brighter than 14.0 magnitudes from SN 1970A to SN 1981A and report no new detections to a limit of $\sim$ 0.5 mJy. Of the 17 sources listed with SN-type designations, 10 are listed as Type I, with the note that none of these are believed to be Type Ibs. In addition to the 14 SNe listed above, Weiler et al. (1989) made 13 more radio observations of SNe as old as SN 1895B, with no new radio detections. Four of this new group were listed as Type I. Eck et al. (1995) report very early (one week before optical maximum, see Chapter 4) radio upper limits for SN 1986G, refining the previous upper limit reported by Sramek et al. (1993), but no detection for this SN Type Ia.

1.2.4 Supernova Remnants (SNRs)

Weiler & Sramek (1988) identify an SNR as having a shell or a partial shell form and a non-thermal radio spectrum. Most SNRs tend to be strong radio emitters (see Table 1). But this broad category can be broken down into smaller ones based on their identifying features: Balmer-dominated, oxygen-rich, plerionic[2]-composite, and evolved SNRs (Weiler & Sramek 1988).

The prototype for the Balmer-dominated SNR is Tycho's supernova (SN 1572,

[2]pulsar-like

SN Name	SNR Name	Distance (kpc)	S_{6cm} (Jy)	Refs.
SN 1006	none	1.0	7	1,2
SN 1054	Crab Nebula	2.0	658	2,3
SN 1181	3C 58	2.6	28	2,3,4
SN 1572	Tycho, 3C 10	2.3	21	1,2
SN 1604	Kepler	4.4	7	1,2
SN $\sim$ 1670	Cas A	2.8	782	1,2

Table 1.1: Table of young Galactic SNRs and data pertaining to them. References—(1) Clark and Caswell (1976), (2) Green (1984), (3) Weiler et al. (1983); Weiler and Panagia (1980), (4) Green and Gull (1982)

Type I) whose identifying features include filamentary shells strong in hydrogen Balmer lines but lacking in or very weak in [O III] and [S II]. This category can include either shell or partial shell shaped remnants. Other examples of this class of SNR are Kepler's supernova (SN 1604, Type I) and SN 1006 (Type I?).

Cas A is a prime example of the next category, the oxygen-rich SNR. As one might guess, it is identified by strong oxygen lines, in particular [O III]. Progenitors for this type of SNR is thought to be the explosion of a massive ($< 25M_{\odot}$) star.

Plerionic-composite SNRs are observed to have a pulsar in the center of a filled remnant that may or may not have an associated shell structure. The Crab Nebula (SN 1054, Type II?) is an example of this type of remnant.

The final category, the evolved SNR, is hard to apply to SNRs due to the difficulty of the observations. This category is identified by the ratio of [S II] to Hα being greater than 0.7 and the presence of a partial shell structure. The difficulty arises because most of the Galactic SNRs have no optical identification. Weiler & Sramek (1988) then suggest that this class could represent the final evolutionary phase of the other 3 classes—a final drop in emission before the remnant fades below detectability.

1.3 Theoretical Models for Radio Emission

Two models will be briefly reviewed in this section to help illuminate the cause for and help our understanding of the radio emission: the Chevalier model for RSNe, and the Gull model for radio SNRs. I will also briefly mention the physical quantities that the models enable us to calculate and compare the model radio light curves with observations as a check of the model.

1.3.1 Chevalier Model for Radio Emission from Supernovae

Chevalier (Chevalier 1982a,b) has proposed the following scenario to generate the radio emission observed from SNe Type II (and possibly Type Ib/c given the similar pre-SN masses of the progenitors). The believed progenitors for Type II SNe are stars with masses around $7 - 30 M_{\odot}$, and these types of stars are expected to have a stellar wind ($v_w =\sim 10$ km/s), and thus a mass-loss during the red giant phase of evolution before explosion. When the SN explodes, an outward moving shock wave ($v_s =\sim 10^4$ km/s) is generated that interacts with the pre-SN stellar wind. The interaction region is Rayleigh-Taylor unstable, which can drive turbulent motions. This turbulence can then compress and amplify the magnetic fields present and accelerate already relativistically moving (via the fast shock or from the energy of the explosion) free electrons; synchrotron radiation results that is characterized by a non-thermal spectral index. The radio emission from the synchrotron radiation is then subject to free-free absorption by the unshocked stellar wind. Recent calculations by Chevalier (1998) indicate that synchrotron self-absorption (previously thought to be unimportant) may be important for SNe with low mass-loss rates and SNe Ib/c at early times. Its

effects on derived quantities will be discussed shortly. There are several assumptions in this scenario: 1) the SN density profile has a power law form in radius (a good approximation), 2) the ratios of the magnetic and electron energy densities to the thermal energy densities are constant, 3) the wind mass-loss rate and stellar wind velocity are constant, 4) the magnetic and electron energies are in equipartition, and 5) spherical symmetry. The radio light curves can be explained as follows. Due to the nature of the free-free absorption, the shorter wavelengths are observed first. The radio luminosity at a given wavelength increases with time as the optical depth from the absorption drops, peaking as the optical depth reaches unity. We then observe the synchrotron emission with its usual negative spectral index.

The model described here seems to work well in describing the general form for the radio light curve at later times for SNe 1979C, 1980K, 1983N, 1984L, and 1990B, and the calculated curves seems to fit well. Note that the fits are good at later times for a range of SN types—II, Ib, and Ic.

Variations on the Model

SN 1979C Weiler et al. (1992b) attempted to account for the short term fluctuations in the 10 year light curve of SN 1979C by modifying the model. The radio light curve shows an apparent periodicity that they show to be statistically significant. Weiler et al. (1992b) achieves a somewhat better fit[3] to the data by incorporating a sinusoidal variation term to the Chevalier (1982a,b) model, but admits the model is still incomplete at this level. They propose several methods that might produce peri-

[3] "better fit" is described as the improvement (reduction) on the minimum error artificially introduced to bring χ^2 to its ideal value of unity for a perfect fit

odic fluctuations ranging from a pulsational instability for the red giant while emitting its wind to changes in mass-loss rates due to the presence of a binary companion.

At an age of only about 20 years, the second rise in radio emission (Weiler et al. 1998) is not likely a result of emission from a SNR (see next section). It *is* likely that the shock is encountering a denser layer of the circumstellar wind material. This denser wind layer could then provide the extra fuel for an increase in radio emission.

SN 1986J Examination and analysis of the radio light curve and data for SN 1986J leads Weiler et al. (1990) to propose a modification of the model to achieve a better fit. They modify the Chevalier (1982a,b) model to account for mixed non-thermal emitters *and* thermal (free-free) absorbers that seems to fit the radio data better than the simpler Chevalier model. Again, the model improved the fit to the data but is still incomplete—SN 1986J was obviously a very different radio SN.

SN 1987A A reasonable explanation may now be proposed for the second rise in radio emission from SN 1987A. Chevalier & Dwarkadas (1995) adopt a mass-loss rate at about 1500 days of 7.5×10^{-8} $M_\odot$ yr^{-1} (with $v_w = 450$ km/s), which is too small to contribute to the free-free absorption observed. Synchrotron self-absorption can account for the initial rise and fall of radio emission, though. The recent (second) turn-on can be explained as the shock *now* encountering a region of enhanced density. It is known that the progenitor for SN 1987A went through a red giant stage and then a blue giant stage before exploding. One explanation for the enhanced circumstellar density is that the SN shock is encountering an H II region created by the blue giant progenitor (Chevalier & Dwarkadas 1995). This H II region is merely the ionized red

giant wind, according to Chevalier & Dwarkadas.

Model Results

An advantage to using the model is that it helps in our understanding of the origin of radio emission, but it also enables calculation of another quantity, provided the model fit is good. In particular, the Chevalier model lets us calculate the mass-loss rate (divided the wind speed, v_w) of the pre-SN star required to produce the emission we observe. With knowledge of the mass-loss rate we may estimate, based on stellar evolution models, the stellar mass required to produce such a wind. Estimated mass-loss rates and pre-SN stellar masses calculated for modeled SNe are in Table 1.2. Excluding the effects of synchrotron self-absorption can cause these derived mass-loss rate to be overestimated for SNe Ib/c and SNe with low mass-loss rates (Chevalier 1998). Chapter 5 briefly addresses this issue with respect to the observations presented in that chapter.

Boffi & Branch (1995) have applied the Chevalier model to Type Ia SNe in symbiotic systems (a red giant in a binary system with a white dwarf) where a white dwarf accretes matter from the stellar wind of the red giant. This has been applied to SN 1986G by Eck et al. (1995) as a test on this symbiotic scenario for this SN with negative results (see Chapter 4).

1.3.2 Gull Model for Radio Emission from SNRs

The basic premise for the Gull model (Gull 1973) involves continuation of the SN shock as it passes into the interstellar medium (ISM). Radio emission has faded by the time the shock passes into the ISM, but the shock sweeps up material as it moves

SN (Type)	Mass-loss ($10^{-5} M_\odot/yr$)	Pre-SN mass ($M_\odot$)	Reference
SN 1979C (II)	12	$\gtrsim 13$	Lundqvist & Fransson (1988) Weiler et al. (1991)
SN 1980K (II)	3	none reported	Lundqvist & Fransson (1988)
SN 1981K (II?)	< 0.50	$<$ that of SNe 1979C and 1980K	Van Dyk et al. (1992)
SN 1983N (Ib)	0.20	none reported	Weiler et al. (1986)
SN 1984L (Ib)	0.0083	none reported	Van Dyk et al. (1993b)
SN 1986J (II)	> 24	$\gtrsim 20 - 30$	Weiler et al. (1990)
SN 1988Z (II)	7.1	$\sim 20 - 30$	Van Dyk et al. (1993b)
SN 1990B (Ic)	0.17	$\sim 6 - 8$	Van Dyk et al. (1993a)
SN 1993J (II)	2 (variable)	none reported	Van Dyk et al. (1994)

Table 1.2: Reported mass-loss rates derived from model fits to the radio light curve and possible stellar masses for the progenitors inferred from the mass-loss rates.

out. Calculations by Cowsik & Sarkar (1984) show that when the shock has swept up approximately one solar mass of interstellar matter (after a minimum of $\sim$ 100 years), the SNR "turns on" due to the Rayleigh-Taylor instabilities generated, and subsequent synchrotron radio emission appears as before. Why have we not seen any SNRs less than $\sim$ 300 yrs old? Since it takes a minimum of about 100 years (or maybe 300 years, depending on the parameters in the model) to brighten as a SNR, we have a possible explanation for the fact that we have not seen any SNRs younger than Cas A.

To investigate radio emission from all types of SNe, I report the results of a search for radio emission from SNe whose ages range from 10 days after explosion to almost 90 years old. With these results, I hope to get a better understanding of why some SNe are radio emitters and others are not.

SN Name	SN Type	Distance[a] (Mpc)	Parent Galaxy	Galaxy[a] Type	Age[b] (yr)	Observed Radio Maximum @ 20 cm: Flux Density (mJy)	Spectral Luminosity (erg s^{-1} Hz^{-1})	Ratio to Cas A	Optically Thin Radio Sp. Index α_6^{20}	Rate of Flux density Decline, β	Refs
SN 1950B	II?	4.7	NGC 5236 (M83)	Sc	30	0.8	2.1×10^{25}	~ 1.1	-0.57 ± 0.08	...	1,2
SN 1957D	II?	4.7	NGC 5236 (M83)	Sc	23	2.6	6.9×10^{25}	~ 3.6	-0.30 ± 0.02	-2.9 ± 0.3	1,2
SN? 1961V	II	9.1	NGC 1058	Sc	24	0.18 ± 0.04	1.8×10^{25}	~ 0.95	-0.60 ± 0.08	...	3
SN 1968D	II	5.5	NGC 6946	Scd	26	0.62 ± 0.04(21cm)	2.2×10^{25}	~ 1.2	-0.92 ± 0.13	...	4
SN 1970G	II	5.4	NGC 5457 (M101)	Scd	3.4	~ 6	2.1×10^{26}	~ 11	-0.56 ± 0.11	-2.0 ± 0.17	5,6
SN 1978K	II	3.7	NGC 1313	SBd	13.5	160	2.6×10^{27}	~ 140	...	...	17
SN 1979C	II	16.8	NGC 4321 (M100)	Sbc	4.0	13.2 ± 1.2	4.5×10^{27}	~ 240	~ -0.75 $[-0.74 \pm 0.1]$	...	7,8
SN 1980K	II	5.5	NGC 6946	Scd	1.5	2.2 ± 0.2	8.0×10^{25}	~ 4.2	~ -0.60 $[-0.52 \pm 0.3]$	...	7,9
SN 1981K	II?	6.8	NGC 4258	Sbc	0.5?	~ 2?	1.1×10^{26}	~ 5.8	0.74 ± 0.5 $[-0.91 \pm 0.07]$	...	10,11
SN 1983N	Ib	4.7	NGC 5236 (M83)	Sc	0.42	4.2 ± 0.2	$\sim 1.1 \times 10^{26}$	~ 5.8	... $[-1.03 \pm 0.06]$	...	7
SN 1984L	Ib	18.8	NGC 991	Sc	0.30	1.01 ± 0.10	4.3×10^{26}	~ 23	... $[-1.01 \pm 0.17]$	...	12
SN 1986J	II	9.6	NGC 891	Sb	5.5	127.6 ± 6.4	1.4×10^{28}	~ 740	-0.33 ± 0.06 $[-0.67 \pm 0.08]$	...	13
SN 1988Z	II	89	MCG +03-28-022		4.9	1.45 ± 0.11[c]	1.4×10^{28}	~ 740	... $[-0.74 \pm 0.05]$	...	14
SN 1990B	Ic	16.8	NGC 4568	Sbc	0.13	1.48 ± 0.11	5.0×10^{26}	~ 26	-0.97 ± 0.27 $[-1.12 \pm 0.08]$	...	15
SN 1993J	II	1.4	NGC 3031 (M81)	Sab	0.3	~ 50[c]	1.2×10^{26}	~ 6.3	... $[-0.99 \pm 0.6]$	...	16

Table 1.3: Summary of data on well-studied radio SNe at 20 cm.

Table 1.3:—Continued

a. From Fully (1988).
b. At peak flux or at highest flux measured if only post-peak measurements are available.
c. Pre-peak observation maximum observation listed.

Quantities enclosed by square brackets are derived from model fits to data using the Chevalier model.

References– 1) Cowan & Branch 1985, 2) Cowan *et al.* 1994, 3) Cowan *et al.* 1988, 4) Hyman *et al.* 1995, 5) Allen *et al.* 1976, 6) Cowan *et al.* 1991, 7) Weiler *et al.* 1986, 8) Weiler *et al.* 1991, 9) Weiler *et al.* 1992a, 10) van der Hulst *et al.* 1983, 11) Van Dyk *et al.* 1992, 12) Panagia *et al.* 1986, 13) Weiler *et al.* 1990, 14) Van Dyk *et al.* 1993b, 15) Van Dyk *et al.* 1993a, 16) Van Dyk *et al.* 1994, 17) Ryder *et al.* 1993

SN Name	SN Type	Distance[a] (Mpc)	Parent Galaxy	Galaxy[a] Type	Observed Radio Maximum @ 6 cm				Optically Thin Radio Sp. Index α_6^{20}	Rate of Flux density Decline, β	Refs
					Age[b] (yr)	Flux Density (mJy)	Spectral Luminosity (erg s^{-1} Hz^{-1})	Ratio to Cas A			
SN 1950B	II?	4.7	NGC 5236 (M83)	Sc	34	0.5	1.3×10^{25}	~ 2	-0.57 ± 0.08	...	1,2
SN 1957D	II?	4.7	NGC 5236 (M83)	Sc	27	1.9	5.0×10^{25}	~ 7	-0.30 ± 0.02	-1.7 ± 0.2	1,2
SN? 1961V	II	9.1	NGC 1058	Sc	24	0.11 ± 0.03	1.1×10^{25}	~ 1.5	-0.60 ± 0.08	...	3
SN 1968D	II	5.5	NGC 6946	Scd	26	0.20 ± 0.03	7.2×10^{24}	~ 1	-0.92 ± 0.13	...	4
SN 1970G	II	5.4	NGC 5457 (M101)	Scd	1.4	~ 2.5	8.7×10^{25}	~ 12	-0.56 ± 0.11	...	5,6
SN 1979C	II	16.8	NGC 4321 (M100)	Sbc	1.2	8.3 ± 0.44	2.8×10^{27}	~ 380	~ -0.75 $[-0.74 \pm 0.1]$	... $[-0.78 \pm 0.03]$	7,8
SN 1980K	II	5.5	NGC 6946	Scd	0.4	2.6 ± 0.12	9.4×10^{25}	~ 13	~ -0.60 $[-0.52 \pm 0.3]$	... $[-0.66 \pm 0.08]$	7,9
SN 1981K	II?	6.8	NGC 4258	Sbc	0.5	~ 2	1.1×10^{26}	~ 15	0.74 ± 0.5 $[-0.91 \pm 0.07]$	... $[-0.5 \pm 0.05]$	10,11
SN 1983N	Ib	4.7	NGC 5236 (M83)	Sc	0.08	18.5 ± 1.0	$\sim 4.9 \times 10^{26}$	~ 67	... $[-1.03 \pm 0.06]$	... $[-1.59 \pm 0.08]$	7
SN 1984L	Ib	18.8	NGC 991	Sc	0.14	0.7 ± 0.18	3×10^{26}	~ 40	... $[-1.01 \pm 0.17]$	... $[-1.46 \pm 0.33]$	12
SN 1986J	II	9.6	NGC 891	Sb	3.6	128.4 ± 6.6	1.4×10^{28}	~ 2000	-0.33 ± 0.06 $[-0.67 \pm 0.08]$	... $[-1.18 \pm 0.04]$	13
SN 1988Z	II	89	MCG +03-28-022		3.4	1.9 ± 0.11[c]	1.8×10^{28}	~ 2500	... $[-0.74 \pm 0.05]$	... $[-1.45 \pm 0.02]$	14
SN 1990B	Ic	16.8	NGC 4568	Sbc	0.08	1.04 ± 0.08	3.5×10^{26}	~ 48	-0.97 ± 0.27 $[-1.12 \pm 0.08]$	... $[-1.27 \pm 0.04]$	15
SN 1993J	II	1.4	NGC 3031 (M81)	Sab	0.3	~ 90[c]	2.1×10^{26}	~ 30	... $[-0.99 \pm 0.6]$	... $[-0.64 \pm 0.25]$	16

Table 1.4: Summary of data on well-studied radio SNe at 6 cm.

Table 1.4:—Continued

a. From Tully (1988).
b. At peak flux or at highest flux measured if only post-peak measurements are available.
c. Pre-peak observation–maximum observation listed.

Quantities enclosed by square brackets are derived from model fits to data using the Chevalier model.

References—1) Cowan & Branch 1985, 2) Cowan *et al.* 1994, 3) Cowan *et al.* 1988, 4) Hyman *et al.* 1995, 5) Allen *et al.* 1976, 6) Cowan *et al.* 1991, 7) Weiler *et al.* 1986, 8) Weiler *et al.* 1991, 9) Weiler *et al.* 1992a, 10) van der Hulst *et al.* 1983, 11) Van Dyk *et al.* 1992, 12) Panagia *et al.* 1986, 13) Weiler *et al.* 1990, 14) Van Dyk *et al.* 1993b, 15) Van Dyk *et al.* 1993a, 16) Van Dyk *et al.* 1994

Chapter 2

SN 1923A: The Oldest Radio Supernova?

2.1 Introduction

In this chapter, the results of a re-analysis of a radio map of M 83 (NGC 5236) will be presented. More specifically, two weak unresolved sources were detected whose positions are coincident with the reported optical position of SN 1923A. One of the sources is closer to the SN position than the other, and both sources are non-thermal with spectral indices of $\alpha = -1.0 \pm 0.30$ for the closer source and -0.69 ± 0.24 for the other source. The non-thermal nature of the radio emission combined with the positional coincidence makes it probable that one of these sources is from the site of SN 1923A.

This probable detection is important for two reasons. First, SN 1923A has been classified as an SN II-P (Patat et al. 1994). This will be the first radio detection of

a Type II-P. Second, at an age of about 70 years, this would be the oldest historical radio supernova yet detected.

2.2 Observations and Data Reduction

SN 1923A was discovered by C. Lampland (Lampland 1936) in M 83, classified as an SABc starburst galaxy at 4.1 Mpc (Saha et al. 1995) and home to 5 other supernovae (SNe 1945B, 1950B, 1957D, 1968L, 1983N). Its position via offsets to the center of M 83 is 109″ E and 58″ N. A recent re-analysis of the map of M 83 from CRB revealed two faint sources near the optical position of SN 1923A.

Observations of M 83 were made at two epochs for each wavelength, 20 and 6 cm, at the Very Large Array (VLA)[1] in different configurations such that the beam sizes were circular and approximately the same for all observations. The different "hybrid" configurations were used at the VLA to obtain circular beam sizes for observations of M 83, at low declination. The phase and pointing centers for all images were at R.A.(1950)= $13^h34^m12^s.2$, Dec.(1950)= $-29°35'36''.0$ and the strong radio source 3C 286 was used as primary flux calibrator for all observations.

Due to the non-thermal nature of the late-time radio emission from supernovae, M 83 was observed initially at 20 cm at the first epoch, and then at 6 cm to determine the spectral index of the observed sources. At the second epoch a problem with the online systems at the VLA corrupted the 20 cm data taken in the hybrid BnA configuration. The observations were repeated later in B configuration instead,

[1]The VLA is a telescope of the National Radio Astronomy Observatory which is operated by Associated Universities, Inc., under a cooperative agreement with the National Science Foundation.

	1983-1984 Observations		1990-1992 Observations	
Wavelength (cm) :	20	6	20	6
Frequency (GHz) :	1.446	4.873	1.515	4.848
Bandwidth per IF (MHz) :	12.5	25	25	25
Number of IFs :	2	2	2	2
Observation dates :	15 Dec 1983	13 Mar 1984	4 Jan 1992	14 Oct 1990
Observing time (hr) :	6	6.5	8	8.5
VLA Configuration :	BnA	CnB	B	CnB
Primary beam HPBW :	30′	8′	30′	8′
Resolution ($\alpha \times \delta$) :	$3\farcs5 \times 3\farcs5$	$3\farcs9 \times 2\farcs8$	$2\farcs3 \times 5\farcs2$	$3\farcs2 \times 2\farcs8$
Rms noise (mJy beam^{-1}) :	0.19	0.054	0.050	0.028

Table 2.1: Parameters for Radio Observations of SN 1923A (M 83).

resulting in a slightly different beam size than at the first epoch at 20 cm. Table 2.1 summarizes the relevant parameters for each wavelength and epoch.

The data reduction was done using the Astronomical Image Processing System (AIPS) software provided by the National Radio Astronomy Observatory. Details of the original data reduction techniques are described in the papers regarding the observations of M 83 (Cowan & Branch 1985, CRB). While a Maximum Entropy Method was used in the original image processing to reconstruct the diffuse structure, CLEAN was used for the second epoch observations to get a higher signal-to-noise for isolated point sources (i.e., SN 1923A) where the diffuse structure was not important. We (Eck et al. 1998a) initially attempted to fit the two nearby point sources with two Gaussian components simultaneously using JMFIT, however, the relatively low signal-to-noise ratio of the two sources prevented convergence. Therefore, all but one of the

flux densities and positions were determined by fitting a quadratic function to each source, using the MAXFIT program of the AIPS package. For the other datum, the fit using MAXFIT failed so that we report the peak flux using the AIPS routine IMSTAT. A background level was estimated using TVSTAT at all wavelengths and epochs. The background level was determined to be on the order of the rms noise so it was included in the error estimation. PBCOR was used to correct the fluxes for primary beam attenuation. Images of the field of view can be seen in Figures 2.1, 2.2, and 2.3. Results for positions and fluxes are given in Table 2.2, along with the optical supernova position from Pennington, Talbot, & Dufour (1982). Figure 2.1 shows approximately half of M 83 at 20 cm along with several sources CRB observed, labeled here as in that paper. Figure 2.2 shows the region surrounding SN 1923A (zoomed in from Figure 2.1) and includes both SN candidates. Figure 2.3 is a 6 cm map of approximately the same region as in Figure 2.2. To within the uncertainties[2], both unresolved sources are coincident with the optical position. Although we tentatively report the western (closer) source as probably being from SN 1923A, we cannot exclude the possibility that either source may be SN 1923A. Calculation of the spectral index, α, ($S \propto \nu^{\alpha}$) between 20 and 6 cm (at second epoch only) reveals that both candidates are non-thermal, with the western source at $\alpha_6^{20} = -1.0 \pm 0.30$ and the eastern source at $\alpha_6^{20} = -0.69 \pm 0.24$. Some caution must be exercised in interpreting this value since the flux densities were measured at slightly different times. we can compare this value to the late-time spectral indices of other Type II SNe ($\alpha_6^{20} = -0.57$ [1950B, CRB], -0.23 [1957D, CRB][3], -0.60 [1961V, Cowan et al. 1988], -0.92 [1968D, Hyman et

[2]Without a fitting routine such as JMFIT to estimate positional uncertainty, we can only report the beamsize as representative of the positional uncertainty although it is probably less than this.

[3]Note: this value is at the first epoch of observations since it is believed the SN has faded below

Source	R.A.(1950)[b]	Dec.(1950)[c]	Peak Flux (mJy) 20 cm	Peak Flux (mJy) 6 cm	Age (yrs)
SN 1923A?[a]	$13^h34^m19^s.92$	$-29°35'46''.3$	< 0.57[d]	···	60.6
			···	0.19 ± 0.05	60.8
			···	0.093 ± 0.03	67.4
			0.30 ± 0.05	···	68.6
Eastern Source	$13^h34^m20^s.18$	$-29°35'46''.6$	< 0.57[d]	···	60.6
			···	0.21 ± 0.05	60.8
			···	0.13 ± 0.03	67.4
			0.29 ± 0.05	···	68.6

[a] Optical position at $\alpha(1950) = 13^h34^m20^s \pm 0^s.02$, $\delta(1950) = -29°35'48'' \pm 0''.24$ from Pennington, Talbot, & Dufour (1982).
[b] $\pm 0^s.18$
[c] $\pm 5''.2$
[d] 3σ upper limit

Table 2.2: Observations of the site of SN 1923A.

al. 1995], −0.59 [1970G, Cowan et al. 1991], −0.74 [1979C, Weiler et al. 1991]).

Since there are 6 cm flux densities at two epochs, it is tempting to try to fit the data to a power-law in time ($S \propto t^\beta$) for comparison with other events ($\beta_{20cm} = -2.9$ [1957D, CRB], $\beta_{6cm} = -1.7$ [1957D, CRB], $\beta_{20cm} = -1.95$ [1970G, Cowan et al. 1991]). For SN 1923A, we find $\beta_{6cm} = -6.9 \pm 4.0$ and -4.7 ± 3.3 for the western and eastern sources, respectively. Since the flux densities appear to be decreasing with time, both sources are consistent with being in the later stages of radio supernova evolution. While it is likely that both sources are fading radio SNe, it is not clear which source is SN 1923A.

the level of an associated H II region at the second epoch (CRB).

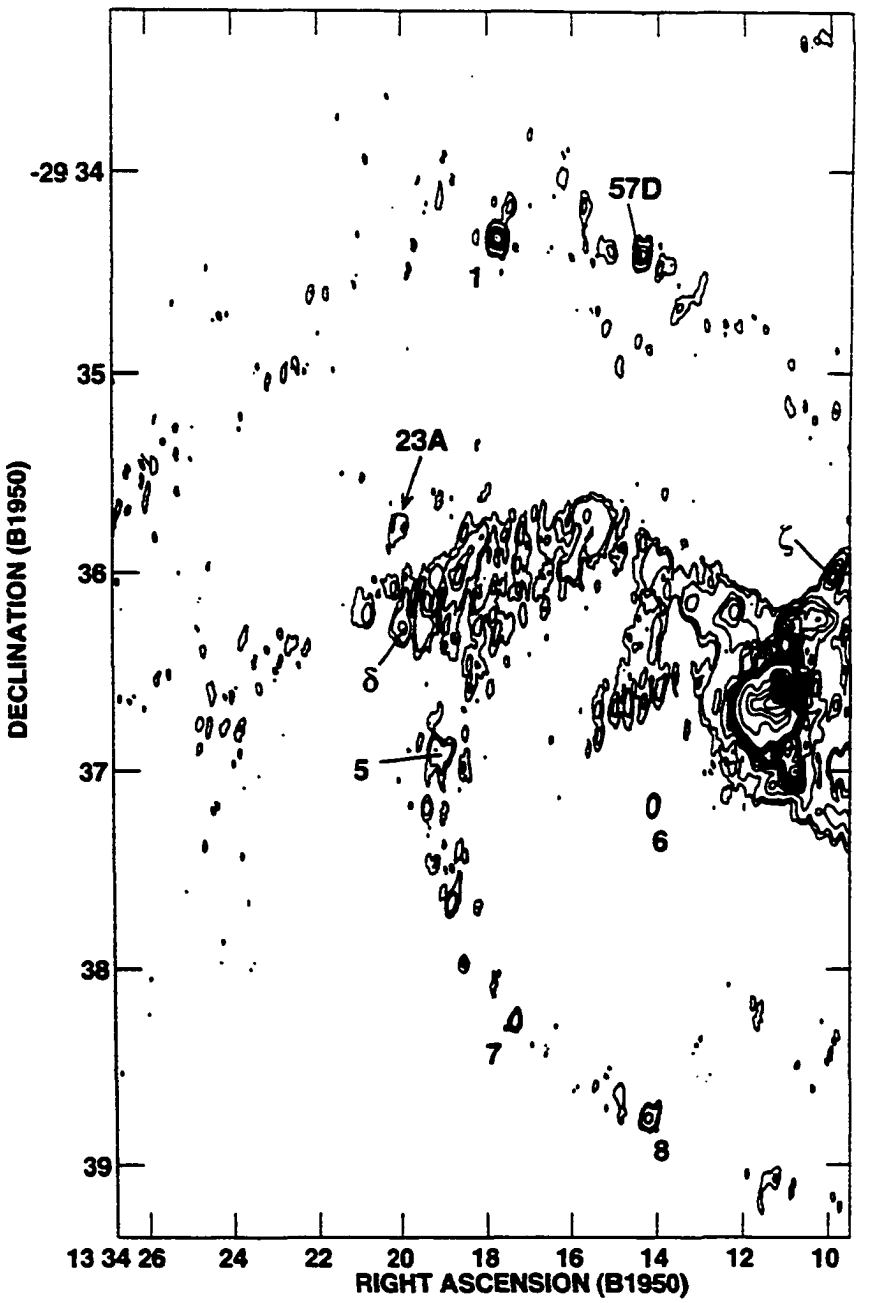

Figure 2.1: A 1.515 GHz (20 cm) contour map of approximately half of the field of view for M 83 taken at the VLA in the B configuration on January 4, 1992. The beam size ($\alpha \times \delta$) is $2''.3 \times 5''.2$ and the rms noise level is 0.050 mJy beam^{-1}. The contour levels are at 0.17, 0.27, 0.60, 0.89, 1.19, 1.49, 1.79, 2.08, 2.38, 2.68, 2.98, 5.95, 8.93, 11.9, 14.9, 17.9, 20.8, 23.8, 26.8, 29.5 mJy beam^{-1}. SN 1957D (CRB) and SN 1923A are both visible in the map as well as several other sources from CRB including the radio bright central regions of M 83.

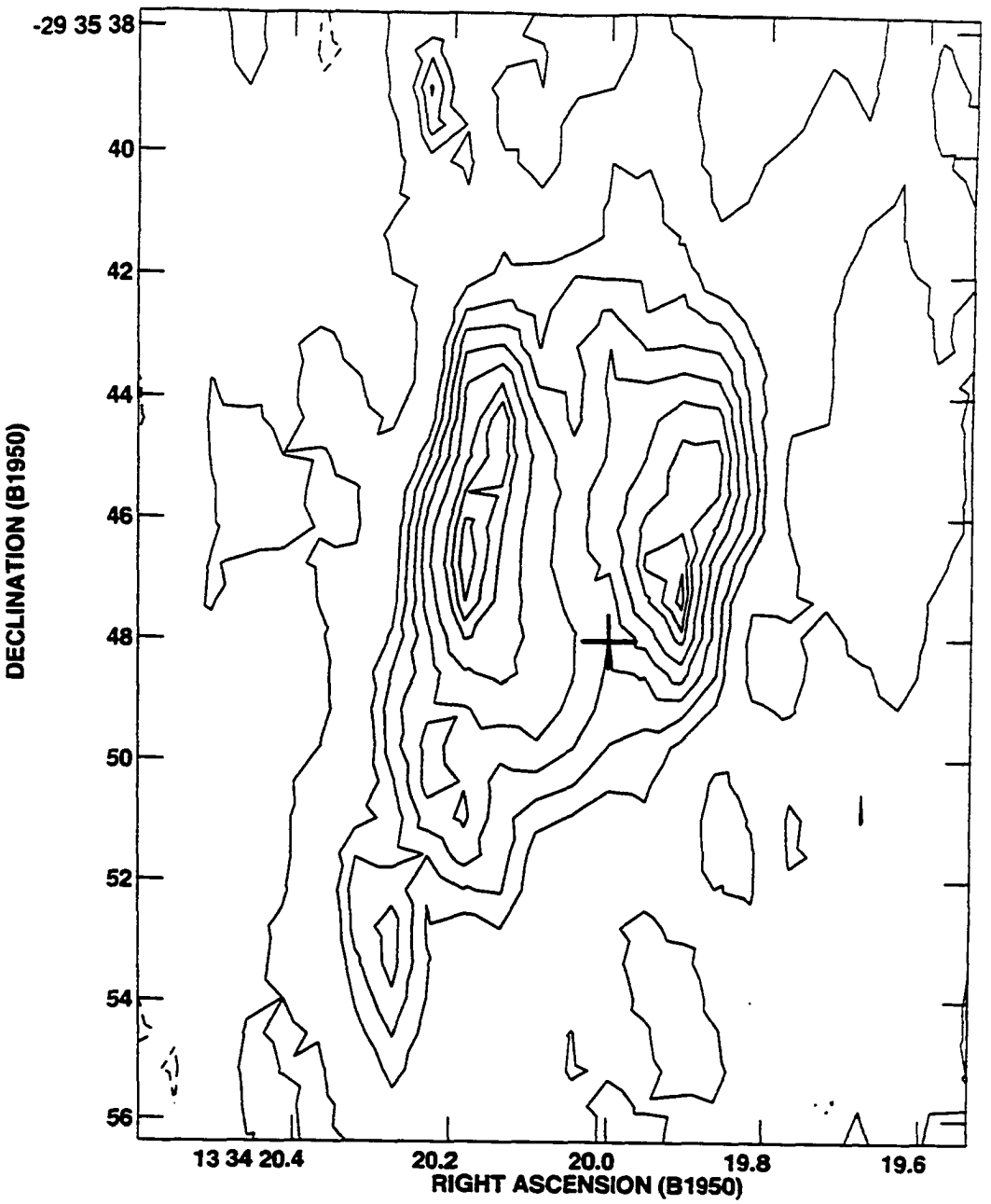

Figure 2.2: A (20 cm) contour map of the region immediately surrounding the site of SN 1923A, magnified from the map in Figure 2.1. Included in the map are both SN candidates visible near the center of the map in Figure 2.1. A cross marks the optical position for SN 1923A from Pennington et al. (1982). The contour levels are -0.071, 0.071, 0.14, 0.17, 0.19, 0.21, 0.24, 0.26, 0.27, 0.29, 0.30 mJy beam^{-1}. The peak flux for the SN 1923A candidate is 0.30 ± 0.05 mJy beam^{-1}.

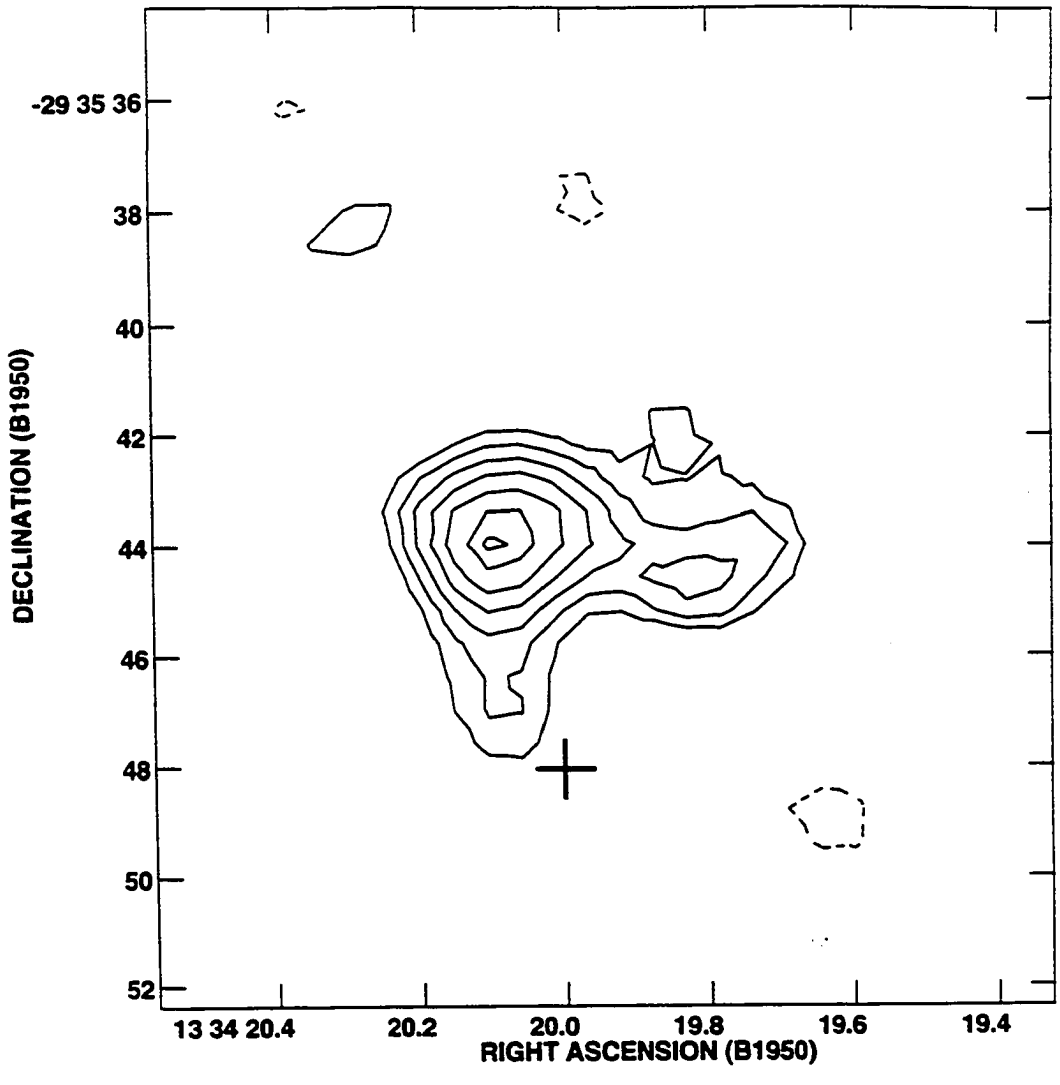

Figure 2.3: A (6 cm) contour map of the region immediately surrounding the site of SN 1923A taken at the VLA in the CnB configuration on October 14, 1990. The beamsize ($\alpha \times \delta$) is $3\farcs5 \times 2\farcs8$ and the rms noise level is 0.028 mJy beam^{-1}. A cross marks the optical position for SN 1923A from Pennington et al. (1982). Both SN candidates are visible with peak flux positions consistent (to within uncertainties) with the 20 cm peak flux positions. The angular separation of the peaks of the two sources is nearly identical ($3\farcs5$) in the 6 cm map and in the 20 cm map. The contour levels are -0.065, 0.065, 0.076, 0.087, 0.098, 0.11, 0.12, 0.13 mJy beam^{-1}. The peak flux for the candidate nearest the optical SN position is 0.093 ± 0.03 mJy beam^{-1}.

2.3 Discussion and Conclusions

Although the detected sources are relatively weak, the non-thermal nature and the apparent positional coincidence with the location of SN 1923A (as shown in Table 2.2) make it probable that we have detected radio emission from this supernova. The sources are separated by about 3.″5 which, at the distance to M 83 (4.1 Mpc), corresponds to almost 70 pc, thus the sources cannot both be from SN 1923A. Past optical studies of the site of SN 1923A have shown evidence for an H II region at or near the supernova site. Rumstay & Kaufman (1983) list an H II region — no. 59 in their paper — within $1'' - 2''$ of the SN position as based upon offsets with respect to the center of its parent galaxy. Richter & Rosa (1984) refer to Rumstay & Kaufman H II region no. 59 as an H II region associated with and lying $1''$ from SN 1923A. Pennington et al. (1982) also note that SN 1923A appears to be coincident with an H II region. A map of H II regions by de Vaucouleurs, Pence, & Davoust (1983), when overlaid with the scaled radio map, has the source for SN 1923A directly over the H II region. Since the progenitor star of SN 1923A has been estimated to have been massive, $\simeq$ 18 $M_\odot$ (Pennington et al. 1982), it should not have moved much prior to explosion, and the H II region near the radio source may be associated with the supernova's progenitor. The presence of an H II region at the SN site reduces the chances that the two sources are actually background sources. There is evidence for other similar associations of radio supernovae (RSNe) and H II regions (Van Dyk 1992), including SN 1957D (also estimated to have resulted from a massive star) in M 83 (CRB). Clearly new examinations of the area surrounding the site of SN 1923A in M 83 are warranted to search for an optical counterpart to the radio source.

On the basis of what is known about the shape of its light curve, SN 1923A has been tentatively designated as a sub-luminous Type II-P (Patat et al. 1994, Schaefer 1996). No Type II-P (other than SN 1987A) has been detected previously in the radio. In Figure 2.4, we plot the radio luminosity at 20 cm of the western source assuming it to be SN 1923A, along with several other extra-galactic RSNe and two Galactic SNRs, as a function of time since outburst. Data and fits (solid lines) in Figure 2.4 for the well-studied Type II-L SN 1979C were taken from Weiler et al. (1986, 1991), for the Type II-L SN 1980K from Weiler et al. (1986, 1992a), for the Type Ib SN 1983N from Weiler et al. (1986) and Cowan & Branch (1985), for the Type II-L SN 1970G from Cowan et al. (1991), for the Type II-L SN 1968D from Hyman et al. (1995) and for SNe 1950B & 1957D from CRB. The distance to M 83 (4.1 Mpc) was taken to be the Cepheid–based distance to NGC 5253, (Saha et al. 1995), a fellow member of the Centaurus group. As Figure 2.4 illustrates, the luminosity of SN 1923A is comparable to, but slightly below, the two other intermediate-age supernovae detected in M 83, SNe 1957D and 1950B. (These two supernovae are suspected to have had massive progenitors but their actual supernova types are unknown.) SN 1957D may actually be somewhat less luminous than plotted, because emission from an associated H II region may have contributed to the observed flux. The radio emission from SN 1923A falls between that of Cas A and the Crab.

At an age of approximately 68 years when last observed, SN 1923A would be the oldest radio supernova yet discovered. Detectable radio emission from supernovae decades after explosion (but before the SNR phase) may in fact be uncommon, as evidenced by the small class of such known objects. Observations of several other supernovae over a number of years also support that conclusion. SN 1979C is still

detectable and SN 1980K has dropped off sharply after a decade of being followed. Recently Montes et al. (1997) have reported early radio emission from SN 1986E, while we were unable to detect this supernova at an intermediate-age despite a deep VLA search (Eck et al. 1996 and Chapter 3). Montes et al. (1997) argue that SN 1986E is a typical Type II-L, similar to SN 1980K and the fading radio emission can be adequately explained in terms of the Chevalier model.

What is the cause of the radio emission of SN 1923A? No Type II-P events have been observed to undergo a prompt, bright circumstellar interaction such as that of radio supernovae. SN 1987A, having been a sub-luminous Type II-P, underwent a prompt but dim circumstellar interaction that would not have been detectable in a galaxy beyond the local group, but now it is beginning what promises to be stronger, delayed interaction with a detached circumstellar shell that originated back in its red giant days. If SN 1923A was a sub-luminous Type II–P, it may now be fading from the kind of delayed interaction that SN 1987A is just beginning.

The key radio observations needed now (apart from more firmly establishing the presence of a non-thermal radio source at the site of SN 1923A) are to trace the radio evolution of these sources, one of which is likely to be SN 1923A, the oldest radio supernova yet detected. While it is noted above that theoretical models have suggested a minimum time of 100 years for the onset of the SNR (and a brightening) phase, radio emission from the supernovae at this age has never been previously detected or studied. These observations at one wavelength seem to indicate that the source closest to the SN position is still fading with time, but the uncertainties are large. Additional observations of SN 1923A will help to understand more about the nature of radio emission as supernovae evolve from intermediate-age to the SNR

phase.

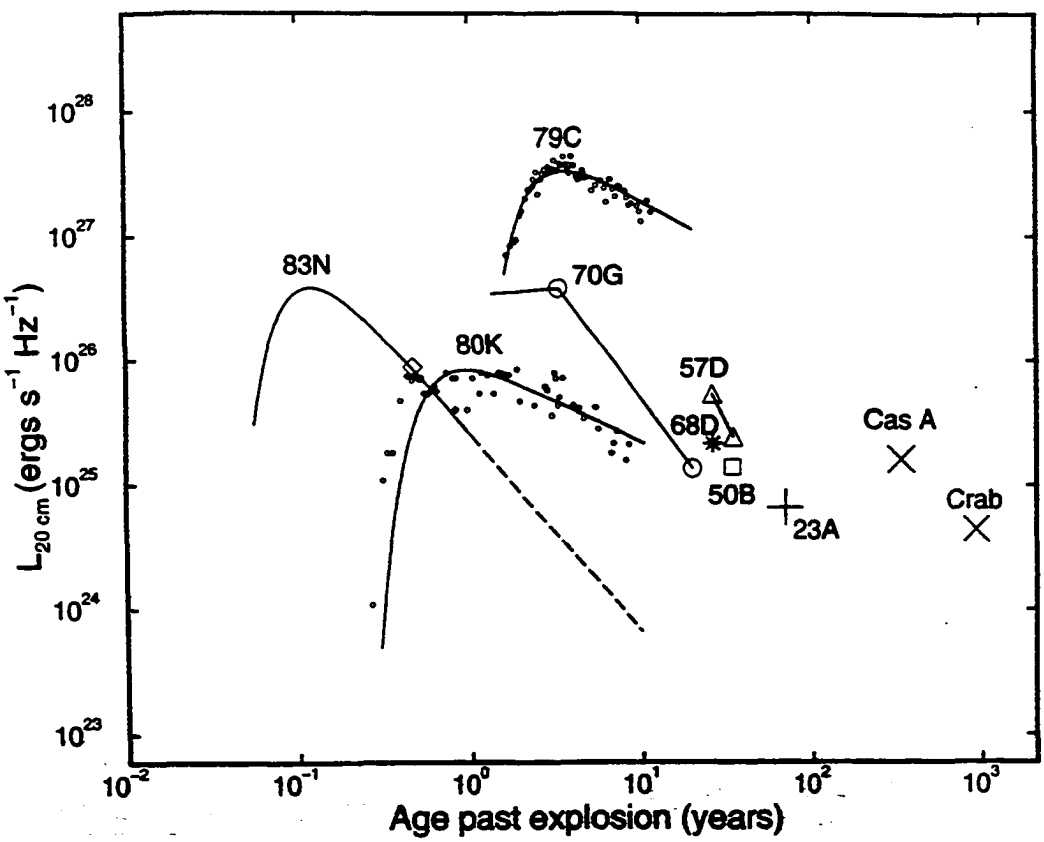

Figure 2.4: Radio luminosity of SN 1923A compared to several extra-galactic intermediate-age supernovae and Galactic SNRs at 20 cm as a function of time since outburst. The peak flux densities for both sources are nearly equal, so only a single data point is plotted as representative of the luminosity for SN 1923A. Data and fits (solid lines) for SN 1979C from Weiler et al. (1986, 1991), SN 1980K from Weiler et al. (1986, 1992a), SN 1983N from Weiler et al. (1986) and Cowan & Branch (1985), SN 1970G from Cowan et al. (1991), SN 1968D from Hyman et al. (1995) and SNe 1950B & 1957D from CRB. The dashed line is an extrapolation to the light curve of SN 1983N based on the Chevalier model.

Chapter 3

SNe 1984E and 1986E

3.1 Introduction

In this chapter, we (Eck et al. 1996) report on the results of an attempt to use the VLA to detect two SNe (1984E and 1986E) that show evidence for circumstellar interaction seen in other wavebands, which is a good indicator that detectable radio emission may be present.

The results were both expected and surprising, since the search for radio emission resulted in non-detections. The absence of radio emission from SN 1984E is not too surprising. The evidence for circumstellar interaction was close to optical maximum and indicated that it was of limited duration compared to the much later radio observations presented here. However, the evidence for circumstellar interaction for SN 1986E (Cappellaro, Danziger, & Turatto 1995) was recent (1994) compared to the date of observation (1995). This result is important, since it is the first supernova with an optical recovery but no accompanying detectable radio emission. Clearly, more

detailed modeling of the optical and radio emission from circumstellar interaction is needed.

3.2 Observations and Data Reduction

Observations of SN 1984E were made at 20 cm (1.425 GHz) on 1995 July 8 at the Very Large Array (VLA) in the A configuration. The search was centered on the NASA/IPAC Extragalactic Database (NED)[1] position of the SN at R.A.(1950) = $10^h11^m35^s.3$, Decl.(1950)= $+03°43'07''.0$. SN 1986E was observed at 20 cm (1.425 GHz) on 1995 July 14 at the VLA in A array centered on the NED position for the SN at R.A.(1950)= $12^h19^m09^s$, Decl.(1950)= $+14°54'33''$, and at 6 cm (4.860 GHz) on 1995 December 4 in B array. About 6 - 6.5 hours were devoted to each source at each wavelength using a bandwidth of 50 MHz in each IF pair.

The data reduction was done using the Astronomical Image Processing System (AIPS) software provided by the National Radio Astronomy Observatory. Table 3.1 lists positions and flux densities for the primary (flux) calibrators and secondary (phase) calibrators used in the data reduction. The derived flux densities for the normally non-thermal phase calibrator 1252+119 imply a spectral index, α ($S \propto \nu^{+\alpha}$), between 20 and 6 cm, of about zero. This is somewhat inconsistent with others' observed spectral indices for this source of $\alpha = -0.24$ (Price et al. 1993) and $\alpha = -0.3$ (White & Becker 1992), but some phase calibrators have variable spectral indices.

[1]The NASA/IPAC Extragalactic Database (NED) is operated by the Jet Propulsion Laboratory, California Institute of Technology, under contract with the National Aeronautics and Space Administration.

	Position		Flux Density	
Source	α_{1950}	δ_{1950}	20 cm (Jy)	6 cm (Jy)
Primary Calibrators				
3C 286	not used	not used	14.64	7.53
3C 48	not used	not used	15.67	···
Secondary Calibrators				
1021−006[a]	$10^h21^m56^s.2$	$-00°37'41''.55$	1.00	···
1252+119[b]	$12^h52^m07^s.7$	$+11°57'20''.87$	0.754	0.748

[a] Flux derived using both primary calibrators.
[b] Flux derived using 3C 286 only.

Table 3.1: Calibrator positions and fluxes for observations of SNe 1984E and 1986E.

Reduction of the data followed standard procedures (FLAG-ing, CALIBration, and then mapping) including CLEAN deconvolution using the MX routine. The data for SN 1986E at 20 cm were affected severely by what is believed to be Radio Frequency Interference (RFI), common at this wavelength in the summer, and therefore show a relatively high rms noise. Rms noise levels were 0.0243 and 0.0562 mJy for SN 1984E and SN 1986E, respectively, at 20 cm, and 0.0126 mJy for SN 1986E at 6 cm.

Assuming a 3σ detection threshold, we found *no* sources within the uncertainties ($\leq 1''$) for the positions of the supernovae. Contour maps of the fields of view for SN 1984E at 20 cm and SN 1986E at 20 cm and 6 cm are shown in Figure 3.1, 3.2, and 3.3, respectively.

Table 3.2 lists upper limits or peak flux densities, and positions for the sources in the fields of view for each map. Since none of the sources, except NGC 3169, have associated IRAS sources to within $1'$ (in the NGC 3169 map) and $2'$ (all sources in the NGC 4302 map), these objects are probably not H II regions. In addition, the fluxes (1-2 mJy) and spectral indices ($+0.6 > \alpha > +0.4$) of sources β and γ are similar to those of background radio galaxies and/or quasars found in Donnelly et al. (1987). Sources β and γ may be such objects. Future observations are recommended to explore this possibility.

Hummel et al. (1991) report 6 cm observations of a source, whose position is $2''$ from source β, with a flux density of 1.8 ± 0.1 mJy. Although they tentatively report their source to be associated with SN 1986E, more accurate positional information on SN 1986E (Danziger 1995) excludes this possibility. From the positional coincidence and similarity of flux density observations, it is likely that source β is the Hummel et

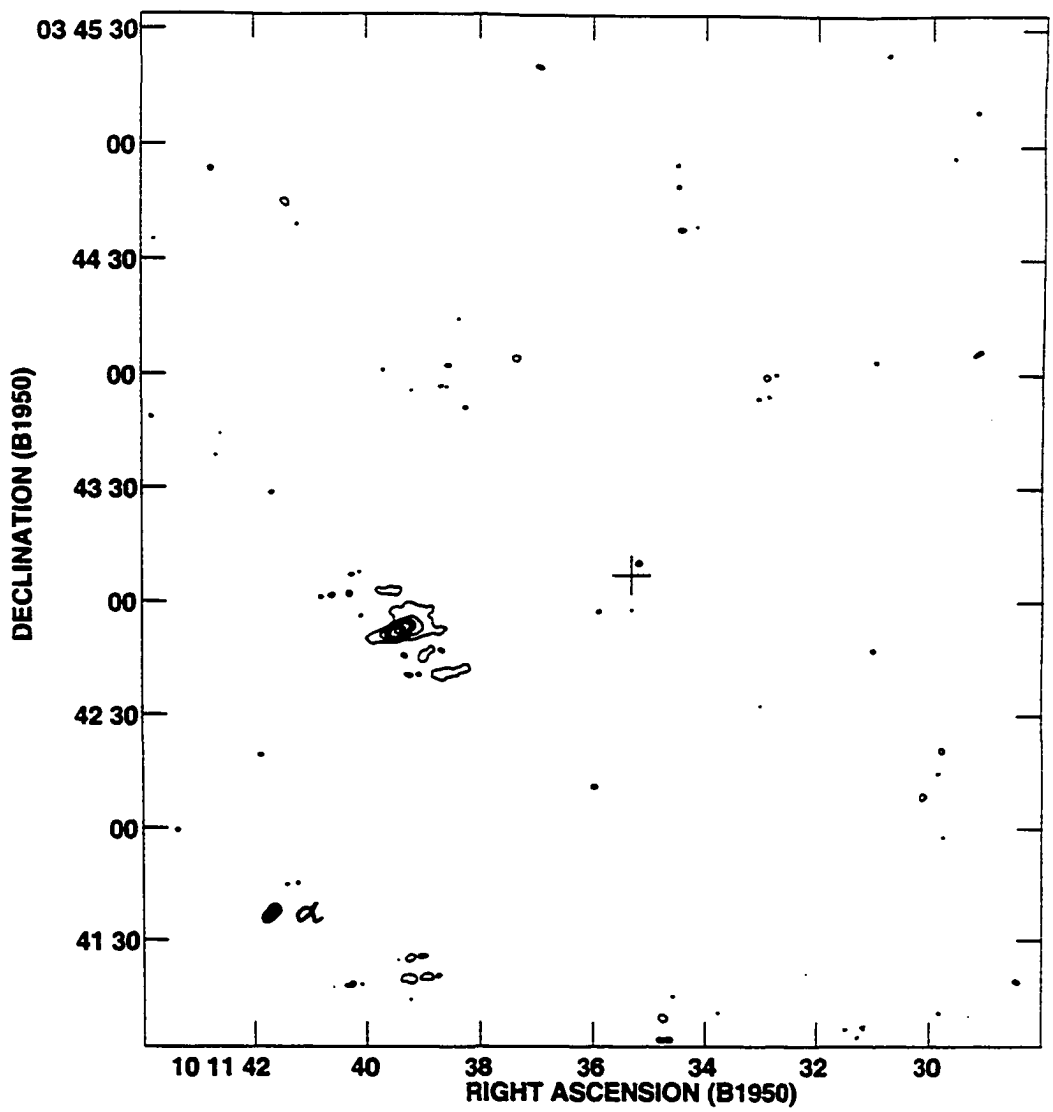

Figure 3.1: A (20 cm) contour map of the field of view of SN 1984E in NGC 3169, observed at the VLA in A array on July 8, 1995 with an rms noise of 0.0243 mJy. The contour levels shown are 0.02, 0.05, 0.10, 0.15, 0.20, 0.60, 0.99 of the peak intensity of 3.78 mJy/beam. The cross marks the optical position (NED) of SN 1984E and α marks the position of an unknown source. Source α has a position $> 2'$ from the SN position. The source located to the northwest of source α is associated with the central regions of NGC 3169.

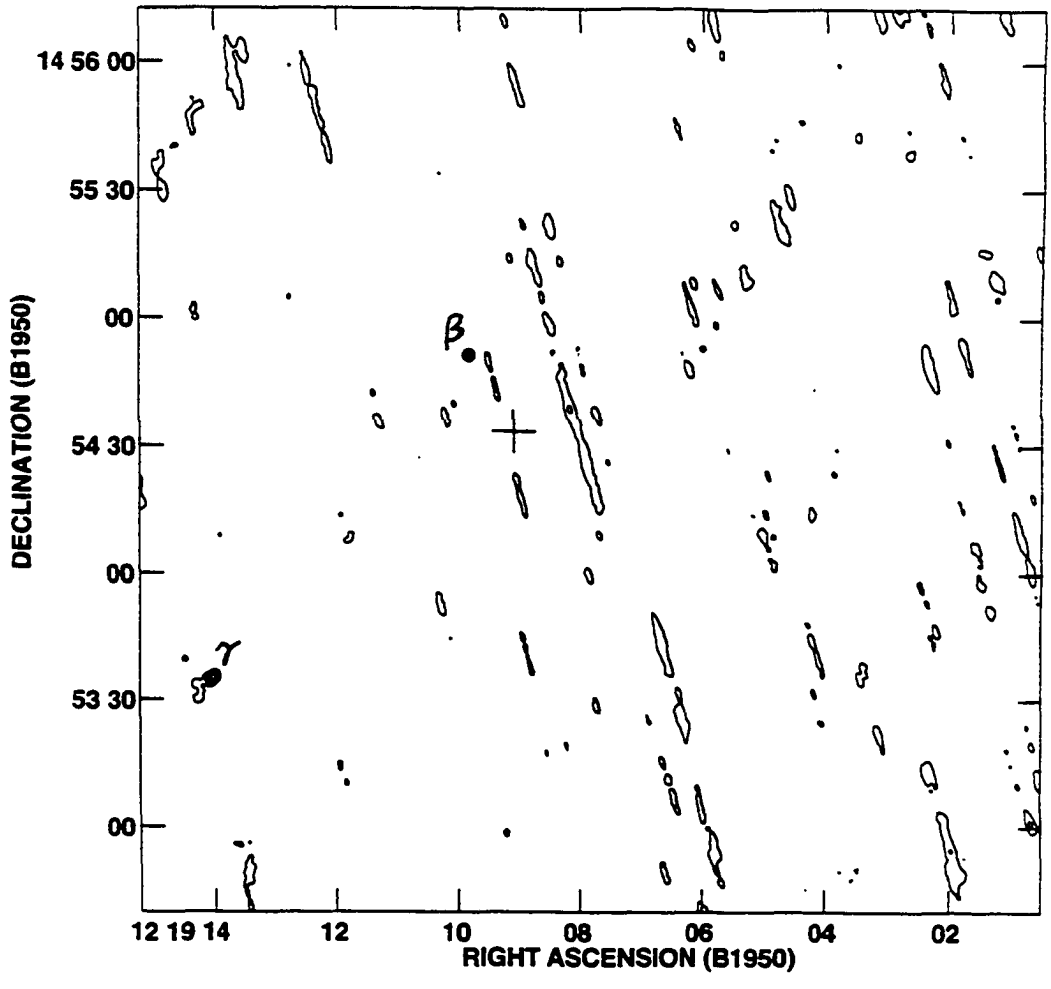

Figure 3.2: A (20 cm) contour map of the field of view of SN 1986E in NGC 4302, observed at the VLA in A array on July 14, 1995 with and rms noise of 0.056 mJy. The contour levels shown are 0.16, 0.32, 0.48, 0.70, 0.90, and 0.99 of the peak intensity of 1.03 mJy/beam. The cross marks the optical position (Danziger 1995) of SN 1986E and β and γ mark the positions of unknown sources. All of the unknown sources have positions $> 21''$ from the SN position.

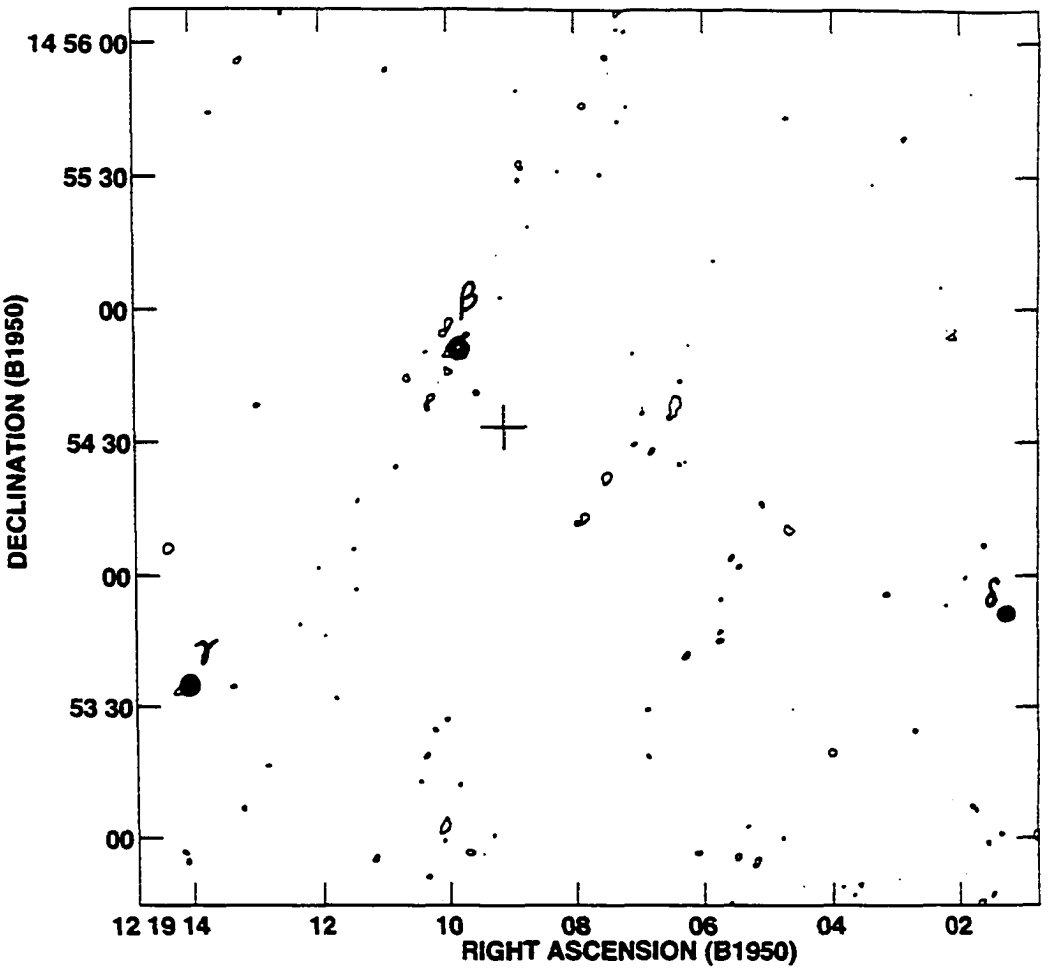

Figure 3.3: A (6 cm) contour map of the field of view of SN 1986E in NGC 4302, observed at the VLA in B array on December 4, 1995 with and rms noise of 0.0126 mJy. The contour levels shown are 0.02, 0.05, 0.10, 0.15, 0.20, 0.60, 0.99 of the peak intensity of 2.08 mJy/beam. The cross marks the optical position (Danziger 1995) of SN 1986E and β, γ, and δ mark the positions of unknown sources. All of the unknown sources have positions $> 21''$ from the SN position.

Wavelength Observed	Source	R.A.(1950)	Decl.(1950)	Peak Flux (mJy)
		Parent Galaxy NGC 3169		
20 cm	SN 1984E	$10^h11^m35^s.3$	$+03°43'07''.0$	$< 0.073^a$
	Center	$10^h11^m39^s.4$	$+03°42'52''.5$	3.8
	α	$10^h11^m41^s.7$	$+03°41'37''.5$	0.66
		Parent Galaxy NGC 4302		
20 cm	SN 1986E	$12^h19^m09^s.1$	$+14°54'33''.3$	$< 0.17^a$
	β	$12^h19^m09^s.8$	$+14°54'51''.3$	1.0
	γ	$12^h19^m14^s.0$	$+14°53'35''.3$	0.91
6 cm	SN 1986E	same position		$< 0.038^a$
	β	same position		2.0
	γ	same position		2.1
	δ	$12^h19^m01^s.3$	$+14°53'51''.2$	0.38

[a] Upper limits are based on 3 sigma noise levels.

Table 3.2: Observations of SNe 1984E and 1986E.

al. source.

3.3 Results and Discussion

In the standard model for supernova radio emission, the level of the emission depends, above all, on $\dot{M}_w/v_w$, the ratio of the mass-loss rate to the velocity of the pre-SN stellar wind, both of which are assumed to have been constant for an extended period of time prior to the explosion. The upper limits to the radio emission can be used, in the framework of the standard model, to constrain the values of $\dot{M}_w/v_w$ for SNe 1984E and 1986E. To simplify the procedure the radio light curves are calculated for SNe 1984E and 1986E for a range of values of $\dot{M}_w/v_w$, while holding all of the other parameters constant at the values that were used by Weiler et al. (1991) for the radio–bright Type II–L SN 1979C. For a more detailed discussion of this simple scaling procedure, see Boffi & Branch (1995), who calculated radio light curves for the Type Ia SN 1986G by scaling against the radio–bright Type Ib SN 1983N. Here it is assumed that NGC 4302, NGC 4321, and NGC 3169, the parent galaxies of SNe 1986E, 1979C, and 1984E, respectively, are at the same distance. NGC 4302 and NGC 4321 are in the Virgo cluster complex; NGC 3169 is not, but its distance probably is comparable (Tully 1988).

Calculated radio light curves for various values of $\dot{M}_w/v_w$ are shown in Figure 3.4 (6 cm) and Figure 3.5 (20 cm). These curves were calculated by assuming that the ejecta density profile is described by a n = 20 power law and that the radio spectral index is $\alpha = 0.72$ (Weiler et al. 1986). Also shown are the 3σ observational upper limits for SNe 1984E and 1986E and recently published upper limits for SN 1984E at

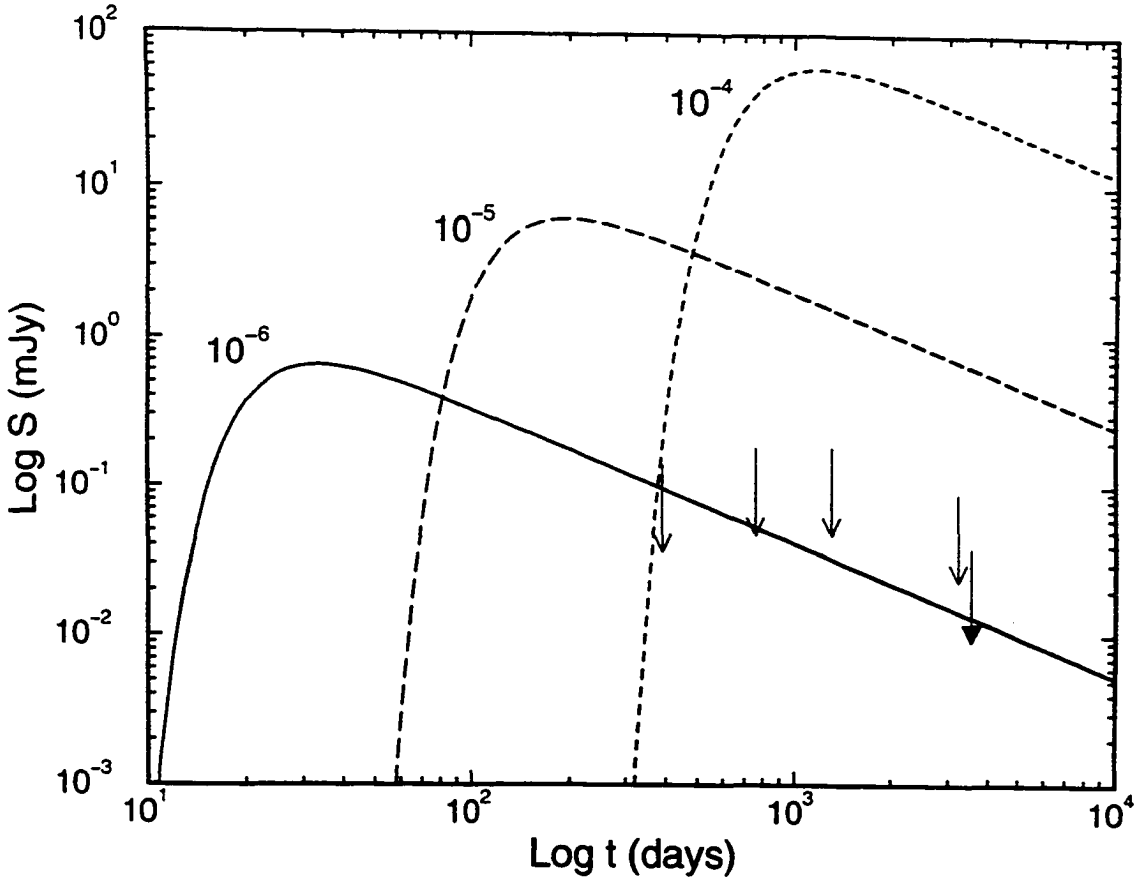

Figure 3.4: Light curves at 6 cm are plotted for three different values of the mass loss rate: 10^{-6} (solid line), 10^{-5} (long-dashed line) and 10^{-4} (short-dashed line) solar masses per year per kilometer per second, with n = 20 and $\alpha = 0.72$ (see text). The higher the mass loss rate the later the light curve turns on. The 3σ upper limit for SN 1986E (solid arrow-head) is at approximately 9 years after explosion, and the upper limits for SN 1984E (all other arrows) from Van Dyk et al. (1996) are at 1.0, 2.0, 3.6 and 8 years.

For SNe 1984E 1986E, Figure 3.4 implies $\dot{M}_w/v_w < 10^{-6}$ (solar masses per year per kilometer per second) and Figure 3.5 gives $\dot{M}_w/v_w < 10^{-6}$ (solar masses per year per kilometer per second). The figures make clear that at all epochs of observations, mass loss rates (per wind velocity) greater than 10^{-6} would have produced a detectable radio emission and are therefore excluded.

In principle, very *high* values of $\dot{M}_w/v_w$ also are allowed, because then the circumstellar shell would still be optically thick to free–free absorption and the radio light

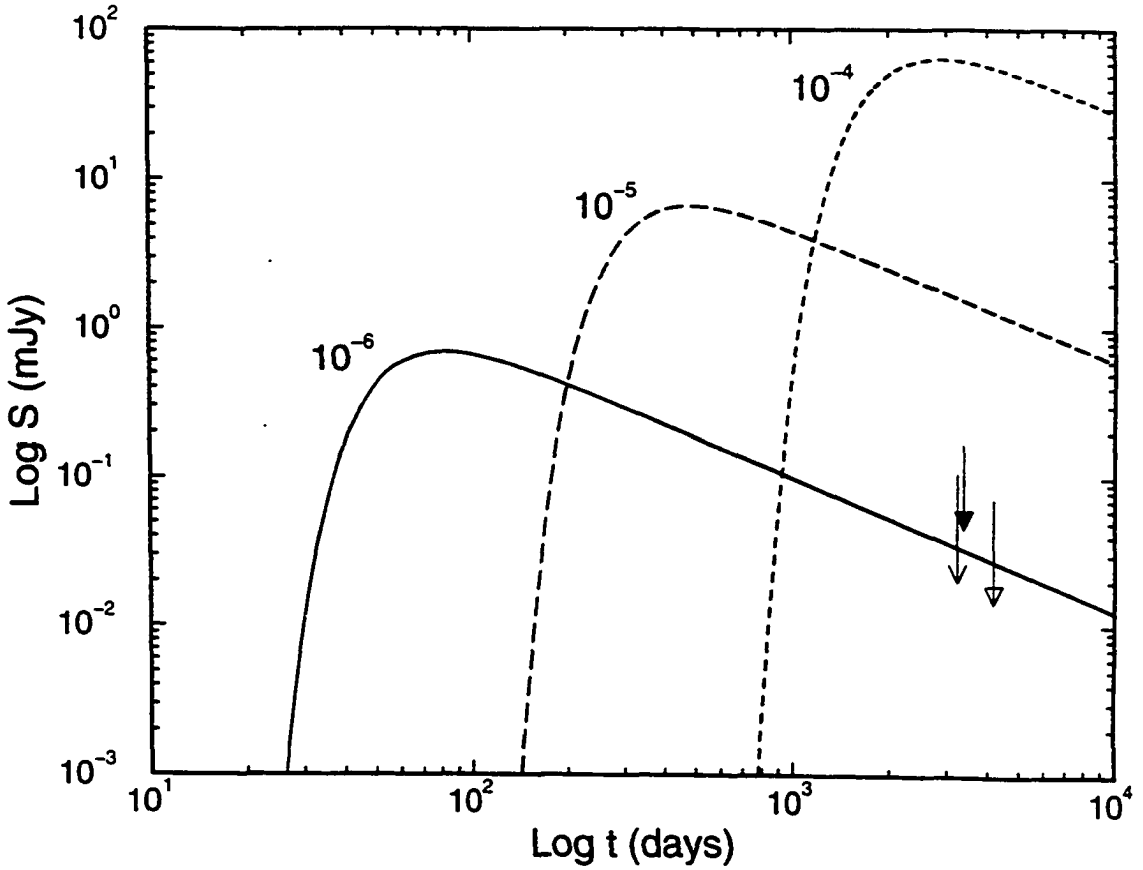

Figure 3.5: Light curves calculated as in Figure 3.4, but at 20 cm. The 3σ upper limits for SN 1984E (hollow arrow-head) and for SN 1986E (solid arrow-head) are at approximately 11 and 9 years after explosion, respectively, and an upper limit for SN 1984E (the other arrow) from Van Dyk et al. (1996) is at 8 years.

curve would not yet have turned on. SN 1979C (Weiler et al. 1991) turned on about a year after explosion, and SNe 1986J (Weiler et al. 1990) and 1988Z (Van Dyk et al. 1993b) took even longer. However, improbably high values of $\dot{M}_w/v_w$ and of total masses of the circumstellar shells would be required to keep SNe 1984E and 1986E optically thick for a decade after their explosions. At the suggestion of M. Dopita, the free-free optical depth of the Hα–emitting region (using the emission measure and assuming that Hα is emitted by recombination) has been worked out and found to be optically thick in the radio. Therefore, if the Hα–emitting region is not far inside the radio–emitting region, up to one half of the radio emission could be blocked. In keeping with the usual practice, this effect is ignored. For a discussion of other effects that are of comparable importance for SN radio light curves but that are not included in the standard model, see Lundqvist & Fransson (1988).

3.3.1 SN 1984E

Dopita et al. (1984) presented a spectrum of SN 1984E near maximum light that showed narrow ($<$ 3000 km/s) P Cygni profiles in the Balmer lines, superimposed on broader profiles that were formed in the high–velocity ($\sim$ 15,000 km/s) supernova ejecta. Dopita et al. concluded that the narrow profiles were formed in a circumstellar shell that had been created by a pre-SN "superwind" for which, on the basis of the fluxes in the narrow Balmer lines, they estimated $2 \times 10^{-6} < \dot{M}_w/v_w < 3 \times 10^{-5}$ (solar masses per year per kilometer per second). If the supernova ejecta that was interacting at that time had been expanding for two weeks at 15,000 km/s, and if prior to explosion the superwind had a velocity between 3000 km/s and a more typical value for a red supergiant of 10 km/s (the superwind subsequently being

radiatively accelerated by the supernova), then the dense circumstellar matter that was interacting at that time had been lost from the progenitor between 10 weeks and 60 years before the explosion. A spectrum of SN 1984E obtained a month after maximum light showed little or no emission from the circumstellar shell (Henry & Branch 1986). At this epoch the spectrum was probing the progenitor's wind between 0.6 and 200 years prior to explosion, so Henry & Branch (1986) concluded that the superwind must have been confined to within the last 200 years before explosion. Gaskell & Keel (1988) presented evidence for the appearance of strong Hα emission at the site of SN 1984E some time between 2.2 and 23 years before the explosion, which they interpreted in terms of an episodic ejection of mass from the pre–supernova rather than a continuous superwind.

The much later radio observations of SN 1984E probe the wind of the pre-SN epoch at much earlier epochs: the first radio observation of Van Dyk et al. (1996) probes the wind from 3 to 1000 years prior to explosion, and this radio observation probes the wind from 33 to 10^4 years prior to explosion. The radio upper limits indicate that no superwind was blowing at these earlier times. One of the explanations of the brief superwind of SN 1984E that was suggested by Henry & Branch (1986), involving a nuclear shell flash in the pre-SN progenitor (Woosley et al. 1980), has been invoked by Van Dyk et al. (1996) to account for the undetectably low levels of late radio emission from a number of Type II supernovae that showed evidence of circumstellar interaction in their earlier optical spectra.

3.3.2 SN 1986E

The inability to detect radio emission from SN 1986E is more surprising. According to Cappellaro et al. (1995), optical spectra of SN 1986E obtained in 1993 and 1994 were showing evidence of strong circumstellar interaction that implied a substantially higher value of $\dot{M}_w/v_w$ than in SN 1980K, for which Weiler et al. (1992a) estimated 2.6×10^{-6} (solar masses per year per kilometer per second) from the radio light curve. Therefore, at practically the same time that SN 1986E was undergoing strong circumstellar interaction, as revealed by its optical spectrum, it was undetectably dim in the radio. As noted by Fesen (1993), although circumstellar interaction can produce both optical and radio emission from old supernovae, the optical and radio do not come from exactly the same place and their emission mechanisms are not the same (cf. Chevalier & Fransson 1994). The non-detectability, in the radio, of SN 1986E, SN 1984E, and other SNe II that have not been seen in the radio (CRB Cowan, Romanishin, & Branch 1994b; Van Dyk et al. 1996; Eck et al. 1996) make it increasingly evident that strong radio emission from old SNe II is the exception, not the rule. More detailed modeling of circumstellar interaction in old supernovae is needed to understand the lack of strong radio emission even in an event such as SN 1986E whose optical spectra show evidence for contemporary circumstellar interaction.

Chapter 4

Radio Observations of SN 1986G

4.1 Introduction

This chapter presents an attempt to detect radio emission from the Type Ia SN 1986G in NGC 5128, using the VLA. As mentioned in Chapter 1, one proposal for detecting radio emission from SNe Ia is with the symbiotic–star scenario, where a white dwarf accretes mass from the wind of a companion red giant (Boffi & Branch 1995).

The observations were made at about 10 days after explosion (one week before optical maximum) and at smaller wavelengths (2 and 6 cm) to maximize the chances for detection. (Recall that the radio emission peaks at smaller wavelengths first due to the nature of the free-free absorption.) These observations are important since they enable earlier and lower limits on SN Ia radio emission than previously available.

4.2 Observations and Data Reduction

Observations were carried out using the VLA in A-configuration at 6 and 2 cm on May 5, 1986, seven days before the estimated optical maximum of SN 1986G. About 20 min were devoted to each of the two wavelengths. The search centered on RA(1950) = $13^h22^m40^s.5$, Dec(1950) = $-42°46'16''$ and used a bandwidth of 50 MHz in each of the two IF pairs. All data reduction was done using the Astronomical Image Processing System (AIPS) software of the National Radio Astronomy Observatory. The calibration of the complex gains, as well as the absolute flux density, was carried out using the radio galaxy 3C 286. In the imaging process, the visibility data were uniformly weighted in order to suppress gain errors on the short baselines. The final beam size was $0''.63 \times 0''.31$, PA = $-19°.4$ and $0''.67 \times 0''.10$, PA = $-16°.8$ for the 6 and 2 cm observations, respectively. Note that the beam size of the 2 cm data was not the full resolution of the A-configuration because of flagging of the long N-S baselines.

In an iterative procedure of imaging, CLEAN deconvolution, and self-calibration, short time scale variations of errors in the complex gains due to atmospheric effects were removed. The iterative self-calibration was carried out using the bright, unresolved core of Centaurus A (2'.4 from the position of SN1986G) independently for the two wavelengths. The poor u-v coverage due to the short length of observation was the dominant factor limiting the fidelity of the final images. The rms noise of the 6 cm image was also affected by a large fraction of corrupted data which required significant editing, further increasing the rms noise. The final images were made with the AIPS task MX and the rms noises were 0.23 and 0.32 mJy at 2 and 6 cm, respectively. The supernova 1986G was *not* detected in these observations with a 3-σ limit

of 0.7 and 1.0 mJy at 2 and 6 cm, respectively. The 6 and 2 cm contour images of the fields of view are illustrated in Figures 4.1 and 4.2, with the optical position (Cragg 1986) of SN 1986G indicated by a cross.

4.3 Discussion

Figure 4.3 shows the flux densities calculated for SN 1986G in the symbiotic-star scenario, at 10 days after explosion which corresponds approximately to one week before optical maximum, as a function of the red giant's wind mass-loss rate, $\dot{M}_w$. The calculations are as in Boffi & Branch (1995), but here the results for 2 and 20 cm, as well as 6 cm, are shown. The calculated behavior of the radio emission can be understood in terms of (1) the non-thermal spectra index of the synchrotron radiation ($S \propto \lambda^{\alpha}$, with α=1 here) emitted by the interaction region, and (2) the wavelength dependence of the free-free absorption ($\tau_{ff} \propto \lambda^{2.1}$) in the ionized gas of the circumstellar medium. At early times the free-free absorption in the circumstellar medium external to the interaction region suppresses the radio emission, especially at longer wavelengths. At later times, after the interaction region has worked its way farther out into the circumstellar medium, the free-free optical depth falls below unity and the circumstellar absorption becomes negligible. Thus, an event with a relatively low $\dot{M}_w$ of 10^{-8} $M_\odot$ yr^{-1} (and therefore a low-density circumstellar medium) is predicted to be radio quiet 10 days after explosion because the emission peaked earlier and already has faded; an event with a relatively high $\dot{M}_w$ of 10^{-5} $M_\odot$ yr^{-1} is predicted to be radio quiet at 10 days because the circumstellar medium is still optically thick to free-free absorption and the light curve has not yet turned on. For

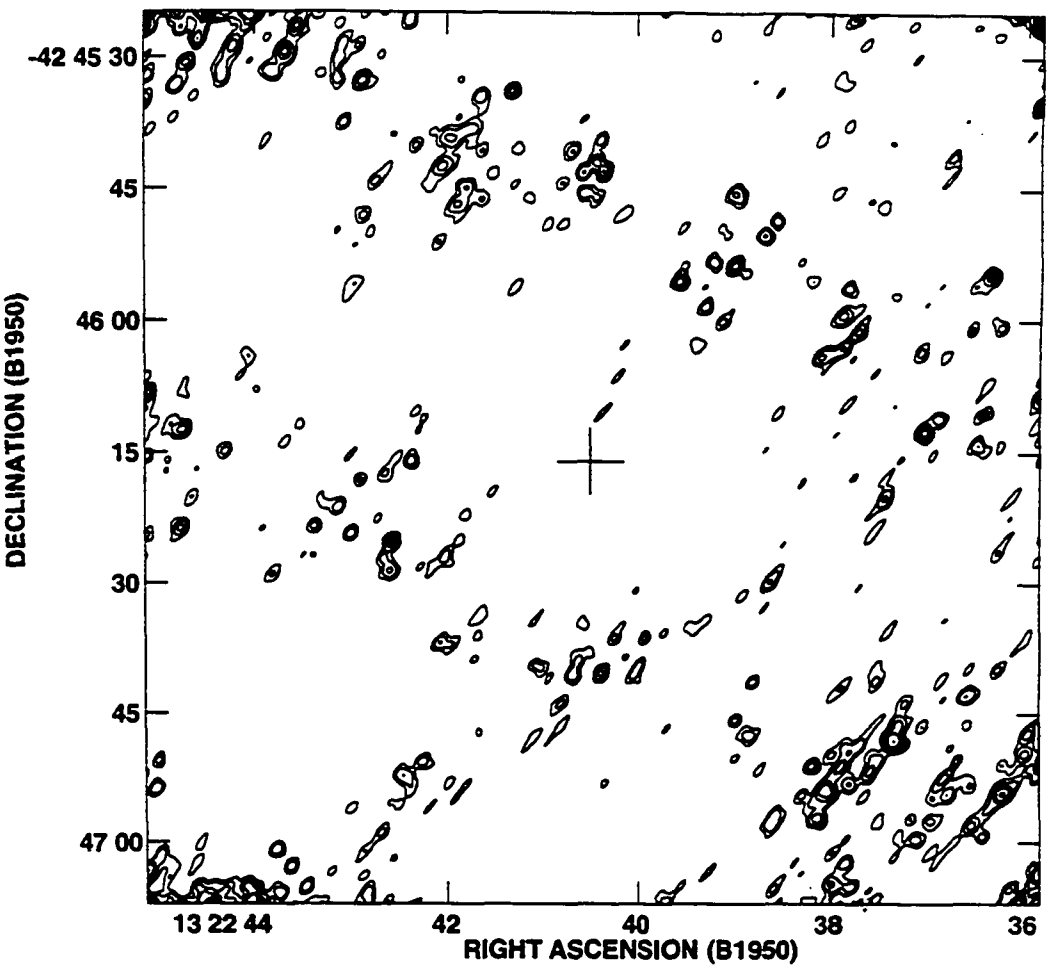

Figure 4.1: A 6 cm contour map of the field of view near SN 1986G in Centaurus A, observed with the VLA in A configuration on May 5, 1986 with a resolution ($\alpha \times \delta$) of $0\overset{s}{.}63 \times 0\overset{s}{.}31$ and an rms noise of 0.32 mJy. The contour levels shown are 0.05, 0.1, 0.20, 0.30, 0.5, 0.7 and 0.9 of the peak intensity of 22.1 mJy beam^{-1}. The cross marks the optical position (Cragg 1986) of SN 1986G.

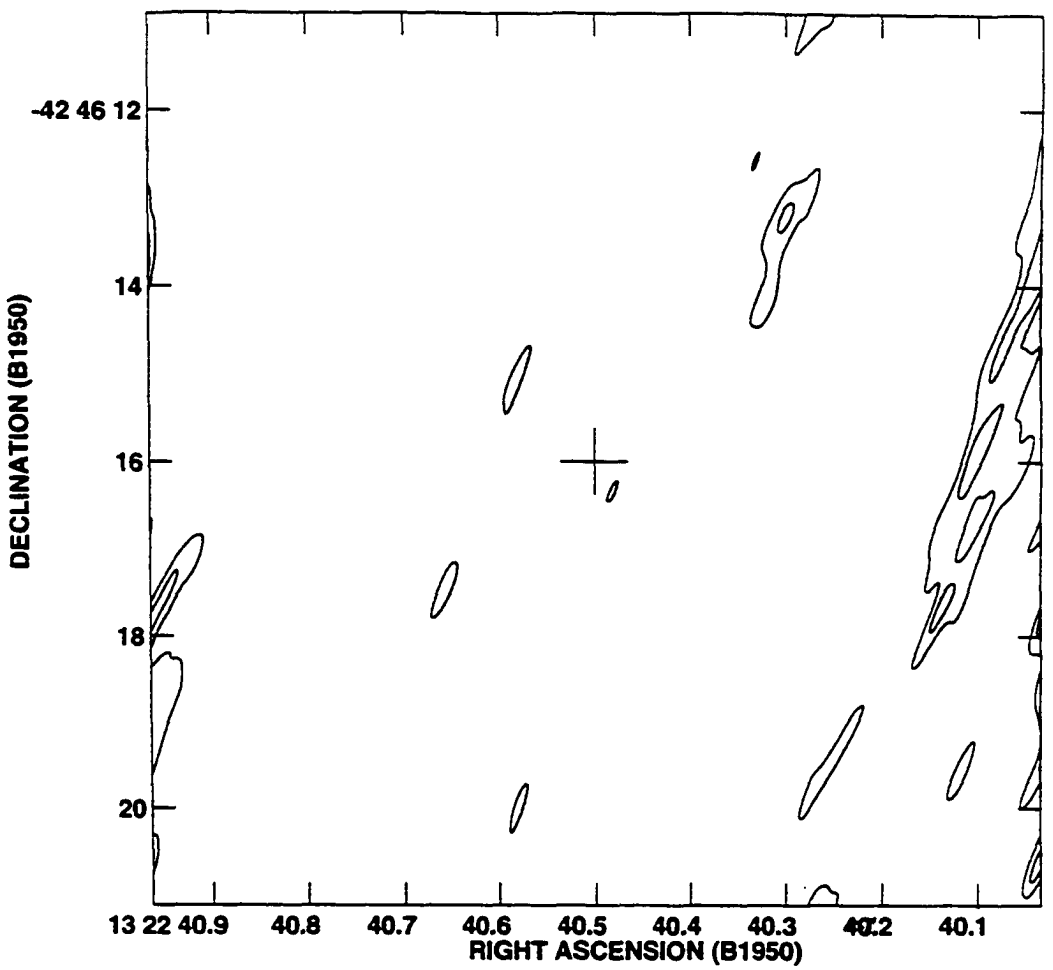

Figure 4.2: A 2 cm contour map of the field of view near SN 1986G in Centaurus A, observed with the VLA A configuration on May 5, 1986 with a resolution ($\alpha \times \delta$) of $0''.84 \times 0''.14$ and an rms noise of 0.23 mJy. The contour levels shown are 0.44, 0.66, 0.88, and 0.99 of the peak intensity of 1.6 mJy beam^{-1}. The cross marks the optical position (Cragg 1986) of SN 1986G.

intermediate values of $\dot{M}_w$, 10^{-6} to 10^{-5} $M_\odot$ yr^{-1}, the radio light curve is near its peak at 10 days. (For further discussion, and details of the calculations made in this chapter, see Boffi & Branch 1995.)

The observational upper limits at 2 and 6 cm also are plotted in Figure 4.3. Taking the figure at face value, the upper limits are in conflict with the range $6 \times 10^{-8} < \dot{M}_w < 7 \times 10^{-6}$ $M_\odot$ yr^{-1}. However, considering that the calculations presented here have been carried out for just one particular set of parameters (those adopted by Weiler et al. [1986] for SN 1983N, including spectral index α=1 and supernova density power-law index n=7), the upper limits more realistically should be regarded to be in clear conflict only with the narrower range $10^{-7} \lesssim \dot{M}_w \lesssim 3 \times 10^{-6}$ $M_\odot$ yr^{-1}. This happens to be the most interesting range in the symbiotic-star progenitor scenario.

It is generally agreed that if a hydrogen-accreting white dwarf is to approach the Chandrasekhar limit, it must avoid both strong mass-ejecting nuclear outbursts of its accumulated hydrogen and helium layers and heavy mass-loss due to expansion of its accreted layers, and therefore its accretion rate should be on the order of 10^{-7} $M_\odot$ yr^{-1} (Wheeler & Harkness 1990, Nomoto & Kondo 1991, Livio 1995). In the symbiotic-star scenario, the efficiency of accretion from the wind of the detached companion would be on the order of 10^{-1} (Yungelson et al. 1995). Therefore, the wind mass-loss rate of the red giant should be on the order of 10^{-6} $M_\odot$ yr^{-1}. In fact, the mass-loss rates from red giants in symbiotic systems are observed to be in the range 10^{-7} to 10^{-5} $M_\odot$ yr^{-1}, somewhat higher than from single red giants (Seaquist & Taylor 1990, Mürset et al. 1991), perhaps owing to stimulated mass loss from the red giant by the hot white dwarf accretion (Munari & Renzini 1992). Although it would be preferable to have radio observations at more than a single epoch, the

strong conflict between the radio upper limits for SN 1986G and the predictions of the symbiotic-star scenario for wind mass-loss rates around 10^{-6} $M_{\odot}$ yr^{-1} indicates that the progenitor of SN 1986G probably was not a symbiotic system.

It would be premature, however, to conclude that no SNe Ia come from symbiotics. SN 1986G was a peculiar SN Ia, both photometrically (Phillips et al. 1987, Phillips 1993) and spectroscopically (Phillips et al. 1987, Branch & van den Bergh 1993, Branch, Fisher, & Nugent 1993). Among the other published upper limits for radio emission from SNe Ia, only a single observation of the normal SN Ia 1981B near its optical maximum (Sramek & Weiler 1990) can be regarded to be in mild conflict with the symbiotic-star scenario (Boffi & Branch 1995). Therefore, further searches for radio emission from SNe Ia, beginning as soon as possible after their discovery, are needed to more thoroughly test the symbiotic-star progenitor scenario.

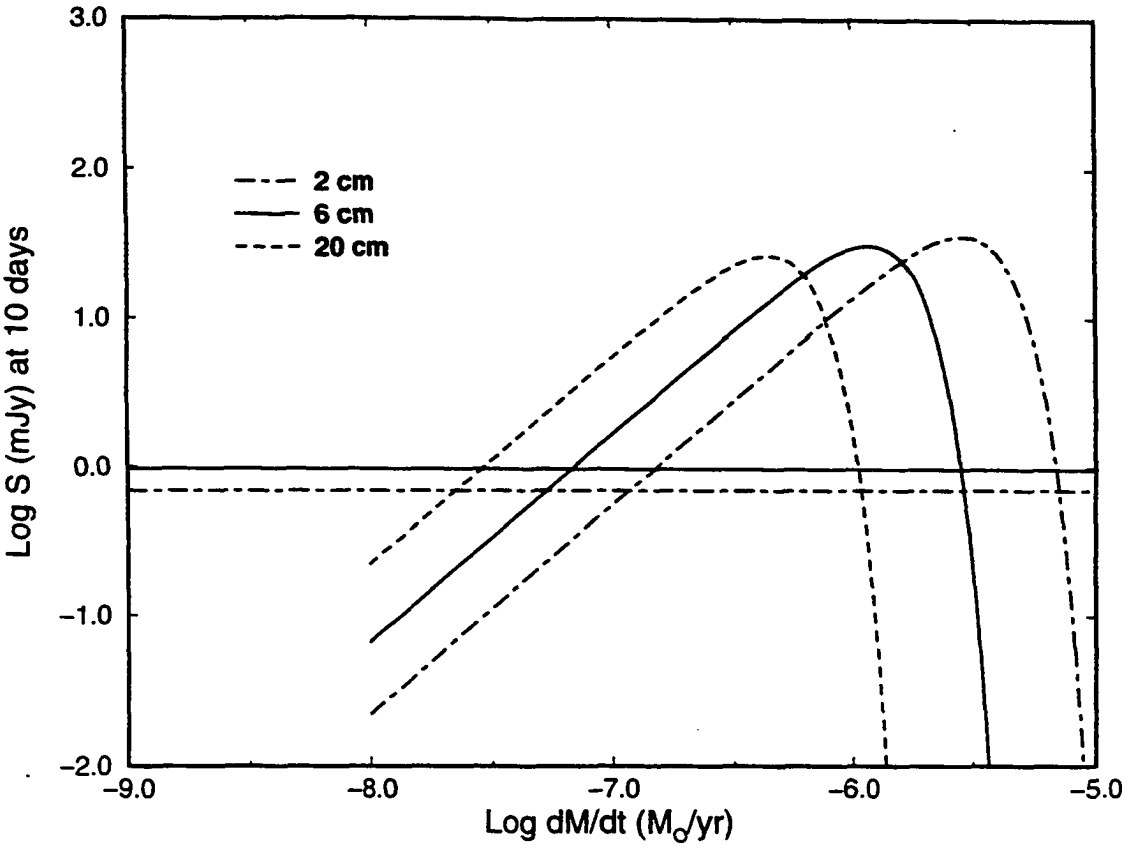

Figure 4.3: Comparison of radio observations and predicted flux densities for symbiotic-star progenitors of Type Ia supernovae. The theoretical curves, as a function of circumstellar mass-loss rates in the progenitors, are for radio emission at 2, 6 and 20 cm. The solid (or dashed) horizontal line represents the 3σ observational upper limit for radio emission at 6 (or 2) cm.

Chapter 5

Observations of Radio SNe up to 90 Yrs Old

5.1 Introduction

This chapter presents VLA radio observations of 29 SNe with ages ranging from 10 days to about 90 years past explosion. Included are detections of known radio SNe 1950B, 1957D, 1970G, 1983N, the suspected radio SN 1923A, and the possible radio SN 1961V. None of the remaining 23 observations resulted in detections implying that most SNe are not detectable radio emitters. To investigate this, Chevalier's "standard model" has been used to derive (upper limits to) the mass-loss rates for the supernova progenitors and various assumptions affecting the calculation are discussed. Provided the model is correct, the upper limits to fluxes are consistent with a lack of circumstellar material needed for detectable radio emission.

Finally, plots of the luminosity upper limits versus age past explosion are presented

for comparison with the data and light curves of the well-studied SNe 1979C, 1980K and 1983N.

5.2 Observations

This program was begun in an attempt to detect radio emission from intermediate-age SNe. If detected, a monitoring program could begin at the VLA to trace its evolution from the radio supernova (RSN) stage to a supernova remnant (SNR). Since there is very little data on the transition of RSNe to SNRs, this would help in understanding this phase of SN evolution.

All of these observations were taken at the VLA over a time span ranging from 1981 to 1995. The SNe observed vary in distance and in ages at the time of observation, and Tables 5.1, 5.2, and 5.3 summarize relevant observational data for the SNe reported here. Table 5.1 gives parameters for each observation, and Table 5.2 shows distances assumed for each SN, most based on Cepheid observations in the parent galaxy or in a galaxy in the same group. Table 5.3 summarizes data on each SN, its parent galaxy, the age at the time of observation and the flux densities for either detections or 3σ upper limits.

In addition to analyzing the region near the SNe sites, we (Eck, Cowan, & Branch 1998) analyzed the non-SNe sources to determine a probable identity based on superpositions with maps made at optical (Hα) wavelengths or on spectral indices, for example. Table B.1 lists the positions and fluxes for these non-SNe sources and a possible identity for each. See Appendix B for descriptions of the analyses of each map.

SN Name	Frequency (GHz)	Date	VLA Config	Duration (hr)
SN 1885A	8.440	08 Jun 1990	A	19.4
SN 1895B	1.452	29 Apr 1981	BnA	3
	1.452	16 Dec 1984	A	9.1
SN 1909A	4.835	22 Nov 1988	A	9.4
SN 1921B	1.452	17 Dec 1983	BnA	3.4
SN 1921C	1.452	17 Dec 1983	BnA	3.4
SN 1923A	1.446	15 Dec 1983	BnA	4.5
	4.873	13 Mar 1984	CnB	4.6
	4.848	14 Oct 1990	CnB	5.9
	1.515	04 Jan 1992	B	6.3
SN 1937C	1.465	02 May 1986	A	7.8
SN 1937F	1.452	17 Dec 1983	BnA	3.4
SN 1945B	1.446	15 Dec 1983	BnA	4.5
	4.873	13 Mar 1984	CnB	4.6
	4.848	14 Oct 1990	CnB	5.9
	1.515	04 Jan 1992	B	6.3
SN 1950B	1.446	15 Dec 1983	BnA	4.5
	4.873	13 Mar 1984	CnB	4.6
	4.848	14 Oct 1990	CnB	5.9
	1.515	04 Jan 1992	B	6.3
SN 1951H	1.425	05 Dec 1992	A	9.1
SN 1954A	1.465	03 May 1986	A	9.7
SN 1954J	1.515	19 Aug 1985	C	7.6
SN 1957D	1.446	15 Dec 1983	BnA	4.5
	4.873	13 Mar 1984	CnB	4.6
	4.848	14 Oct 1990	CnB	5.9
	1.515	04 Jan 1992	B	6.3
SN 1959D	1.465	19 Aug 1985	C	7.7
	1.465	18 Apr 1986	A	9.3
	4.885	11 Aug 1986	B	9.2

Table 5.1: Observational parameters for the SNe in this survey.

SN Name	Frequency (GHz)	Date	VLA Config	Duration (hr)
SN 1961V	1.452	16 Nov 1984	A	9.1
	4.885	14 Aug 1986	B	9.3
SN 1966B	1.465	01 Aug 1987	A	4.3
SN 1968L	1.446	15 Dec 1983	BnA	4.5
	4.873	13 Mar 1984	CnB	4.6
	4.848	14 Oct 1990	CnB	5.9
	1.515	04 Jan 1992	B	6.3
SN 1969L	1.452	16 Nov 1984	A	9.1
	4.885	14 Aug 1986	B	9.3
SN 1970G	1.490	01 May 1990	A	9.1
	8.415	15 Nov 1990	C	6.5
SN 1972E	1.452	29 Apr 1981	BnA	3
	1.452	16 Dec 1984	A	9.1
SN 1973R	1.465	01 Aug 1987	A	3.9
SN 1980D	1.465	03 Aug 1987	A	4.5
SN 1983K	4.835	03 Aug 1987	A	4.2
SN 1983N	1.446	15 Dec 1983	BnA	4.5
	4.873	13 Mar 1984	CnB	4.6
	4.848	14 Oct 1990	CnB	5.9
	1.515	04 Jan 1992	B	6.3
SN 1984E	1.425	08 Jul 1995	A	6.4
SN 1986E	1.425	14 Jul 1995	A	6.3
	4.860	04 Dec 1995	B	5.9
SN 1986G	4.860	05 May 1986	A	0.3
	14.94	05 May 1986	A	0.3
SN 1989B	4.885	02 Feb 1989	A	2.5
	8.415	02 Feb 1989	A	2.3

Table 5.1:—Continued

SN Name	SN Type	Parent Galaxy	Distance (Mpc)	References
SN 1885A	I pec	NGC 0224	0.76	Madore & Freedman (1991)
SN 1895B	Ia	NGC 5253	4.1	Saha et al. (1995)
SN 1909A	II(-P)	NGC 5457	7.4	Kelson et al. (1996)
SN 1921B	II	NGC 3184	8.7	Tully (1988)
SN 1921C	I	NGC 3184	8.7	Tully (1988)
SN 1923A	II-P	NGC 5236	4.1	Saha et al. (1995)
SN 1937C	Ia	IC 4182	4.7	Saha et al. (1994)
SN 1937F	II(-P)	NGC 3184	8.7	Tully (1988)
SN 1945B	?	NGC 5236	4.1	Saha et al. (1995)
SN 1950B	?	NGC 5236	4.1	Saha et al. (1995)
SN 1951H	II	NGC 5457	7.4	Kelson et al. (1996)
SN 1954A	Ib	NGC 4214	4.7	Saha et al. (1994)
SN 1954J	V	NGC 2403	3.6	Sandage & Tammann (1974)
SN 1957D	?	NGC 5236	4.1	Saha et al. (1995)
SN 1959D	II-L	NGC 7331	15.1	Hughes et al. (1998)
SN 1961V	II pec (V)	NGC 1058	9.3	Silbermann et al. (1996)
SN 1966B	II-L	NGC 4688	17.1	Tully (1988)
SN 1968L	II-P	NGC 5236	4.1	Saha et al. (1995)
SN 1969L	II-P	NGC 1058	9.3	Silbermann et al. (1996)
SN 1970G	II-L	NGC 5457	7.4	Kelson et al. (1996)
SN 1972E	I	NGC 5253	4.1	Saha et al. (1995)
SN 1973R	II-P	NGC 3627	11.4	Saha et al. (1997)
SN 1980D	II-P	NGC 3733	22.1	Tully (1988)
SN 1983K	II-P	NGC 4699	25.7	Tully (1988)
SN 1983N	Ib	NGC 5236	4.1	Saha et al. (1995)
SN 1984E	II-L	NGC 3169	19.7	Tully (1988)
SN 1986E	II-L	NGC 4302	16.8	Tully (1988)
SN 1986G	Ia	NGC 5128	4.1	Saha et al. (1995)
SN 1989B	Ia	NGC 3627	11.4	Saha et al. (1997)

Table 5.2: Distances assumed for the SNe in this survey based on Cepheid observations in the parent galaxy or in the same group of galaxies as the parent galaxy.

SN Name	SN position[a] α_{1950} δ_{1950}	SN Type	Parent Galaxy	α^a_{1950} δ_{1950}	Galaxy Type[a]	Age (yr)[b]	Flux Density (mJy)[c] 20 cm	6 cm	Other λ	Notes
SN 1885A	$00^h39^m58^s.6$ $+40°59'38''$	I pec	NGC 0224 (M31)	$00^h40^m00^s.1$ $+40°59'42''.8$	SA(s)b	105	...	...	< 0.015	1, 2
SN 1895B	$13^h37^m06^s.6$ $-31°23'01''$	Ia	NGC 5253	$13^h37^m05^s.1$ $-31°23'13''.2$	Im pec	85.8 89.5	< 0.9 < 0.15	... ...	... ...	3, 4
SN 1909A	$14^h00^m17^s.2$ $+54°42'22''$	II(-P)	NGC 5457 (M101)	$14^h01^m26^s.3$ $+54°35'17''.9$	SAB(rs)cd	79.7	...	< 0.034	...	3
SN 1921B	$10^h15^m19^s.6$ $+41°37'20''$	II	NGC 3184	$10^h15^m17^s.2$ $+41°40'29''.0$	SAB(rs)cd	62.7	< 0.51	...	...	3, 4
SN 1921C	$10^h15^m23^s.7$ $+41°36'04''$	I	NGC 3184	$10^h15^m17^s.2$ $+41°40'29''.0$	SAB(rs)cd	62.0	< 0.51	...	...	4, 5
SN 1923A	$13^h34^m20^s.0$ $-29°35'48''.0$	II-P	NGC 5236 (M83)	$13^h34^m11^s.6$ $-29°36'42''.2$	SAB(s)c	60.6 60.8 67.4 68.6	< 0.57 ... ... 0.30	... 0.19 0.093 ...	... ...	
SN 1937C	$13^h03^m33^s.1$ $+37°53'10''$	Ia	IC 4182	$13^h03^m30^s.2$ $+37°52'20''.0$	SA(s)m	48.7	< 0.10	...	...	
SN 1937F	$10^h15^m17^s.2$ $+41°37'31''$	II(-P)	NGC 3184	$10^h15^m17^s.2$ $+41°40'29''.0$	SAB(rs)cd	46.0	< 0.51	...	...	4
SN 1945B	$13^h34^m02^s.8$ $-29°39'43''$	?	NGC 5236 (M83)	$13^h34^m11^s.6$ $-29°36'42''.2$	SAB(s)c	38.4 38.7 45.2 46.5	< 0.57 ... ... < 0.15	... < 0.16 < 0.084 ...	... ...	

Table 5.3: Summary of data on intermediate-age SNe and younger SNe in this survey.

SN Name	SN position[a] α_{1950} δ_{1950}	SN Type	Parent Galaxy	α^{a}_{1950} δ_{1950}	Galaxy Type[a]	Age (yr)[b]	Flux Density (mJy)[c] 20 cm	6 cm	Other λ	Notes
SN 1950B	$13^h34^m03^s.7$	?	NGC 5236	$13^h34^m11^s.6$	SAB(s)c	33.8	0.7	...	...	
	$-29°36'39''.0$		(M83)	$-29°36'42''.2$		34.0	...	0.36	...	
						40.6	...	0.37	...	
						41.8	0.72	...	...	
SN 1951H	$14^h02^m07^s.2$	II	NGC 5457	$14^h01^m26^s.3$	SAB(rs)cd	42.1	< 0.044	...	...	3
	$+54°36'21''$		(M101)	$+54°35'17''.9$						
SN 1954A	$12^h13^m15^s.2$	Ib	NGC 4214	$12^h13^m08^s.0$	IAB(s)m	32.0	< 0.068	...	...	
	$+36°32'54''$			$+36°36'22''.0$						
SN 1954J	$07^h32^m08^s.6$	V	NGC 2403	$07^h32^m05^s.5$	SAB(s)cd	30.8	< 0.35	...	...	3, 6
	$+65°44'22''$			$+65°42'40''.0$						
SN 1957D	$13^h34^m14^s.4$	?	NGC 5236	$13^h34^m11^s.6$	SAB(s)c	26.0	2.7	...	...	
	$-29°34'24''.3$		(M83)	$-29°36'42''.2$		26.2	...	2.1	...	
						32.8	...	1.4	...	
						34.0	1.2	...	...	
SN 1959D	$22^h34^m44^s.4$	II-L	NGC 7331	$22^h34^m46^s.7$	SA(s)b	26.1	< 0.058	...	...	3
	$+34°09'33''.1$			$+34°09'20''.9$		26.8	< 0.079	...	...	
						27.1	...	< 0.042	...	

Table 5.3:—Continued

SN Name	SN position[a] α_{1950} δ_{1950}	SN Type	Parent Galaxy	α^a_{1950} δ_{1950}	Galaxy Type[a]	Age (yr)[b]	Flux Density (mJy)[c] 20 cm	6 cm	Other λ	Notes
SN 1961V	$02^h40^m29^s.7$ $+37°08'01''.8$	II pec (V)	NGC 1058	$02^h40^m23^s.2$ $+37°07'45''.0$	SA(rs)c	22.9	0.27			3, 7
						24.7	...	0.13	...	
SN 1966B	$12^h45^m12^s.1$ $+04°35'58''$	II-L	NGC 4688	$12^h45^m14^s.0$ $+04°36'27''.0$	SB(s)cd	21.5	< 0.16	...	...	
SN 1968L	$13^h34^m11^s.3$ $-29°36'42''.6$	II-P	NGC 5236 (M83)	$13^h34^m11^s.6$ $-29°36'42''.2$	SAB(s)c	15.4	< 0.57	...	...	
						15.7	...	< 0.16	...	
						22.3	...	< 0.084	...	
						23.5	< 0.15	...	...	
SN 1969L	$02^h40^m38^s.6$ $+37°05'58''$	II-P	NGC 1058	$02^h40^m23^s.2$ $+37°07'45''.0$	SA(rs)c	14.9	< 0.09	...	...	3, 10
						16.7	...	< 0.042		
SN 1970G	$14^h01^m14^s.4$ $+54°28'55''.8$	II-L	NGC 5457 (M101)	$14^h01^m26^s.3$ $+54°35'17''.9$	SAB(rs)cd	19.8	0.21	...	...	3
						20.3	...	...	0.076	2
SN 1972E	$13^h37^m02^s.4$ $-31°25'04''$	Ia	NGC 5253	$13^h37^m05^s.1$ $-31°23'13''.2$	Im pec	9.0	< 0.9	...	...	3, 4
						13.6	< 0.15	...	...	
SN 1973R	$11^h17^m35^s.0$ $+13°16'13''$	II-P	NGC 3627 (M66)	$11^h17^m38^s.5$ $+13°15'55''.6$	SAB(s)b	13.6	< 0.28	...	...	3
SN 1980D	$11^h32^m13^s.4$ $+55°09'30''.0$	II-P	NGC 3733	$11^h32^m17^s.1$ $+55°07'43''.0$	SAB(s)cd	7.4	< 0.094	...	...	

Table 5.3:—Continued

Table 5.3:—Continued

SN Name	SN position[a] α_{1950} δ_{1950}	SN Type	Parent Galaxy	α^a_{1950} δ_{1950}	Galaxy Type[a]	Age (yr)[b]	Flux Density (mJy)[c] 20 cm	6 cm	Other λ	Notes
SN 1983K	$12^h46^m36^s.4$ $-08°21'21''.0$	IIB-P	NGC 4699	$12^h46^m26^s.5$ $-08°23'34''$	SAB(rs)b	4.1	...	< 0.052	...	8
SN 1983N	$13^h34^m02^s.0$ $-29°38'45''.2$	Ib	NGC 5236 (M83)	$13^h34^m11^s.6$ $-29°34'42''.4$	SAB(s)c	0.47	4.4	...	...	
						0.70	...	0.52	...	
						7.3	...	< 0.084	...	
						8.5	< 0.15	...	...	
SN 1984E	$10^h11^m35^s.4$ $+03°43'07''.7$	II-L	NGC 3169	$10^h11^m39^s.4$ $+03°42'52''.0$	SA(s)a pec	11.3	< 0.073	...	...	
SN 1986E	$12^h19^m09^s.0$ $+14°54'33''.0$	II-L	NGC 4302	$12^h19^m10^s.1$ $+14°52'30''.3$	Sc	9.3	< 0.17	...	...	
							...	< 0.038	...	
SN 1986G	$13^h22^m40^s.4$ $-42°46'18''.0$	Ia	NGC 5128	$13^h22^m31^s.6$ $-42°45'32''.9$	S0 pec	-0.02	...	< 0.96	...	
							...	...	< 0.69	9
SN 1989B	$11^h17^m37^s.4$ $+13°16'45''.0$	Ia	NGC 3627 (M66)	$11^h17^m38^s.5$ $+13°15'55''.6$	SAB(s)b	-0.008	...	< 0.11	...	
							...	...	< 0.089	2

a. Supernovae and galaxy positions and types taken from NED. Positions have been rounded to the nearest $0^s.1$ and $0''.1$ when applicable.

b. Age of the supernova past maximum brightness or past date of discovery (if the date of maximum is not known) at the time of observation. A negative age stands for a pre-maximum observation.

c. Flux densities are 3σ upper limits.

Table 5.3:—Continued

Notes

1) This upper limit provided by Crane et al. (1992).
2) Observation was made at 3.6 cm.
3) Brown & Marscher (1978) report radio observations of these SNe resulting in upper limits to detection.
4) The upper limits from observations of these SNe are quoted from Cowan & Branch (1982) and *Branch & Cowan (1985) since a map was unavailable for independent analysis.*
5) There is some dicrepancy with the NED reported position for SN 1921C and the astrometric position reported in Branch & Cowan (1985).
6) There is not much evidence that the explosion associated with SN 1954J was an actual SN.
7) It is not certain that SN 1961V was actually an SN explosion (Fillipenko et al. 1995).
8) NGC 4699 is also home to SN 1948A, but its position lies outside of the field of view for our map.
9) Observation was made at 2 cm.
10) The 20 cm upper limit for SN 1969L is quoted from Branch & Cowan (1985) since a map was unavailable for independent analysis.

5.3 Discussion

5.3.1 The Model

To estimate upper limits to mass-loss rates from pre-SN progenitors, one begins with the expression for the radio luminosity for Type II SNe based on the well-established Chevalier (1982a,b) mini-shell model. According to this model, The outward moving shock from the SN explosion encounters circumstellar material, compresses it and creates Rayleigh-Taylor instabilities. The magnetic fields locked in the material compress and amplify, accelerating free electrons. Synchrotron radiation results and is responsible for the radio luminosity. This luminosity has the form (following Chevalier [1982b], see Appendix A for the derivation)

$$L \propto \left(\frac{\dot{M}}{v_w}\right)^{(\gamma-7+12m)/4} t^{-(\gamma+5-6m)/2} m^{(5+\gamma)/2} U^{3(1-m)} \nu^{-(\gamma-1)/2} e^{-\tau_{\nu,ff}} \qquad (5.1)$$

where

$$\tau_{\nu,ff} = C \left(\frac{\dot{M}}{v_w}\right)^{(5-3m)} t^{-3m} \nu^{-2.1}. \qquad (5.2)$$

$\dot{M}$ is the mass-loss rate of the pre-SN progenitor in $M_\odot$ yr^{-1}, v_w is the wind speed in km/s, γ is the electron energy index, related to the radio spectral index, α, by $\gamma = 2\alpha+1$, t is the time since explosion in days, m is defined by the ratio $(n-3)/(n-2)$, and n is the power law index for the ejecta density profile defined by $\rho \propto r^{-n}$. U is a parameter that depends on the density of the supernova ejecta at a given ejecta speed, $\tau_{\nu,ff}$ is the frequency dependent optical depth due to free-free absorption experienced by the radio emission as it escapes outward from the interaction region into the surrounding circumstellar material, and C is a constant. Initially, the optical depth

is large, depressing the emission, but as the shock moves out, the optical depth falls with circumstellar density and the radio emission peaks. Due to the frequency dependence of the optical depth, shorter wavelengths peak first. According to the model, after peaking the radio emission falls monotonically to undetectability. The radio emission may eventually rise again either from a second phase of interaction with a denser layer of circumstellar material (e.g., SNe 1979C, 1987A) or from the onset of the SNR phase.

How does the model apply to different SN types? For core-collapse SNe (Type II, Ib/c) the interaction occurs between the outgoing shock and the pre-SN progenitor wind. For SNe Type Ia the interaction can take place between the outgoing shock front of the white dwarf explosion and the wind of a companion red giant (Boffi & Branch 1995, Eck et al. 1995). For detectable radio emission, there must be enough circumstellar material (high enough $\dot{M}/v_w$) to fuel the synchrotron emission, so for small $\dot{M}/v_w$ (of the progenitor or companion) no strong radio emission is expected.

For detected SNe, the data follow this "standard model" very well (e.g., Weiler et al. 1986, Weiler et al. 1990, Van Dyk et al. 1993a) albeit with occasional minor modifications such as periodicities folded into the model and interpreted (Weiler et al. 1991) to better fit the data. Recent calculations by Chevalier (1998) indicate that synchrotron self-absorption may be important for SNe Ib/c and SN 1987A as well as for SN whose progenitors have low mass-loss rates. Ignoring this effect may cause an overestimate of mass-loss rates.

By knowing the luminosity, the frequency and the age of an observation the mass-loss rate of the pre-SN progenitor can be predicted provided the other parameters can be determined. Since most of the observations are non-detections and only upper

limits to flux densities, there is not enough data to determine all the parameters with a fitting routine. However, the data may be salvaged by scaling the SNe Type II data to the parameters of the well-known SN 1979C and scaling the SNe Type I data to SN 1983N, a Type Ib with similar (derived) properties to another Type Ib, SN 1984L. Of course calculations performed in this way must be taken only as rough estimates since every SN is not exactly like SNe 1979C or 1983N. We are effectively forcing every SN in the data set to look like either SN 1979C or SN 1983N, which has only limited validity, but the results can be useful where no data were previously available.

The relevant parameters for the mass-loss rate calculations were determined in the following manner. With different values inferred from the observations for the parameter n (Chevalier & Fransson 1994), we choose a value of $n = 20$ ($m = 0.94$) (Eck et al. 1996) for the SNe Type II. The radio spectral index for SN 1979C is $\alpha = -0.72$ ($\gamma = 2.4$) from Weiler et al. (1986) and the constants K, U, and $m^{(5+\gamma)/2}$ can be incorporated into one constant and determine its value by substituting all other known parameters and solving. The constant C can be determined by knowing the optical depth, age, frequency and mass-loss rate of an observation. Weiler et al. (1986) have fitted data to determine their parameter K_2, representative of the optical depth at 5 GHz at $t = 1$ day. We also use the mass-loss rate calculated by Weiler et al. (1986) for SN 1979C. The resulting luminosity equation is

$$L = 1.8 \times 10^{37} \left(\frac{\dot{M}}{v_w/10 \text{ km s}^{-1}}\right)^{1.7} \left(\frac{t}{1 \text{ day}}\right)^{-0.88} \left(\frac{\nu}{5 \text{ GHz}}\right)^{-0.7} e^{-\tau_{\nu,ff}} \text{ erg s}^{-1} \quad (5.3)$$

where

$$\tau_{\nu,ff} = 2.6 \times 10^{16} \left(\frac{\dot{M}}{v_w/10 \text{ km s}^{-1}}\right)^{2.18} \left(\frac{t}{1 \text{ day}}\right)^{-2.8} \left(\frac{\nu}{5 \text{ GHz}}\right)^{-2.1}. \quad (5.4)$$

For SNe Type I, the SN density power law index is typically $n = 7$ ($m = 0.8$), and for SN 1983N, Weiler et al. (1986) report $\alpha = -1.03$ ($\gamma = 3.1$). Determining the other constants in the same manner for Type II SNe results in a luminosity equation for SNe Type I of

$$L = 9.1 \times 10^{36} \left(\frac{\dot{M}}{v_w/10 \text{ km s}^{-1}} \right)^{1.4} \left(\frac{t}{1 \text{ day}} \right)^{-1.6} \left(\frac{\nu}{5 \text{ GHz}} \right)^{-1.0} e^{-\tau_{\nu,ff}} \text{ erg s}^{-1} \quad (5.5)$$

where

$$\tau_{\nu,ff} = 3.5 \times 10^{17} \left(\frac{\dot{M}}{v_w/10 \text{ km s}^{-1}} \right)^{2.6} \left(\frac{t}{1 \text{ day}} \right)^{-2.4} \left(\frac{\nu}{5 \text{ GHz}} \right)^{-2.1} \quad (5.6)$$

We take the commonly assumed value for the wind speed, 10 km s^{-1}. For simplicity we use this wind speed for all SN Types although it is noted that for Types Ib/c, the wind speed may be higher. Calculated values for $\dot{M}$ are shown in Tables 5.4, 5.5, 5.6. In many cases the observation age has been calculated from the time of maximum brightness or from the time of discovery since data on the explosion date are not available, especially for the older SNe. Thus, the ages may be in error by about 30 days. For any SNe (in this survey) with observation ages older than that of SN 1983K ($\sim$ 1500 days) this amounts to an error in the ages of less than 2%. For the SNe with observation ages less than 1500 days, we were able to obtain data on the explosion date for a better calculation of the (upper limit to the) mass-loss rate.

For all but a couple of the upper limits, the observation age is large enough that the radio emission can be assumed to be fading. However, observations for the Type Ia SNe 1986G and 1989B are at 10 and 14 days past explosion, respectively. It is possible that the radio emission at this age could be rising (pre-peak) or falling (post-peak).

SN Name	SN Type	Distance (Mpc)	Age at Observation (days)	Flux Density (mJy) 20 cm	6 cm	Other λ	$\dot{M}$
SN 1885A	I pec	0.76	38280	...	...	< 0.015	< 4.3
SN 1895B	Ia	4.1	31343	< 0.9	...	...	< 260
			32680	< 0.15	...	...	< 73
SN 1921C	I	8.7	22650	< 0.51	...	...	< 410
SN 1937C	Ia	4.7	17784	< 0.10	...	...	< 34
SN 1954A	Ib	4.7	11703	< 0.068	...	...	< 23
SN 1972E	I	4.1	3276	< 0.9	...	...	< 19
			4968	< 0.15	...	...	< 8.6
SN 1983N	Ib	4.1	170	4.4	...	...	2.1
			256	...	0.52	...	1.7
			2664	...	< 0.084	...	< 6.6
			3111	< 0.15	...	...	< 5.1
SN 1986G	Ia	4.1	10	...	< 0.96	...	< 0.064
				...	...	...	> 2.8
			10	...	...	< 0.69	< 0.11
				...	...	...	> 7.1
SN 1989B	Ia	11.4	15	...	< 0.11	...	< 0.093
				...	...	...	> 4.1
			15	...	...	< 0.089	< 0.12
				...	...	...	> 6.4

Table 5.4: Parameters and (upper limits to) derived mass-loss rates for the SNe I in this survey based on the Chevalier model. Units for the mass-loss rates are 10^{-6} $M_\odot$ yr^{-1}.

SN Name	SN Type	Distance (Mpc)	Age at Observation (days)	Flux Density (mJy) 20 cm	6 cm	Other λ	$\dot{M}$
SN 1909A	II(-P)	7.4	29107	···	< 0.034	···	< 5.2
SN 1921B	II	8.7	22899	< 0.51	···	···	< 17
SN 1923A	II-P	4.1	22126	< 0.57	···	···	< 7.2
			22212	···	0.19	···	6.2
			24620	···	0.093	···	4.3
			25067	0.30	···	···	5.3
SN 1937F	II(-P)	8.7	16791	< 0.51	···	···	< 14
SN 1951H	II	7.4	15390	< 0.044	···	···	< 2.7
SN 1954J	V	3.6	11250	< 0.35	···	···	< 3.3
SN 1959D	II-L	15.1	9545	< 0.058	···	···	< 5.7
			9787	< 0.079	···	···	< 6.9
			9902	···	< 0.042	···	< 7.8
SN 1961V	II pec (V)	9.3	8382	0.27	···	···	7.4
			9018	···	0.13	···	8.2
SN 1966B	II-L	17.1	7853	< 0.16	···	···	< 11
SN 1968L	II-P	4.1	5636	< 0.57	···	···	< 3.6
			5722	···	< 0.16	···	< 2.8
			8129	···	< 0.084	···	< 2.3
			8577	< 0.15	···	···	< 2.0
SN 1969L	II-P	9.3	5460	< 0.09	···	···	< 3.1
			6096	···	< 0.042	···	< 3.4
SN 1970G	II-L	7.4	7215	0.21	···	···	4.5
			7413	···	···	0.076	5.1
SN 1973R	II-P	11.4	4968	< 0.28	···	···	< 7.3
SN 1980D	II-P	22.1	2697	< 0.094	···	···	< 6.1
SN 1983K	II-P	25.7	1502	···	< 0.052	···	< 6.3
SN 1984E	II-L	19.7	4116	< 0.073	···	···	< 5.7
SN 1986E	II-L	16.8	3395	< 0.17	···	···	< 7.1
			3539	···	< 0.038	···	< 4.9

Table 5.5: Parameters and (upper limits to) derived mass-loss rates for the SNe II in this survey based on the Chevalier model. Units for the mass-loss rates are 10^{-6} $M_\odot$ yr^{-1}.

SN Name	SN Type	Distance (Mpc)	Age at Observation (days)	Flux Density (mJy) 20 cm	6 cm	Other λ	$\dot{M}$ SN I	SN II
SN 1945B	?	4.1	14032	< 0.57	...	...	< 74	< 5.7
			14119	...	< 0.16	...	< 71	< 4.5
			16526	...	< 0.084	...	< 53	< 3.3
			16974	< 0.15	...	...	< 35	< 2.9
SN 1950B	?	4.1	12328	0.7	...	...	74	6.0
			12414	...	0.36	...	110	6.7
			14822	...	0.37	...	140	7.5
			15269	0.72	...	...	97	6.9
SN 1957D	?	4.1	9489	2.7	...	...	160	12
			9576	...	2.1	...	200	17
			11983	...	1.4	...	280	15
			12431	1.2	...	...	110	8.3

Table 5.6: Parameters and (upper limits to) derived mass-loss rates for the unknown Type SNe in this survey based on the Chevalier model. Note that SNe 1950B and 1957D are likely SNe II (see text). Units for the mass-loss rates are 10^{-6} $M_\odot$ yr^{-1}.

This would result in two different derived mass-loss rates—a larger mass-loss rate corresponding to the optically thick case when the emission has not peaked yet and a smaller mass-loss rate corresponding to the optically thin case when the emission has already peaked (see Eck et al. 1995 and Chapter 4 for details and previously calculated results for SN 1986G). For SNe Ia one may be able to test whether the progenitor system is a symbiotic (white dwarf accreting matter from the wind of a red giant companion) using early radio observations such as this. By comparing the range of derived mass-loss rates to the mass-loss rate expected from red giants in symbiotic systems (10^{-7} to 10^{-5} $M_\odot$ yr^{-1} [Seaquist & Taylor 1990, Mürset et al. 1991]) one may test the symbiotic scenario. Inspection of Table 5.4 reveals that the derived range of mass-loss rates for SNe 1986G and 1989B are in mild conflict with that expected for the symbiotic red giant companion. These were probably not symbiotic systems (in agreement with original calculations by Eck et al. [1995] for SN 1986G).

Model Assumptions

We now examine some of the assumptions in the Chevalier model and their possible effects on the derived luminosities and mass-loss rates. One of the key assumptions in the theory of the origin of the synchrotron radio luminosity concerns the efficiency of conversion of the thermal energy density of electrons into the magnetic energy density and relativistic electron energy density. It has been assumed that this value is constant at about 1% (Chevalier 1982b), but this assumption is now being questioned based on observations of SN 1987A. Also inherent is the assumption that the density of the circumstellar wind material and the outer layers of the SN ejecta are described by time-independent power laws, $\rho_{csm} \propto r^{-2}$ and $\rho_{SN} \propto r^{-n}$. While the assumptions on

the density profile of the SN ejecta have been shown to be good assumptions, some cases have shown evidence for a circumstellar power law density that looks different from the assumed form, i.e. $\rho_{csm} \propto r^{-3/2}$ (SN 1993J: Van Dyk et al. 1994). This has been interpreted as a changing presupernova mass-loss rate. Other radio SNe have shown evidence for clumpiness in the pre-SN wind or non-spherical symmetry of the shock and a mix of internal absorbers and emitters along the line of sight (SNe 1986J: Weiler et al. 1990, SN 1988Z: Van Dyk et al. 1993b). In these particular cases, the model was modified to better fit the data. Finally, if synchrotron self-absorption is important, the derived upper limits to mass-loss rates may be overestimated. Since these are only upper limits, we do not include these effects.

For detected SNe, the data can be used to derive mass-loss rates directly. Equation (16) from Weiler et al. (1986) gives an expression for the mass-loss rate as a function of several parameters, one of which, τ_{ff}, the optical depth, can be derived by fitting the data. Some common assumptions on the other parameters are $v_{shock} = 10^4$ km s^{-1}, $v_w = 10$ km s^{-1}, and $T_e = 10^4$ K in the wind. How sensitive are the mass-loss rates to these values? While the functional form for the dependence of these parameters on the mass-loss rate is obvious from the expression from Weiler et al. (1986), there are other considerations. For example, Lundqvist & Fransson (1988) report that the assumption of a fully ionized wind may underestimate the mass-loss rate by a factor of 2 or more. To review this and some other considerations affecting the radio emission, see Lundqvist & Fransson (1988).

5.3.2 Comparisons

Self-consistency

By comparing the results of the calculated mass-loss rates here with those reported previously for SNe 1986G, 1984E & 1986E, we find them to be in good agreement. Eck et al. (1995) report the calculated mass-loss rate for SN 1986G to be outside of the range $6 \times 10^{-8} \lesssim \dot{M} \lesssim 7 \times 10^{-6}$ $M_\odot$ yr^{-1}. This compares to the current calculations, which limit the mass-loss rate to be outside of the range $6.4 \times 10^{-8} \lesssim \dot{M} \lesssim 2.8 \times 10^{-6}$ $M_\odot$ yr^{-1}. The results from Eck et al. (1996) for SNe 1984E & 1986E also are slightly different ($< 10^{-6}$ $M_\odot$ yr^{-1} for Eck et al.), versus $< 4.9 \times 10^{-6}$ $M_\odot$ yr^{-1} for the present work.

Other Radio Comparisons

Montes et al. (1997) recently reported a detection of SN 1986E at an age of about 8 months. By scaling some of the parameters to those of SNe 1979C & 1980K and using the detection of SN 1986E as well as some tight upper limits, they derive a light curve and a subsequent mass-loss rate of $> 4.7 \times 10^{-5}$ $M_\odot$ yr^{-1}. While these upper limits are consistent with their radio light curve (i.e., their derived radio light curve predicts the radio emission to be less than these upper limits at the epochs of the observation), the derived mass-loss rate, here, is in conflict, at $< 4.9 \times 10^{-6}$ $M_\odot$ yr^{-1}, by an order of magnitude. The disagreement may be due to the very approximate nature of this calculation and an artifice of the differences in assumptions between us and Montes et al. By using their assumptions for SN 1986E on α and m (or δ), as well as their reported value for K_2 (for SN 1980K), the upper limit for SN 1986E is

calculated, here, to be $< 2.1 \times 10^{-5}$ which approaches the Montes et al. value. The assumptions can clearly be important and indicate that these results may be good only to within an order of magnitude.

Brown & Marscher (1978) report radio upper limits to 46 SNe at two wavelengths and at ages varying from a few months to more than 70 years. Their sample contains many of the SNe in the present sample (SNe 1895B, 1909A, 1921B, 1921C, 1937F, 1951H, 1954J, 1959D, 1961V, 1969L, 1970G, 1972E and 1973R), but with relatively high upper limits (by todays standards) in the range $3 - 30$ mJy; they reported no detections. By applying these models to their data on upper limits, upper limits to mass-loss rates may be derived similarly to what we have done with the data here. Despite some early observations from Brown & Marscher at less than a year after explosion, no new upper limits to mass-loss rates were obtained that are lower than the observations here.

Weiler et al. (1989) performed a procedure very similar to what we have done in calculating upper limits to mass-loss rates for 24 SNe observed by them at 6 cm, including SNe I and II. They calculate mass-loss rates by scaling all Type II to SNe 1979C & 1980K and all Type I to SN 1983N, but they do not include absorption effects (except for the fluxes from SNe 1979C & 1980K). At late times absorption is negligible, but it can be important at earlier epochs. By not including an absorption term, this could cause an underestimate in mass-loss rates. We calculate mass-loss rates for the 24 SNe in Weiler et al. (1989) and derive upper limits that are $10\% - 60\%$ greater than theirs for their Type II SNe. For the Type I SNe in Weiler et al. (1989), including absorption effects depresses the emission enough that any physically reasonable mass-loss rate would have produced emission below their flux density upper

limits for many of their older, more distant SNe. For the closer SNe I observed early enough to restrict mass-loss rates, these upper limits to the mass-loss rates are greater than theirs. The discrepancies in the results from this paper and Weiler et al. are probably due to a combination of free-free absorption effects and of parameter differences.

Radio and optical emission

Can radio emission be predicted? Since radio emission is the result of the interaction of the shock with circumstellar matter (radio SNe) or of the shock with interstellar matter (radio SNR), any evidence for interaction (in other wavebands) might be used as a predictor for radio emission.

Since most SNe have faded in the optical by an age of about 2 years, indications of optical emission beyond 2 years may be the result of some type of enhanced circumstellar interaction. There are 9 SNe that have been detected in the optical at an age of greater than 2 years: SN 1885A at 103 yrs (Fesen, Hamilton, & Saken 1989, Fesen 1997), SN 1957D at 30-32 yrs (Long, Blair, & Krzeminski 1989), SN 1961V at 22-24 yrs (Goodrich et al. 1989), SN 1978K at 12 and 14 yrs (Ryder et al. 1993, Chugai, Danziger, & Della Valle 1995), SN 1979C at 10 yrs (Fesen 1993), SN 1980K at 7-9 yrs (Fesen & Becker 1990), SN 1986E at 7-8 yrs (Cappellaro et al. 1995), SN 1986J at 4-7 yrs (Leibundgut et al. 1991) and SN 1987A at about 10 years (Sonneborn et al. 1998). SN 1885A has been optically detected in the optical via absorption; this is not evidence for circumstellar interaction, so it is removed from the group of 9. SN 1987A has been detected in the radio at an age of about 10 yrs but at a flux level that would be undetectable at greater distances. SNe 1957D and 1961V were

recovered in the optical only after detection in the radio. (It is not clear whether SN 1961V was an SN or an LBV outburst [Goodrich et al. 1989, Filippenko et al. 1995]). A model fit to the 0.843 GHz data from Ryder et al. (1993) for SN 1978K indicates that the radio emission is fading at the time of the optical observations, but with only 3 data points. More observations are needed. Observations of SN 1979C indicated fading radio emission (albeit with approximate sinusoidal variations [Weiler et al. 1992b]) at the time of optical recovery, but more recent observations indicate that it is now brightening in the radio (Weiler et al. 1998). SN 1980K was optically recovered when the radio emission was fading, and recent radio results now indicate a sharper drop than previously reported (Weiler et al. 1998). Although still fading from its initial rise, SN 1986J was emitting strongly in the radio at an age of 6 yrs. SNe 1885A (Crane, Dickel, & Cowan 1992) and 1986E (Eck et al. 1996) do not show detectable radio emission near the time of optical recovery although, SN 1986E did show one radio detection at an age of 8 months (Montes et al. 1997).

Of all 8 SNe (without SN 1885A) with optical recoveries, 7 show radio emission. Of these 7, only two (SNe 1979C and 1987A) show a rise in radio emission within a few years after optical recovery. It is unlikely that SNe 1979C and 1987A are entering a radio SNR phase at an age of only 10-20 yrs. Thus, optical recovery precedes an increase in radio emission while still in a RSN phase for SNe 1979C and 1987A. Is optical recovery a good indicator (in general) of radio emission as the SN shock encounters circumstellar material? For a majority of the cases (7 out of 8), it would seem to be true. Although both radio and late-time optical emission may be indicative of enhanced circumstellar interaction, the emission mechanisms are different as may be the regions where the emission originates.

5.3.3 Luminosity-Age Plots

Figures 5.1, 5.2, 5.3, 5.4, and 5.5 are plots of the radio luminosities for (3σ) upper limits versus age of observation for all of the SNe in the sample, here. The plots are separated by SN Type and wavelength. Each plot shows upper limits (as upside-down triangles), detections (larger unfilled polygons), and at least one SN of the same type with its model light curve (solid and dashed curves) and observational data (smaller unfilled circles). Because of its unknown SN type, SN 1945B (Liller 1990) was included on both SN Type I and II plots. Although SNe 1950B and 1957D are both of unknown type, they are likely to be SN Type II (CRB, Eck et al. 1998a) and were included only in the Type II plots.

Type II SNe

Inspection of the Type II plots at both 20 and 6 cm reveal that upper limits for SNe 1980D, 1984E & 1986E are below the data for SN 1979C but above the data for SN 1980K. Given that the radio emission from SN 1980K has fallen sharply to undetectable limits, it is possible that most of the other upper limits (for the older SNe) *could* have fluxes above that of SN 1980K. Recent data from Weiler et al. (1998) indicate that radio emission from SN 1979C is now rising again instead of continuing to fade. It is probably reasonable to say that these upper limits are inconsistent with data from SN 1979C. This may indicate that the Type II SNe in this survey have properties more like SN 1980K than SN 1979C. The fact that these upper limits are more consistent with the data from SN 1980K suggests that SN 1980K may be a more typical Type II radio emitter than SN 1979C.

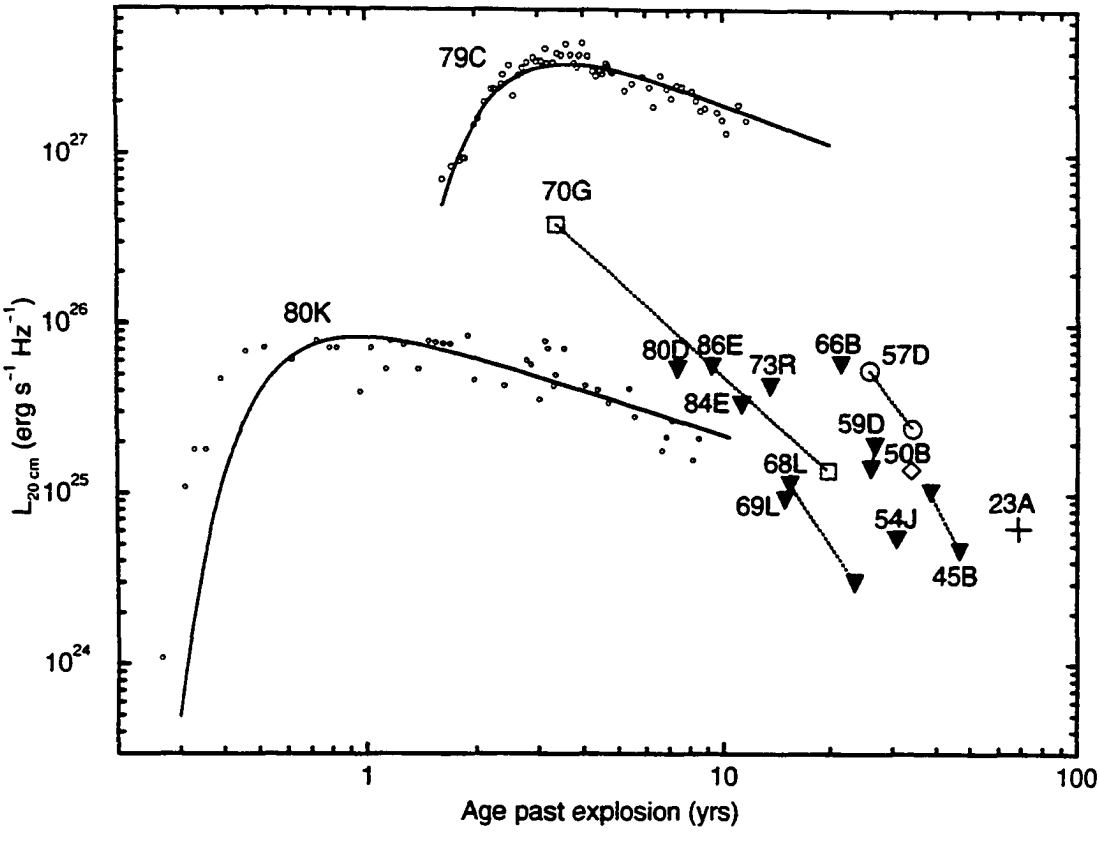

Figure 5.1: A plot of luminosity versus age for the SNe II in this survey at 20 cm. The upper limits are designated as upside-down triangles, the unfilled shapes (squares for SN 1970G, larger circles for SN 1957D, diamond for SN 1950B, plus sign for SN 1923A) are data for the radio detections in this survey. Included are data (small unfilled circles) and model fits (solid curves) to the data for two well-observed SNe II, SNe 1979C (Weiler et al. [1986,1991]) and 1980K (Weiler et al. [1986,1992a]).

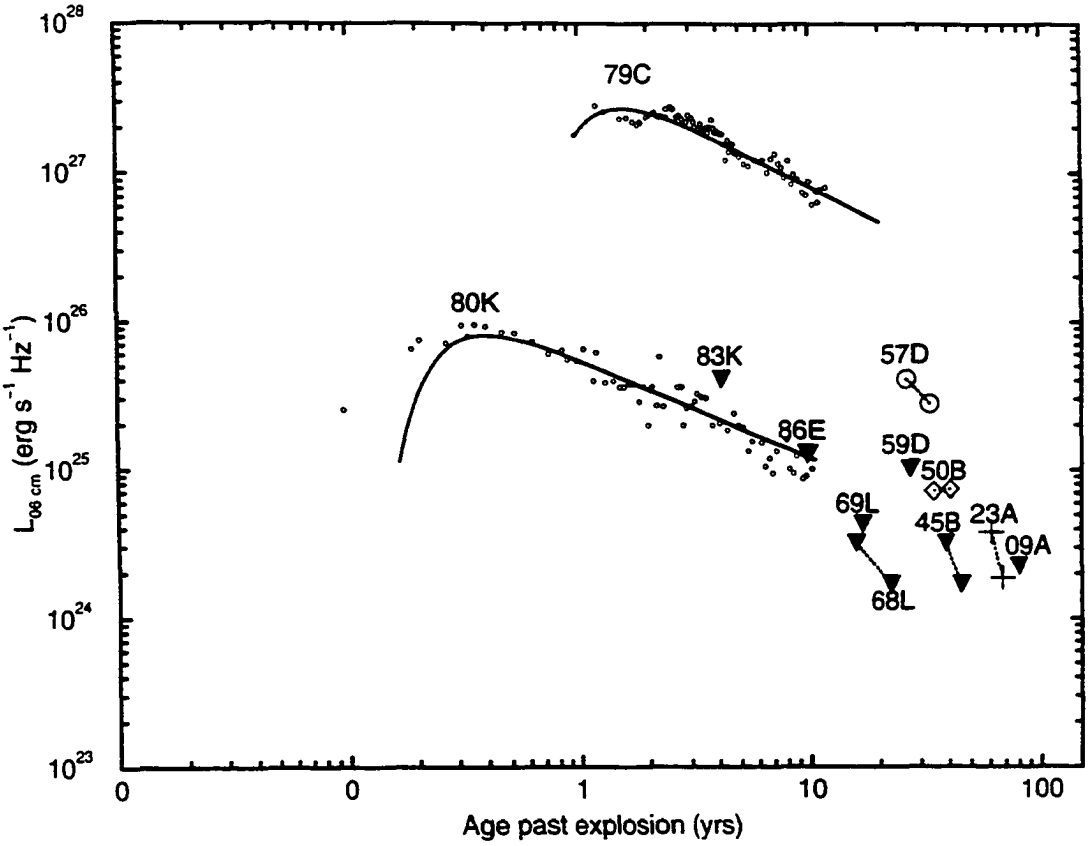

Figure 5.2: A plot of luminosity versus age for the SNe II in this survey at 6 cm. The data and curves are labeled as in Figure 1. The data and light curves for SNe 1979C and 1980K are from Weiler et al. (1986, 1991) and Weiler et al. (1986,1992a), respectively.

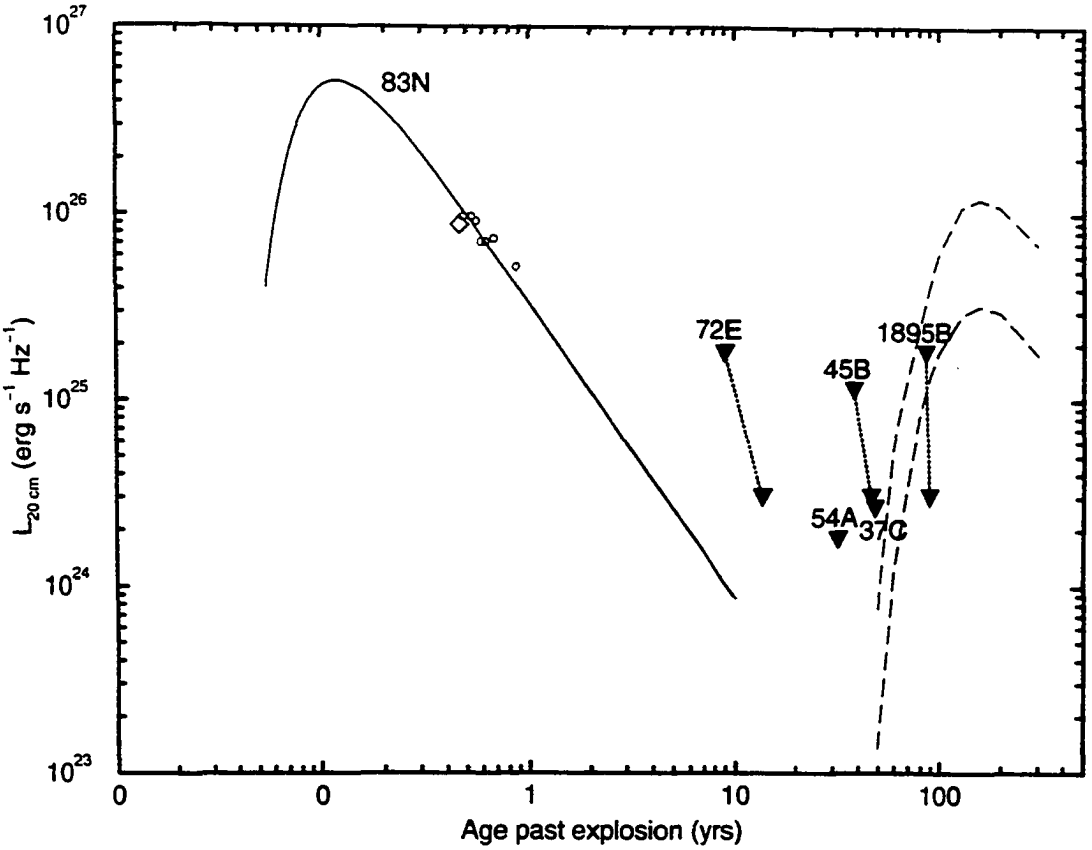

Figure 5.3: A plot of luminosity versus age for the SNe I in this survey at 20 cm. The upper limits are designated as upside-down triangles and the diamond represents the datum for SN 1983N. The smaller unfilled circles and the solid curve are data and a model fit to the data from Weiler et al. (1986) for SN 1983N. The dashed curves are light curves for the onset of the SNR phase from calculations by Cowsik & Sarkar (1984) based on the Gull (1973) model. The two curves are for different model assumptions (see text).

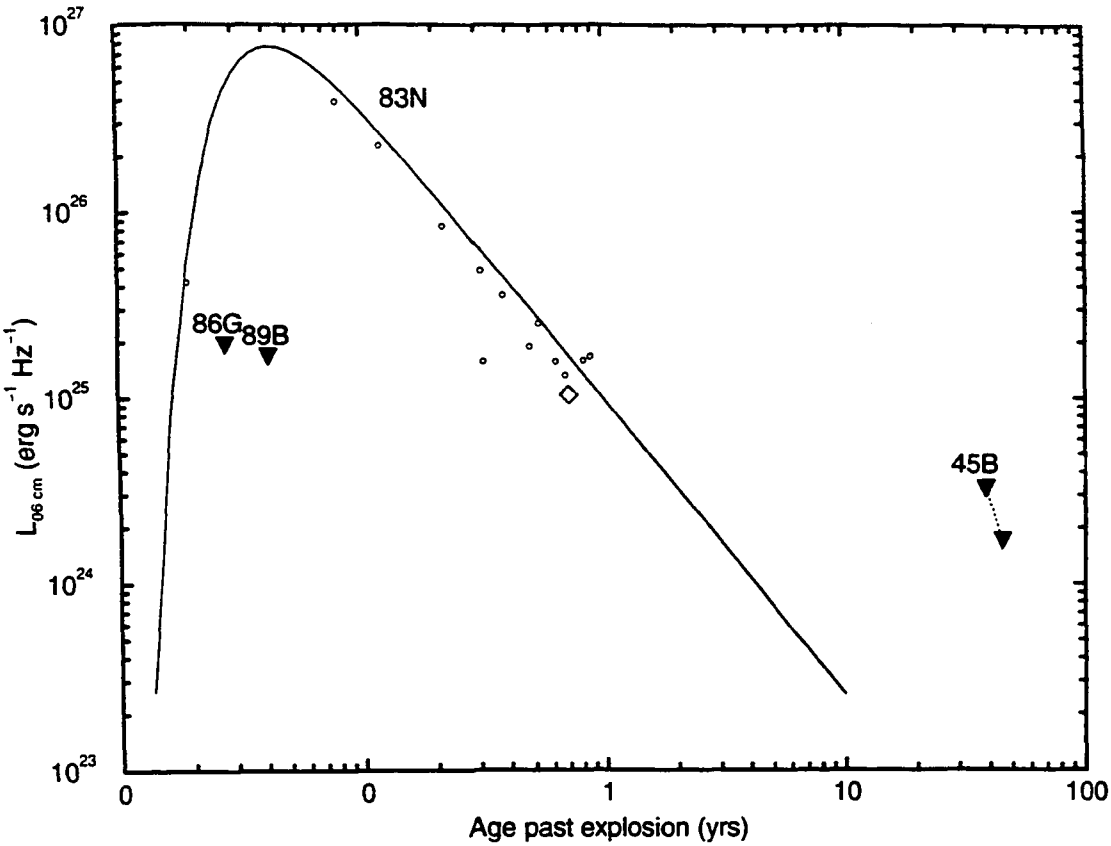

Figure 5.4: A plot of luminosity versus age for the SNe I in this survey at 6 cm. Designations are as in Figure 3.

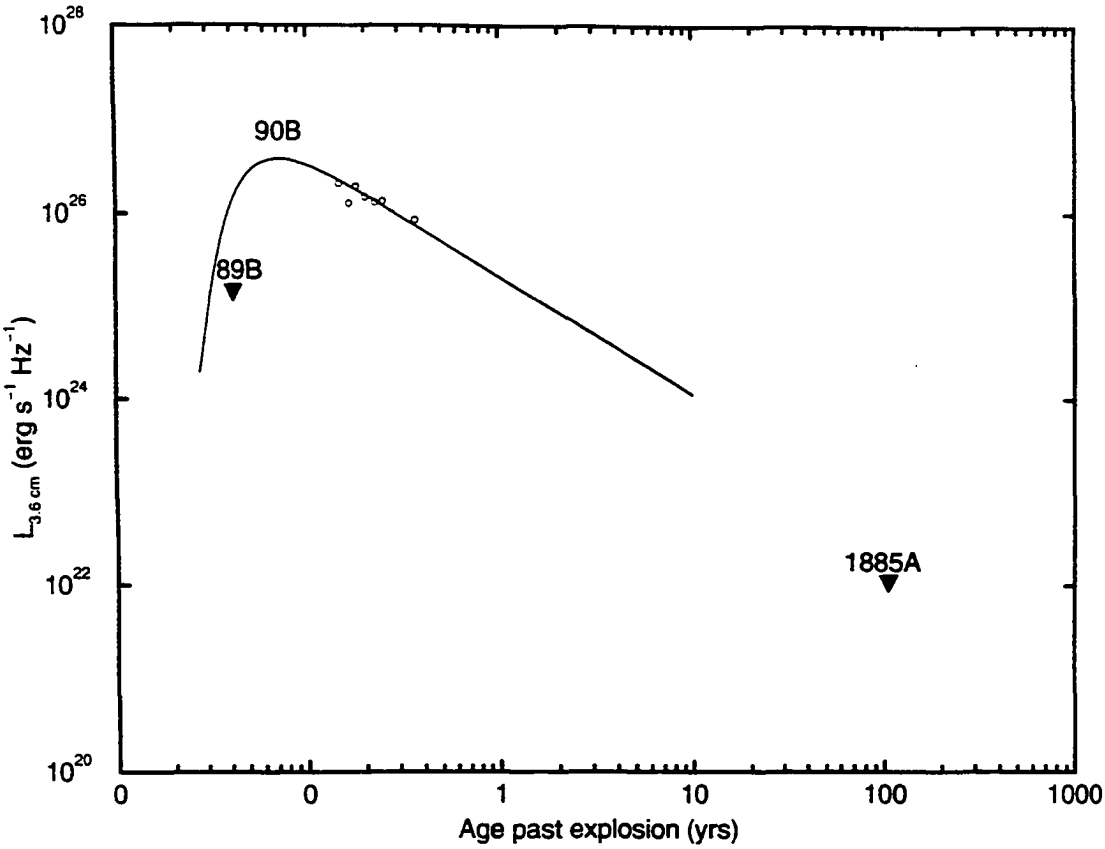

Figure 5.5: A plot of luminosity versus age for the SNe I in this survey at 3.6 cm. Upper limits are designated as upside-down triangles. The upper limit for SN 1885A is from Crane et al. (1992). Data (small circles) and light curve (solid curve) are from the Type Ic SN 1990B (Van Dyk et al. 1993a) since data at 3.6 cm was unavailable for SN 1983N.

In the same manner, the flux from the detected SNe 1957D (CRB) and 1970G (Cowan et al. 1991) can be compared with the data and light curves from SNe 1980K (Weiler et al. 1986, Weiler et al. 1992a) and 1979C (Weiler et al. 1986, Weiler et al. 1991). If it is assumed that SN 1980K doesn't brighten again for the next 30 years and that SN 1979C doesn't drop off any more sharply in the next 20 years, then the fluxes for SNe 1957D and 1970G are bracketed by the light curves for SNe 1980K and 1979C. This suggests that SNe 1957D and 1970G have properties intermediate to those of SNe 1980K and 1979C. Comparing the mass-loss rates reveals that the derived values for the $\dot{M}$ of SNe 1957D and 1970G lie between the mass-loss rates calculated by Lundqvist & Fransson (1988) for SNe 1980K and 1979C (3×10^{-5} and 1.4×10^{-4}, respectively). Some caution must be exercised in comparing mass-loss rates since the properties and parameters of SN 1979C were used to derive the mass-loss rates of SNe 1957D and 1970G. (A lower flux, compared to SN 1979C, naturally leads to a smaller mass-loss rate with all other properties being equal).

Type I SNe

Inspection of the Type I plot at 20 cm reveals that the upper limits lie above the extrapolated curves for the Type Ib SN 1983N, no conclusions can be drawn about similarities (especially between SNe of different sub-types). The observation age of SN 1895B makes it interesting to consider. We may compare it with model curves (dashed curves) for the radio turn-on of a SNR as calculated by Cowsik & Sarkar (1984). The dashed curves correspond to models c) (constant density piston) and d) (isothermal piston) and assume an explosion energy of 10^{51} ergs, 0.5 solar masses of ejected material, an interstellar density of 1 baryon cm^{-1} and a spectral index,

$\alpha \simeq -1$. It is clear that SN 1895B *could* be in the SNR phase, but the high upper limit does not exclude the possibility that it may still be fading as a RSN. At 6 cm, this data is very limited for Type I SNe. The SNe with upper limits (SN 1986G and 1989B) are SN Type Ia compared to the Type Ib SN 1983N. Since no SNe Type Ia have been detected in the radio, we cannot conclude much about the comparison of the upper limits and the SN 1983N light curve, except that the upper limits are below the light curve. For the 3.6 cm plot, no data was available for SN 1983N so we plot data and curves from the only other SN I with 3.6 cm data, the Type Ic SN 1990B. Without more radio light curves to compare these upper limits to, it is difficult to say anything with confidence about the upper limits (for the Type Ia SNe 1885A and 1989B) except that they are in mild conflict with the SN 1990B data.

5.4 Conclusions

The results of the analysis of these radio observations can be summarized:

1. Most SNe are not detectable radio emitters with current radio telescopes, due to either large distances or intrinsically faint radio supernovae (or observations not taken early enough).

2. No SNe Ia have been detected despite some early and/or deep observations (SNe 1895B, 1937C, 1986G, 1989B).

3. While most of the Type II SNe observed in this survey were *not detected* in the radio, it was found that most of the *detected* ones (of all the SN types) are Type II SNe.

4. Assuming the Chevalier model, the flux upper limits imply a lack of circumstellar material (or fuel) for detectable radio emission.

5. Using the Chevalier model for Type Ia SNe, one scenario for which one would get radio emission is the symbiotic-star progenitor scenario (Boffi & Branch 1995). The non-detections of SNe 1986G and 1989B indicate that the derived upper limits to mass-loss rates are in mild conflict with the mass-loss rates inferred from red giants in symbiotic systems. These SNe are probably not symbiotics. The other SNe Ia (SNe 1895B, 1937C) have higher upper limits to the mass-loss rates so that we cannot discount the symbiotic-star scenario as a progenitor scenario.

6. By applying the Chevalier model to the SNe II observations, it is seen that no SNe II have been detected with a derived value for the mass-loss rate of $\dot{M} \lesssim 10^{-6}\ M_{\odot}\ yr^{-1}$, implying a lack of circumstellar material. This value is very dependent on the scaling of the parameters of the SNe to those of the well-observed SN 1979C, and the uncertainty in the derived mass-loss rates may be as high as a factor of 10 due to dependences on parameters (see SN 1986E).

7. The derived mass-loss rates can also have a dependence on the assumptions inherent in the Chevalier model. The effects of these assumptions on the radio luminosity are not trivial to calculate and warrant further study (see Lundqvist & Fransson [1988] for an investigation of some of these effects).

8. There are 8 SNe in this survey with optical recoveries (indicating circumstellar interaction) at an age of greater than 4 years. Of the SNe with optical recoveries,

7 have been detected as radio emitters and for 2 cases of these 7, the optical emission preceded a (second) rise of radio emission. This implies that radio emission may be associated with optical recovery.

9. Since the upper limits for SNe II in this survey are more consistent with SN 1980K than with SN 1979C, the non-detected SNe II in this survey may have radio properties more similar to SN 1980K than SN 1979C.

10. The detected intermediate-age SNe in this survey have luminosities that lie between the extrapolated behaviors of the light curves for SNe 1979C and 1980K, implying radio properties (including mass-loss rates) intermediate to SNe 1979C and 1980K.

Finally, it is noted that despite more than two decades of theoretical and observational work in radio supernovae, radio emission from supernovae is not well understood. As the intermediate-age radio supernovae are followed, one hopes to explore further the transition of radio supernovae into supernova remnants. More sensitive observations of young and intermediate-age SNe, as well as more theoretical work, are needed to help us fully understand the origin and evolution of RSNe.

Chapter 6

Summary

"She blinded me with science," Thomas Dolby

In this chapter, I will summarize the results of this thesis.

I was fortunate to have helped contribute the probable detection of SN 1923A to the realm of science. The positional coincidence (with the reported optical position) and non-thermal nature of the radio emission makes it likely that one of the sources detected is from SN 1923A. This detection is unique in many ways. It would be the oldest historical radio SN yet detected and if confirmed, would be the only SN II-P to be observed as a radio emitter. As the oldest radio SN of known age, this important detection will help us follow the unobserved transition of radio SNe into SNRs.

Somewhat more surprising is the non-detection of SN 1986E despite the low noise level. With clear optical evidence for circumstellar interaction (Cappellaro et al. 1995), it is surprising that there was no accompanying radio emission, although the emission mechanisms are not the same and the radio and optical emission may not originate in the same region. The re-analysis of observations at an age of about 8

months by Montes et al. (1997) revealed a single detection and some tight upper limits. This allowed them to determine a rough light curve which was consistent with our upper limits (i.e., the light curve was below our upper limit to luminosity at the age of our observation). The non-detection of SN 1984E was less surprising given the evidence for a mass-loss episode of limited duration before explosion. Our luminosity upper limit constrains the duration of the mass-loss episode, depending on the speed that the material left the pre-SN star (the wind speed, v_w).

With an opportunity to observe the Type Ia SN 1986G so early (10 days past explosion) and at short wavelengths (6 and 2 cm), it is disappointing that radio emission was not detected from this SN. However, using the symbiotic-star progenitor scenario (white dwarf accreting matter from a red giant companion) for SNe Ia (Boffi & Branch 1995) and the Chevalier model, the mass-loss rate for the red giant can be constrained by our flux density upper limits at 6 and 2 cm. These constraints are in mild conflict with the usual mass-loss rate for red giants in binary systems, so this SN was not likely in a symbiotic system. It is noted that SN 1986G was peculiar spectroscopically and photometrically, so this is not to say that no SNe Ia occur in symbiotic systems.

What conclusions can be drawn from examining all of the data?

- 23 of the 29 SNe observed were non-detections, which continues the observed trend (e.g., Weiler et al. 1989) that most SNe are not detectable radio emitters with current radio telescope capabilities. Probable reasons for the lack of detectable radio emission from most SNe include the large distances to some SNe, intrinsically faint radio SNe, and observations made at large ages.

- 4 of the SNe observed in this sample are classified as SNe Ia and none were detected despite some observations prior to maximum light (SNe 1986G and 1989B) and some deep upper limits (SNe 1885A [Crane et al. 1992], 1895B, 1937C, 1986G, 1989B).

- Of the 6 SNe in this survey with detections (including SN 1923A and SN 1961V), 5 of them are SNe II. This continues the observed trend that most radio SNe are Type II.

- Chevalier's "standard model" (not including synchrotron self-absorption effects) may be applied to these observations to derive (upper limits to) mass-loss rates.

  - For SNe Ia, one scenario for which one might observe radio emission is the symbiotic-star scenario (see Chapter 4 and Boffi & Branch 1995). The non-detections of SNe 1986G and 1989B indicate that the derived ranges of mass-loss rates are in mild conflict with the mass-loss rates inferred from red giants in symbiotic systems. These SNe are probably not symbiotics. The upper limits to mass-loss rates derived for the other SNe Ia are high enough that one cannot discount the symbiotic-star scenario as a progenitor scenario.

  - For SNe II, the derived mass-loss rates imply that no SNe in this survey have been detected with a mass-loss rate of $\dot{M} \lesssim 10^{-6}$ $M_{\odot}$ yr^{-1}, implying a lack of circumstellar material. The uncertainty in this number could be as high as a factor of 10 due to dependencies on parameters determined by scaling to SN 1979C.

- The assumptions inherent in the Chevalier model may contribute to the uncertainty in derived mass-loss rates. The effects of some of the assumptions on the form for the model have been investigated by Chevalier (1998) and Lundqvist & Fransson (1988) but are not easy to calculate.

- Of the 8 SNe that have shown late-time (more than about 4 years) optical emission indicative of circumstellar interaction, 7 (SNe 1957D, 1961V, 1978K, 1979C, 1980K, 1986J, and 1987A) have been detected as radio emitters. Of these 7, SNe 1979C and 1987A were recovered optically before the radio emission began to rise for the second time. This seems to imply that radio emission may be associated with optical recovery.

- The luminosity upper limits for the Type II SNe in this survey are more consistent with SN 1980K than with SN 1979C. These SNe II may have radio properties more similar to SN 1980K than SN 1979C.

- The intermediate-age SNe in this survey with detections (SN 1923A, 1950B, 1957D, 1961V, and 1970G) have luminosities that lie between the extrapolated behaviors of the light curves for SNe 1980K and 1979C. This implies that these SNe have radio properties intermediate to those of SNe 1980K and 1979C.

The discovery of SN 1970G in the radio opened up a new regime in which to study SNe, and in the nearly 30 years of observational and theoretical work done since then, the radio emission from SN is still not completely understood. In the coming decades, it is hoped that more sensitive observations of both young and intermediate-age SNe and more theoretical work will help us fully understand the origin and evolution

of RSNe. As the intermediate-age RSNe are followed, we hope to more completely explore the transition of RSNe into SNRs which has been previously unobservable.

Bibliography

[Allen et al. 1976] Allen, R. J., Goss, W. M., Ekers, R. D., & de Bruyn, A. G. 1976, *Astronomy and Astrophysics*, 48, 253

[Becker et al. 1995] Becker, R. H., White, R. L., & Helfand, D. J. 1995, *Astrophysical Journal*, 450, 559

[Boffi & Branch 1995] Boffi, F. R., & Branch, D. 1995, *Publications of the Astronomical Society of the Pacific*, 107, 347 (BB95)

[Branch & Cowan 1985] Branch, D., & Cowan, J. J. 1985, *Astrophysical Journal*, 297, L33

[Branch et al. 1991] Branch, D., Nomoto, K., & Filippenko, A. V. 1991, Comments Astrophys., 15, 221

[Branch et al. 1993] Branch, D., Fisher, A., & Nugent, P. 1993, *Astronomical Journal*, 106, 2383

[Branch & van den Bergh 1993] Branch, D., & van den Bergh, S. 1993, *Astronomical Journal*, 105, 2231

[Branch et al. 1995] Branch, D., Livio, M., Yungelson, L. R., Boffi, F. R., & Baron, E. 1995, *Publications of the Astronomical Society of the Pacific*, 107, 1019

[Brown & Marscher 1978] Brown, R. L., & Marscher, A. P. 1978, *Astrophysical Journal*, 220, 467

[Cappellaro & Turatto 1988] Capppellaro, E., Turattto, M., 1988, *IAU Circ.*, No. 4691

[Cappellaro et al. 1995] Cappellaro, E., Danziger, I. J., & Turatto, M. 1995, *Monthly Notices of the Royal Astronomical Society*, 277, 106

[Chevalier 1982a] Chevalier, R. A. 1982a, *Astrophysical Journal*, 258, 790

[Chevalier 1982b] Chevalier, R. A. 1982b, *Astrophysical Journal*, 259, 302

[Chevalier 1984] Chevalier, R. A. 1984, *Astrophysical Journal*, 285, L63

[Chevalier & Fransson 1994] Chevalier, R. A., & Fransson, C. 1994, *Astrophysical Journal*, 420, 268

[Chevalier 1998] Chevalier, R. A. 1998, *Astrophysical Journal*, 499, 810

[Chugai et al. 1995] Chugai, N. N., Danziger, I. J., Della Valle, M. 1995, *Monthly Notices of the Royal Astronomical Society*, 276, 530

[Clark & Caswell] Clark, D. H., Caswell, J. L., 1976, *Monthly Notices of the Royal Astronomical Society*, 174, 267

[Clark & Stephenson 1982] Clark, D. H., & Stephenson, F. R. 1982, in Supernovae: A Survey of Current Research, eds. M. J. Rees & R. J. Stoneham (D. Reidel Publishing Company), p. 355

[Condon 1987] Condon, J. J. 1987, *Astrophysical Journal Supplement Series*, 65, 485

[Cowan & Branch 1982] Cowan, J. J., & Branch, D. 1982, *Astrophysical Journal*, 258, 31

[Cowan & Branch 1985] Cowan, J. J., & Branch, D. 1985, *Astrophysical Journal*, 293, 400

[Cowan, Henry, & Branch 1988] Cowan, J. J., Henry, R. B. C., & Branch. D. 1988, *Astrophysical Journal*, 329, 116

[Cowan et al. 1991] Cowan J. J., Goss, W. M., & Sramek, R. A. 1991, *Astrophysical Journal*, 379, L49

[Cowan, Roberts, & Branch 1994a = CRB] Cowan, J. J., Roberts, D. A., & Branch, D. 1994a, *Astrophysical Journal*, 434, 128

[Cowan et al. 1994b] Cowan, J. C., Romanishin, W. R., & Branch, D. 1994b, *Astrophysical Journal*, 439, L139

[Cowsik & Sarkar 1984] Cowsik, R., & Sarkar, S. 1984, *Monthly Notices of the Royal Astronomical Society*, 207, 745

[Crane 1977] Crane, P. C. 1977, Thesis, Massachusetts Institute of Technology

[Crane et al. 1992] Crane, P. C., Dickel, J. R. & Cowan, J. J. 1992, *Astrophysical Journal*, 390, L9

[Cragg 1986] Cragg, T. 1986, IAU Circ., 4208

[Danziger 1995] Danziger, I. J. 1995, private communication

[de Vaucouleurs, Pence, & Davoust 1983] de Vaucouleurs, D. G., Pence, W. D., & Davoust, E. 1983, *Astrophysical Journal Supplement Series*, 53, 17

[Donnelly et al. 1987] Donnelly, R. H., Partridge, R. B., & Windhorst, R. A. 1987, *Astrophysical Journal*, 321, 94

[Dopita et al. 1984] Dopita, M. A., Evans, R., Cohen, M., & Schwartz, R. D. 1984, *Astrophysical Journal*, 287, L69

[Dopita & Ryder 1990] Dopita, M. A., Ryder, S. D., 1990, *IAU Circ*, No. 4950

[Eck et al. 1995] Eck, C. R., Cowan, J. J., Roberts, D., Boffi, F. R., & Branch, D. 1995, *Astrophysical Journal*, 451, L53

[Eck et al. 1996] Eck, C. R., Cowan, J. J., Boffi, F. R., & Branch, D. 1996, *Astrophysical Journal*, 472, L25

[Eck et al. 1998a] Eck, C. R., Roberts, D., Cowan, J. J., & Branch, D. 1998, *Astrophysical Journal*, in press

[Eck et al. 1998b] Eck, C. R., Cowa, J. J., & Branch, D., 1998, *Astrophysical Journal*, in preparation

[Evans 1983] Evans, R., 1983, *IAU Circ.*, No. 3835

[Evans 1984] Evans, R., 1984, *IAU Circ.*, No. 3979

[Fesen et al. 1989] Fesen, R. A., Hamilton, A. J. S. & Saken, J. M. 1989, *Astrophysical Journal*, 341, L55

[Fesen & Becker 1990] Fesen, R. A. & Becker, R. H. 1990, *Astrophysical Journal*, 351, 437

[Fesen & Matonick 1993] Fesen, R. A. & Matonick, D. M. 1993, *Astrophysical Journal*, 407, 110

[Fesen 1993] Fesen, R. A. 1993, *Astrophysical Journal*, 413, L109

[Fesen 1997] Fesen, R. A. 1997, *BAAS*, 29, 1268

[Filippenko et al. 1995] Filippenko, A. V., Barth, A. J., Bower, G. C., Ho, L. C., Stringfellow, G. S., Goodrich, R. W., & Porter, A. C. 1995, *Astronomical Journal*, 110, 2261

[Gaensler et al. 1997] Gaensler, B. M., Manchester, R. N., Staveley-Smith, L., Tzioumis, A. K., Reynolds, J. E., & Kesteven, M. J. 1997, *Astrophysical Journal*, 479, 845

[Gallouët et al. 1975] Gallouët, L., Heidmann, N., & Dampierre, F. 1975, *Astronomy and Astrophysics Supplement Series*, 19, 1

[Gaskell & Keel 1988] Gaskell, C. M., & Keel, W. C. 1988, in Supernova 1987A in the Large Magellanic Cloud, ed. M. Kafatos & A. Michelitsianos (Cambridge University Press, Cambridge), p. 13

[Goodrich et al. 1989] Goodrich, R. W., Stringfellow, G. S., Penrod, G. D., & Filippenko, A. V. 1989, *Astrophysical Journal*, 342, 908

[Goss et al. 1992] Goss, W. M., Sramek, R. A., & Cowan, J. J. 1992, private communication

[Gottesman et al. 1972] Gottesman, S. T., Broderick, J. J., Brown, R. L., Balick, B., & Palmer, P. 1972, *Astrophysical Journal*, 174, 383

[Green & Gull 1982] Green, D. A., Gull, S. F., 1982, Nature, 299, 606

[Green 1984] Green, D. A., 1984, *Monthly Notices of the Royal Astronomical Society*, 209, 449

[Gull 1973] Gull, S. F. 1973, *Monthly Notices of the Royal Astronomical Society*, 161, 47

[Hartmann et al. 1986] Hartmann, L. W., Geller, M. J., & Huchra, J. P. 1986, *Astronomical Journal*, 92, 1278

[Henry & Branch 1986] Henry, R. B. C., & Branch, D. 1986, *Publications of the Astronomical Society of the Pacific*, 99, 112

[Hodge 1974] Hodge, P. W. 1974, *Astrophysical Journal Supplement Series*, 27, 114

[Hodge et al. 1990] Hodge, P. W., Gurwell, M., Goldader, J. D., & Kennicutt, R. C., Jr. 1990, *Astrophysical Journal Supplement Series*, 73, 661

[Hughes et al. 1998] Hughes, S. M. G., Mingsheng, H., Hoessel, J., Freedman, W. L., Kennicutt, Jr., R. C., Mould, J. R., Saha, A., Stetson, P. B., Madore, B. F., Silbermann, N. A., Harding, P., Ferrarese, L., Ford, H., Gibson, B. K., Graham, J. A., Hill, R., Huchra, J., Illingworth, G. D., Phelps, R. & Sakai, S. 1998, in press

[Hummel et al. 1987] Hummel, E., van der Hulst, J. M., Keel, W. C., & Kennicutt, R. C., Jr. 1987, *Astronomy and Astrophysics Supplement Series*, 70, 517

[Hummel et al. 1991] Hummel, E., Beck, R., & Dettmar, R.-J. 1991, *Astronomy and Astrophysics Supplement Series*, 87, 313

[Hyman et al. 1995] Hyman, S. D., Van Dyk, S. D., Weiler, K. W., & Sramek, R. A. 1995, *Astrophysical Journal*, 443, L77

[Israel et al. 1975] Israel, F. P., Goss, W. M., & Allen, R. J. 1975, *Astronomy and Astrophysics*, 40, 421

[Johnson 1979] Johnson, G. E., 1979, *IAU Circ.*, No. 3348

[Kelson et al. 1996] Kelson, D. D., Illingworth G. D., Freedman, W. F., Graham, J. A., Hill, R., Madore, B. F., Saha, A., Stetson, P. B., Kennicutt, Jr., R. C., Mould, J. R., Hughes, S. M., Ferrarese, L., Phelps, R., Turner, A., Cook, K. H., Ford, H., Hoessel, J. G. & Huchra, J. 1996, ApJ, 463, 26

[Klemola 1986] Klemola, A., 1986, *Publications of the Astronomical Society of the Pacific*, 98, 464

[Lampland 1936] Lampland, C. O., 1936, *Publications of the Astronomical Society of the Pacific*, 48, 320

[Leibundgut et al. 1991] Leibundgut, B., Kirshner, R. P., Pinto, P. A., Rupen, M. P., Smith, R. C., Gunn, J. E. & Schneider, D. P. 1991, *Astrophysical Journal*, 372, 531

[Liller 1990] Liller, W. 1990, IBVS No. 3497

[Livio 1995] Livio, M. 1995, in Millisecond Pulsar: A Decade of Surprise, eds. A. S. Fruchter, M. Tavani, & D. C. Backer, ASP Conference Series, Vol. 72, p. 105

[Long et al. 1989] Long, K. S., Blair, W. P. & Krzeminski, W. 1989, *Astrophysical Journal*, 340, L25

[Lundqvist & Fransson 1988] Lundqvist, P., & Fransson, C. 1988, *Astronomy and Astrophysics*, 192, 221

[Madore & Freedman 1991] Madore, B. F. & Freedman, W. L. 1991, *Publications of the Astronomical Society of the Pacific*, 103, 933

[Matonick & Fesen] Matonick, D. M. & Fesen, R. A. 1997, *Astrophysical Journal Supplement Series*, 112, 49

[Montes et al. 1997] Montes, M. J., Van Dyk, S. D., Weiler, K. W., Sramek, R. A., & Panagia, N. 1997, *Astrophysical Journal*, 482, L61

[Montes et al. 1998] Montes, M. J., Van Dyk, S. D., Weiler, K. W., Sramek, R. A., & Panagia, N. 1998, *Astrophysical Journal*, in press.

[Munari & Renzini 1992] Munari, U., & Renzini, A. 1992, *Astrophysical Journal*, 397, L87

[Mürset et al. 1991] Mürset, U. Nussbaumer, H., Schmidt, H. M., & Vogel, M. 1991, *Astronomy and Astrophysics*, 248, 458.

[Nomoto & Kondo 1991] Nomoto, K., & Kondo, Y. 1991, *Astrophysical Journal*, 367, L19

[Nomoto et al. 1996] Nomoto, K., Iwamoto, K., Suzuki, T., Pols, O. R., Yamaoka, H., Hashimoto, M., Höflich, P., & Van Den Heuvel, E. P. J. 1996, in Compact Stars in Binaries, eds. J. van Paradijs et al., IAU (Netherlands), p. 119

[Panagia et al. 1986] Panagia, N., Sramek, R. A., & Weiler, K. W. 1986, ApJ, 300, L55

[Patat et al. 1994] Patat, F., Barbon, R., Cappellaro, E., & Turatto, M. 1994, *Astronomy and Astrophysics*, 282, 731

[Pennington et al. 1982] Pennington, R. L., Talbot, R. J., & Dufour, R. 1982, *Astronomical Journal*, 87, 1538

[Pennington & Dufour 1983] Pennington, R.L., Dufour, R., 1983, *Astrophysical Journal*, 270, L7

[Perlmutter & Pennypacker 1990] Perlmutter, S., Pennypacker, C., 1990, *IAU Circ.*, No. 4959

[Phillips et al. 1987] Phillips, M. M., et al. 1987, *Publications of the Astronomical Society of the Pacific*, 99, 592

[Phillips et al. 1990] Phillips, M. M., Hamuy, M., Maza, J., Ruiz, M. T., Barney, B. W., & Graham, J. A. 1990, *Publications of the Astronomical Society of the Pacific*, 102, 299

[Phillips 1993] Phillips, M. M. 1993, *Astrophysical Journal*, 413, L105

[Pollas 1988] Pollas, C., 1988, *IAU Circ.*, No. 4691

[Price et al. 1993] Price, R., Gower, A. C., Hutchings, J. B., Talon, S., Duncan, D., & Ross, G. 1993, *Astrophysical Journal Supplement Series*, 86, 365

[Richter & Rosa 1984] Richter, O.-G., & Rosa, M. 1984, *Astronomy and Astrophysics*, 140, L1

[Ripero 1993] Ripero, J., 1993, *IAU Circ.*, No. 5731

[Romanishin 1997] Romanishin, W. 1997, private communication

[Rumstay & Kaufman 1983] Rumstay, K. S., & Kaufman, M. 1983, *Astrophysical Journal*, 274, 611

[Ryder et al. 1993] Ryder, S., Stavely-Smith, L., Dopita, M., Petre, R., Colbert, E., Malin, D., & Schlegel, E. 1993, *Astrophysical Journal*, 416, 167

[Saha et al. 1994] Saha, A., Labhardt, L., Schwengeler, H., Macchetto, F. D., Panagia, N., Sandage, A., & Tammann, G. A. 1994, *Astrophysical Journal*, 425, 14

[Saha et al. 1995] Saha, A., Sandage, A., Labhardt, L., Schwengler, H., & Machetto, F. D. 1995, *Astrophysical Journal*, 438, 8

[Saha et al. 1997] Saha, A., Sandage, A., Labhardt, L., Tammann, G. A., Macchetto, F. D. & Panagia, N. 1997, *Astrophysical Journal*, 486, 1

[Sandage & Tammann 1974] Sandage, A. & Tammann, G. A., 1974, *Astrophysical Journal*, 194, 223

[Sandage & Tammann 1982] Sandage, A. & Tammann, G. A., 1982, *Astrophysical Journal*, 256, 339

[Schaefer 1996] Schaefer, B. E. 1996, *Astrophysical Journal*, 464, 404

[Seaquist & Taylor 1990] Seaquist, E. R., & Taylor, A. R. 1990, *Astrophysical Journal*, 349, 313

[Silbermann et al. 1996] Silbermann, N. A., Harding, P., Madore, B. F., Kennicutt, Jr., R. C., Saha, A., Stetson, P. B., Freedman, W. L., Mould, J. R., Graham, J. A., Hill, R. J., Turner, A., Bresolin, F., Ferrarese, L., Ford, H., Hoessel, J. G., Han. M., Huchra, J., Hughes, S. M. G., Illingworth, G. D., Phelps, R. & Sakai, S. 1996, *Astrophysical Journal*, 470, 1

[Sivan et al. 1990] Sivan, J. -P., Petit, H., Compte, G., & Maucherat, A. J. 1990, *Astronomy and Astrophysics*, 237, 23

[Sonneborn et al. 1987] Sonneborn, G., Altner, B., & Kirshner, R. P. 1987, *Astrophysical Journal*, 323, L35

[Sonneborn et al. 1998] Sonneborn, G., Pun, C. S. J., Kimble, R. A., Gull, T. R., Lundqvist, P., McCray, R., Plait, P., Boggess, A., Bowers, C. W., Danks, A. C., Grady, J., Heap, S. R., Kraemer, S., Lindler, D., Loiacono, J., Maran, S. P., Moos, H. W., & Woodgate, B. E. 1988, *Astrophysical Journal*, 492, L139

[Sramek et al. 1984] Sramek, R. A., Panagia, N., & Weiler, K. W. 1984, *Astrophysical Journal*, 285, L59

[Sramek & Weiler 1990] Sramek, R. A. & Weiler, K. W. 1990, in Supernovae, ed. A. G. Petschek (Berlin, Springer), Chapter 4

[Sramek et al. 1993] Sramek, R. A., Weiler, K. W., Van Dyk, S. D., & Panagia, N. 1993, in Sub-Arcsecond Radio Astronomy, eds. R. J. Davis & R. S. Booth (Cambridge, Cambridge Un. Press), p. 32

[Stathakis & Sadler 1991] Stathakis, R. A., & Sadler E. M. 1991, *Monthly Notices of the Royal Astronomical Society*, 250, 786

[Stockdale et al. 1998] Stockdale, C., et al. 1998, in press

[Tammann & Sandage 1968] Tammann, G. A., & Sandage, A. 1968, *Astrophysical Journal*, 151, 825

[Tully 1988] Tully, R. B. 1988, The Catalog of Nearby Galaxies (Cambridge, Cambridge University Press)

[Turner & Ho 1994] Turner, J. L., & Ho, P. T. 1994, *Astrophysical Journal*, 421, 122

[Turtle et al. 1987] Turtle, A. J., Campbell-Wilson, D., Bunton, J. D., Jauncey, D. L., Kesteven, M. J., Manchester, R. N., Norris, R. P., Storey, M. C., & Reynolds, J. E. 1987, *Nature*, 327, 38

[Utrobin 1984] Utrobin, V. P. 1984, *Ap. Space Sci.*, 98, 115

[van der Hulst et al. 1983] van der Hulst, J. M., Hummel, E., Davies, R. D., Pedlar, A., & van Albada, G. D. 1983, Nature, 306, 566

[Van Dyk 1992] Van Dyk, S. D., *Astronomical Journal*, 103, 1788

[Van Dyk et al. 1992] Van Dyk, S. D., Weiler, K. W., Sramek, R. A., Panagia, N., 1992, *Astrophysical Journal*, 396, 195

[Van Dyk et al. 1993a] Van Dyk, S. D., Sramek, R. A., Weiler, K. W., & Panagia, N. 1993, *Astrophysical Journal*, 409, 162

[Van Dyk et al. 1993b] Van Dyk, S. D., Weiler, K. W., Sramek, R. A., & Panagia, N. 1993, *Astrophysical Journal*, 419, L69

[Van Dyk et al. 1994] Van Dyk, S. D., Weiler, K. W., Sramek, R. A., Rupen, M. P., & Panagia, N. 1994, *Astrophysical Journal*, 432, L115

[Van Dyk et al. 1996] Van Dyk, S. D., Weiler, K. W., Sramek, R. A., Schlegel, E. M., Filippenko, A. V., Panagia, N., & Leibundgut, B. 1996, *Astronomical Journal*, 111, 1271

[Van Dyk 1997] Van Dyk, S. 1997, private communication

[van Gorkom et al. 1986] van Gorkom, J., Rupen, M., Knapp, G, Gunn, J., 1986, *IAU Circ.*, No. 4248

[Weiler & Panagia 1980] Weiler, K.W., Panagia, N, 1980, *Astronomy and Astrophysics*, 90, 269

[Weiler et al. 1983] Weiler, K.W., Sramek, R.A., van der Hulst, J.M., Panagia, N., 1983 in IAU Symposium 101, Supernova Remnants and their X-ray Emission, eds J. Danziger and P. Gorenstein, p 171

[Weiler et al. 1986] Weiler, K. W., Sramek, R. A., Panagia, N., van der Hulst, J. M., & Salvati, M. 1986, *Astrophysical Journal*, 301, 790

[Weiler & Sramek 1988] Weiler, K. W., & Sramek, R. A. 1988, *Annual Review of Astronomy and Astrophysics*, 26, 295

[Weiler et al. 1989] Weiler, K. W., Panagia, N., Sramek, R. A., van der Hulst, J. M., Roberts, M. S. & Nguyen, L. 1989, *Astrophysical Journal*, 336, 421

[Weiler et al. 1990] Weiler, K. W., Panagia, N., & Sramek, R. A. 1990, *Astrophysical Journal*, 364, 611

[Weiler et al. 1991] Weiler, K. W., Van Dyk, S. D., Panagia, N., Sramek, R. A., & Discenna, J. L. 1991, *Astrophysical Journal*, 380, 161

[Weiler et al. 1992a] Weiler, K. W., Van Dyk, S. D., Panagia, N., & Sramek, R. A. 1992a, *Astrophysical Journal*, 398, 248

[Weiler et al. 1992b] Weiler, K. W., Van Dyk, S. D., Pringle, J. E., & Panagia, N. 1992b, *Astrophysical Journal*, 399, 672

[Weiler et al. 1998] Weiler et al. 1998, in preparation

[Wheeler & Harkness 1990] Wheeler, J. C., & Harkness, R. P. 1990, *Rep. Prog. Phys.* 53, 1467

[White & Becker 1992] White, R. L., & Becker, R. H. 1992, *Astrophysical Journal Supplement Series*, 79, 331

[Wild 1980] Wild, P., 1980, *IAU Circ.*, No. 3532

[Wild 1983] Wild, P., 1983, *IAU Circ.*, No. 3803

[Willis et al. 1976] Willis, A. G., Oosterbaan, C. E., de Ruiter, H. R. 1976, *Astronomy and Astrophysics Supplement Series*, 25, 453

[Woosley et al. 1980] Woosley, S. E., Weaver, T. A., & Taam, R. E. 1980, in Type I Supernovae, ed. J. C. Wheeler (Austin, University of Texas Press), p. 96

[Young & Branch 1989] Young, T. R., & Branch, D. 1989, *Astrophysical Journal*, 342, 79

[Yungelson et al. 1995] Yungelson, L., Livio, M., Tutukov, A., & Kenyon, S. J. 1995, *Astrophysical Journal*, 447, 656

[Zhang et al. 1993] Zhang, X., Wright, M., Alexander, P. 1993, *Astrophysical Journal*, 418, 100

Appendix A

Derivation of the Chevalier Model Luminosity

Starting with the expression for the intensity of synchrotron radiation resulting from a relativistically moving, homogeneous, and isotropic distribution of electrons, I will show a derivation of Chevalier's (1982b) expression for the radio luminosity originating from a shock encountering a shell of circumstellar material and using the assumptions stated in Chapter 1.

The expression for the intensity of this type of synchrotron radiation is

$$I_\nu = Kl\alpha(\gamma)\frac{\sqrt{3}}{8\pi}\frac{e^3}{m_e c^2}\left[\frac{3e}{4\pi m_e^3 c^5}\right]^{(\gamma-1)/2} H_\perp^{(\gamma+1)/2}\nu^{-(\gamma-1)/2},$$

where K is from $N(E)dE = KE^{-\gamma}dE =$ the power law spectrum for the number of electrons of charge e per unit volume per steradian moving along the line-of-sight towards the observer with an energy between E and $E + dE$. The function $\alpha(\gamma)$ is a weakly varying function of γ, the electron spectral index, of order 1. $H_\perp$ is the component of H along the line of sight and l is the length of the column of electrons

along the line-of-sight. ν is the frequency of radiation and m_e is the mass of an electron.

If the total energy density, $u_{\rm tot}$, is constant then

$$u_{\rm tot} = u_e + u_H = \text{constant},$$

where u_e and u_H are the electron energy densities and magnetic energy densities, respectively. The assumption of equipartition says that

$$u_e = \frac{4}{3} u_H,$$

and substitution into the expression for $u_{\rm tot}$ implies

$$u_{\rm tot} = \frac{4}{3} u_H + u_H = \frac{7}{3} u_H.$$

Now, the expression for the magnetic energy density is

$$u_H = \frac{1}{8\pi} H^2,$$

so the expression for the total energy density becomes

$$u_{\rm tot} = \frac{7}{24\pi} H^2.$$

Recall for a gas of relativistic particles,

$$u_{\rm tot} = 3P,$$

where P is the pressure of the gas. Since the the synchrotron radiation originates at the shock front, and if we assume the thickness of the shock is negligible compared to the distance from the SN, we can use Chevalier's (1982b) expression for the pressure at the outside of the shock front, P_1. Chevalier's self-similar solutions reveal that

$$P_1 = \frac{q}{R^2} \dot{R}^2,$$

where

$$q = \frac{\dot{M}}{4\pi v_w},$$

and R is the radius of the shock front, found by Chevalier to have a time dependence of

$$R = A\, t^{(n-3)/(n-2)},$$

where $A \propto (U^n/q)^{1/(n-2)}$. Recall that U is a parameter that depends on the density of the supernova ejecta at a given ejecta speed, and n is the index for the power law density profile ($\rho_{SN} \propto r^{-n}$). Taking the derivative of R ...

$$\dot{R} \propto \frac{n-3}{n-2}\, t^{-\frac{1}{(n-2)}}.$$

Substitution of R and $\dot{R}$ into the expression for the pressure, it is found that ...

$$P_1 = q\left(\frac{n-3}{n-2}\right)^2 t^{-2} = q\, m^2 t^{-2},$$

where $m = (n-3)/(n-2)$. Equating the two expressions for $u_{\rm tot}$ ...

$$u_{\rm tot} = \frac{7}{24\pi} H^2 = 3P_1 = 3\, q\, m^2 t^{-2}.$$

Solving this equation for H in terms of t ...

$$H = \left(\frac{72\pi}{7}\, q\, m^2 t^{-2}\right)^{1/2} = \left(\frac{72\pi}{7}\, q\right)^{1/2} m\, t^{-1}.$$

Using this expression for H into the expression for the synchrotron intensity implies

$$I_\nu = K l \alpha(\gamma) \frac{\sqrt{3}}{8\pi} \frac{e^3}{m_e c^2} \left[\frac{3e}{4\pi m_e^3 c^5}\right]^{(\gamma-1)/2} \left(\frac{72\pi}{7}\, q\, m^2 t^{-2}\right)^{(\gamma+1)/4} \nu^{-(\gamma-1)/2}.$$

BUT since K is in units of $\left[\frac{\#\,\text{electrons}}{\text{cm}^3}\ \text{erg}^\gamma\right]$, we are not in the right units for intensity. We need to multiply the expression for I_ν by the average energy per electron, u_e. The

expression for u_e in terms of H is

$$u_e = \frac{4}{3} u_H = \frac{1}{6\pi} H^2.$$

If we multiply this expression for u_e by I_ν, we get

$$I_\nu = K l \alpha(\gamma) \frac{\sqrt{3}}{8\pi} \frac{e^3}{m_e c^2} \left[\frac{3e}{4\pi m_e^3 c^5} \right]^{(\gamma-1)/2} \left(\frac{72\pi}{7} q\, m^2 t^{-2} \right)^{(\gamma+1)/4} \frac{H^2}{6\pi} \nu^{-(\gamma-1)/2},$$

or

$$I_\nu = K l \alpha(\gamma) \frac{\sqrt{3}}{8\pi} \frac{e^3}{m_e c^2} \left[\frac{3e}{4\pi m_e^3 c^5} \right]^{(\gamma-1)/2} \left(\frac{72\pi}{7} q\, m^2 t^{-2} \right)^{(\gamma+5)/4} \frac{1}{6\pi} \nu^{-(\gamma-1)/2}.$$

Now the luminosity for radiation of intensity I_ν, at a the distance of the shell, R, is (l is now also equivalent to R)

$$L_\nu = 4\,\pi R^2 (\pi\, I_\nu)^2,$$

$$L_\nu \propto R^3 \left(q\, m^2 t^{-2} \right)^{(\gamma+5)/4} \nu^{-(\gamma-1)/2}.$$

To get the dependence of the luminosity on the mass-loss rate we eliminate R, using its time dependence and substituting for the constant A,

$$L_\nu \propto \left[U^{n/(n-2)} q^{-1/(n-2)} t^m \right]^3 \left(q\, m^2 t^{-2} \right)^{(\gamma+5)/4} \nu^{-(\gamma-1)/2},$$

$$L_\nu \propto (U^n)^{3(1-m)} q^{(12m-7+\gamma)} m^{(\gamma+5)/2} t^{-(\gamma+5-6m)/2} \nu^{-(\gamma-1)/2},$$

and then eliminate q, ...

$$L_\nu \propto (U^n)^{3(1-m)} (\dot{M}/v_w)^{(12m-7+\gamma)} m^{(\gamma+5)/2} t^{-(\gamma+5-6m)/2} \nu^{-(\gamma-1)/2}.$$

QED.

Appendix B

Description of Radio Analyses

This section will give some of the basic information on each SN and describe the analysis of each radio map, including possible identifications of any non-SN sources present when possible. The data for the non-SN sources are summarized in Table B.1.

SN 1885A Discovered in the nearby galaxy NGC 224 (M 31), SN 1885A is an SN I pec and has a position according to NED at $\alpha(1950) = 00^{h}40^{m}00^{s}.1$ and $\delta(1950) = +40°59'42''.8$ with a large uncertainty of 150″ (see explanation in the section on SN 1909A for why the uncertainty is so large), but this is not representative of the actual uncertainty. The SN position calculated via offsets from the galaxy center is consistent to within about 5″ of the NED position, so I assume a little more uncertainty to be safe and adopt a (typical) value of 10″ as representative of the uncertainty in the SN position (see the section on SN 1909A).

Details of the observations and data reduction can be found in Crane et al. (1992). Since a radio map was unavailable for independent analysis, the rms noise level (and upper limit) are quoted from Crane et al. (1992).

Crane et al. (1992) report no detection of radio emission from SN 1885A with a 3σ upper limit at 20 cm of 0.015 mJy.

SN 1895B This SN was discovered by Fleming in March in NGC 5253 and is classified as an SN Ia. It has a NED position at $\alpha(1950) = 13^h37^m06\overset{s}{.}6$ and $\delta(1950) = -31°23'01''$. The positions reported for this SN from various sources (Sternberg Astronomical Catalog, NED) are consistent to within 10″ of the position as determined via offsets from the center of the galaxy so I use this is representative of the uncertainty in SN position.

Details of the observations and data reduction can be found in Cowan & Branch (1982) and Branch & Cowan (1985). Since a radio map was unavailable for independent analysis, I quote the rms noise levels and upper limits from those papers.

I report no detection of radio emission from SN 1895B with 3σ upper limits at 20 cm of 0.9 and 0.15 mJy for the 1981 and 1983 observations, respectively.

SN 1909A SN 1909A is classified as a Type II, and proposed as a Type II-P by Young & Branch (1989), occurring in the spiral galaxy NGC 5457 (M 101). It was discovered by Wolf in late January, 1909 with a position given by NED to be $\alpha_{1950} = 14^h00^m17\overset{s}{.}2$ and $\delta_{1950} = +54°42'22''$ and a large [1] uncertainty of $150'' \times 150''$

Normally, one could adopt the uncertainty in the galaxy center as representative of the uncertainty of the SN, since the SN position is usually computed by offsets

[1]Communication with NED reveals the reason for the large uncertainty in the position. NED uses uncertainty in the galaxy center as the uncertainty in the SN position (since the SN position is computed via offsets from the galaxy center). For galaxies whose centers are not well-determined, the uncertainty is listed at one arcminute and NED uses this value at the 95% confidence level, 150″ in this case, for the SN uncertainty.

from the galaxy center. Since the SN position as determined by offsets is inconsistent with the SN position given by NED, I cannot adopt the uncertainty in the galaxy center for the positional uncertainty of the SN. I adopt an uncertainty of 10″ and acknowledge that it may be greater than this due to the lack of accurate positions available at the time of SN discovery.

A radio map of the region near the SN site is visible in Figure B.1. The map had some ringing in it despite a low noise level of 0.0114 mJy. There are no obvious sources in the map but a deep search of the area in the map near the SN position reveals a 4σ "source" about 6″ from the reported SN position. Since negative contours are still visible at the 3σ level, one cannot say much beyond the possibility that this source might be SN 1909A. A better astrometric position and a deeper radio map would be needed to confirm or exclude the possibility that this is from SN 1909A.

Brown & Marscher (1978) report upper limits to detection of radio emission from the site of SN 1909A at a 3σ level of 4 mJy at 8.085 GHz.

I report no detection of radio emission from the site of SN 1909A with a 3σ upper limit of 0.0343 mJy at 6 cm.

SNe 1921B and 1921C SN 1921B was discovered by Zwicky and Hubble in April and classified as an SN II, while SN 1921C was discovered by Jones with a maximum in December, 1921 and classified as an SN I. Both SNe are found in the spiral galaxy NGC 3184, whose positions from various references are consistent. NED reports positions for these SNe at $\alpha(1950) = 10^{h}15^{m}17^{s}.2$, $\delta(1950) = +41°37'20''$ and $\alpha(1950) = 10^{h}15^{m}23^{s}.7$, $\delta(1950) = +41°36'04''$ for SNe 1921B and 1921C, respectively. This is inconsistent with the positions for these SNe as determined via offsets from

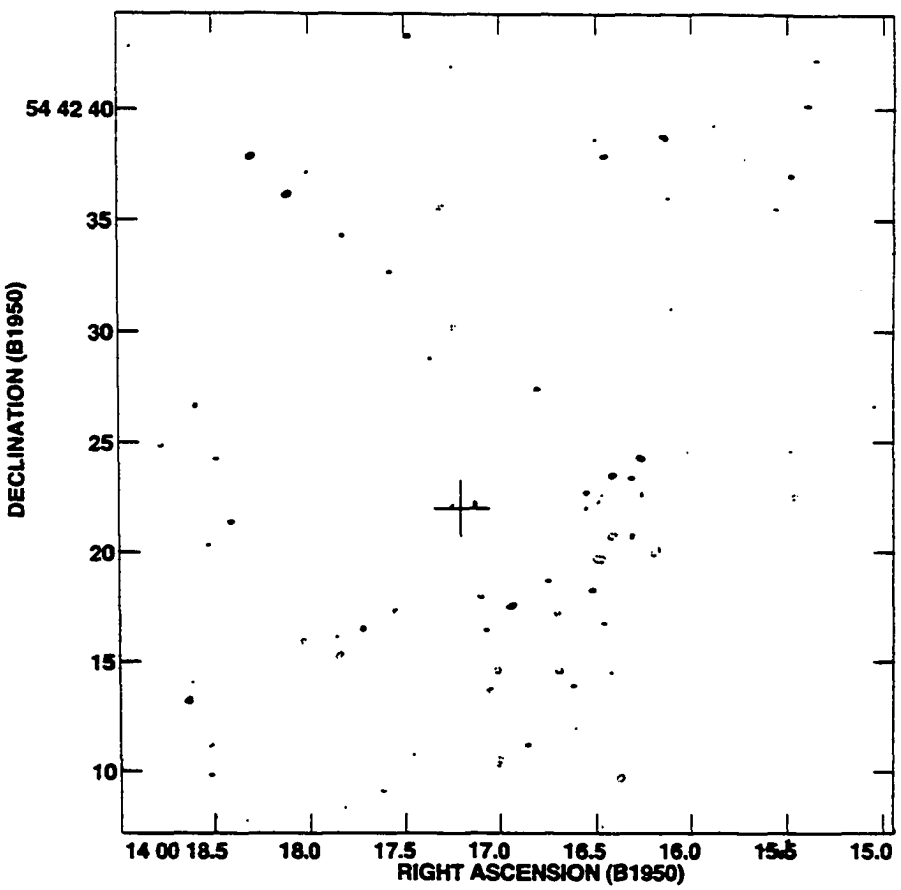

Figure B.1: A (6 cm) contour map of the region immediately surrounding the site of SN 1909A. The (NED) SN position is denoted by a cross whose bars are 2.″5 from one side to the other. The contour levels are -0.037, 0.037, 0.043, 0.049, 0.055, and 0.061 mJy beam^{-1} and the rms noise level is 0.011 mJy beam^{-1}.

the galaxy center. Assuming the position for the galaxy center is correct, an error has probably occurred in NED since the relative differences in NED positions are the same as the relative differences in offsets. I adopt an uncertainty of 10″ for each SN since the NED uncertainty is reported at 150″.

Details of the observations and data reduction can be found in Branch & Cowan (1985). Since a radio map was unavailable for independent analysis, I quote the rms noise level and upper limit from this paper. Branch & Cowan (1985) report the detection of a 0.5 mJy source (3σ); however they report the source 24″ from the astrometrically determined position (from M. Liller and C. Y. Shao) of SN 1921C ($\alpha(1950) = 10^h15^m24\overset{s}{.}1$, $\delta(1950) = +41°36'34\overset{''}{.}1$). The low signal-to-noise level and the distance of the source from the position of SN 1921C make it improbable that this is radio emission from SN 1921C.

No detection is reported of radio emission from SNe 1921B and 1921C with a 3σ upper limit of 0.51 mJy at 20 cm.

SN 1923A Details on this SN and the analysis of the radio maps are found in Chapter 1.

SN 1937C The Type Ia SN 1937C was discovered by Zwicky and had a maximum on August 23, 1937. The position, given by NED is $\alpha(1950) = 13^h03^m33\overset{s}{.}1, \delta(1950) = +37°53'10''$ with an uncertainty of 150″ × 150″. Since the uncertainty for the galaxy center reported by NED is rather small (2″.5 × 2″.0) I adopt an uncertainty of 3″ as representative of the uncertainty for the SN position. The parent galaxy, IC 4182, is classified as an Sm (spiral irregular) and has a Cepheid distance of 4.7 Mpc (Saha et

al. 1994) which compares with Tully's (1988) distance of 4.4 Mpc.

A radio map of the region near the SN site can be seen in Figure B.2. Although no sources were visible in the radio map near the SN position, two prominent sources were visible in the middle west side of the field of view. The peak fluxes for the sources designated α and δ are 0.38 and 1.1, respectively. The field of view coincides with a portion of the sky covered by the Faint Images of the Radio Sky at Twenty-centimeters (FIRST) (Becker et al. 1995) survey underway at the VLA in B array. The survey is at 1.4 GHz with noise level of 0.15−0.2 mJy for most maps. The FIRST survey detects two sources whose positions lie within 2.″5 and 1.″0 of sources α and δ, respectively. Both the shape of the emission regions and the observed fluxes are somewhat different, however, when compared to these observations, but the FIRST observations were made in a different VLA configuration (B array) with a different beamsize. I believe the two sources observed by the FIRST survey coincide with our sources α and δ.

No other obvious attempts to observe this galaxy at the VLA were found.

A Westerbork Synthesis Radio Telescope survey conducted by Willis, Oosterbaan & de Ruiter (1976) at 1.415 GHz observed a source whose position is within 3″ of source α and 11″ of source β. It seems likely that the first Westerbork source and source α are the same, although the peak flux reported by Willis et al. is almost 19 mJy.

No IRAS sources were found to lie near these source positions.

I report no detection for radio emission from the site of SN 1937C at an age of 48.7 years. The rms noise level is measured at 0.0332 mJy so the 3σ upper limit is to detection is 0.0996 mJy.

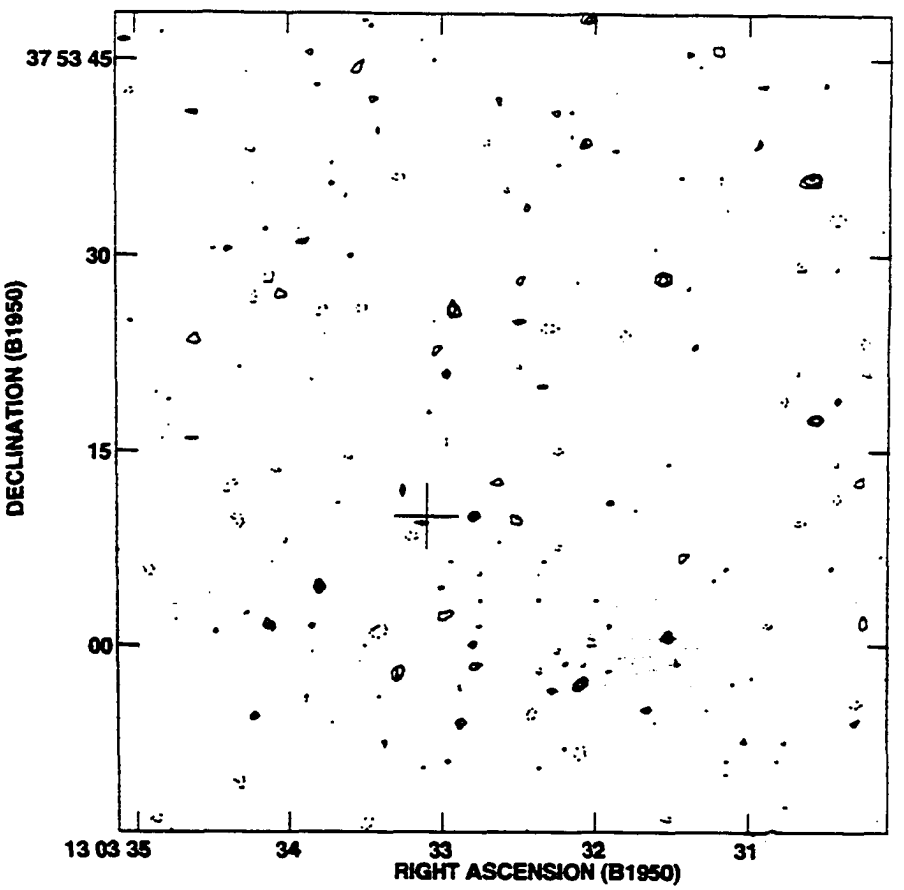

Figure B.2: A (20 cm) contour map of the region immediately surrounding the site of SN 1937C. The (NED) SN position is denoted by a cross whose bars are 5″ from one side to the other. The contour levels are −0.079, 0.079, 0.10, 0.14, 0.17, and 0.26 mJy beam^{-1} and the rms noise level is at 0.033 mJy beam^{-1}.

SN 1937F This SN is classified as an SN II found in NGC 3184 by Zwicky and Jones in December, 1937. Its NED position is at $\alpha(1950) = 10^h15^m17^s.2$ and $\delta(1950) = +41°37'31''$. I adopt a positional uncertainty of 10″ for this SN.

See discussion on SNe 1921B and 1921C for a discussion on the analysis of the radio map for this SN.

No detection is reported of radio emission from SN 1937F with a 3σ upper limit of 0.51 mJy at 20 cm.

SN 1945B This SN is of an unknown type and was discovered on archival plates only recently by Liller (1990). It resides in the spiral NGC 5236 whose center is a matter of some debate. NED reports the center of NGC 5236 at $\alpha(1950) = 13^h34^m11^s.6$ and $\delta(1950) = -29°36'42''$, which differs slightly from the position of the radio peak at the center of the galaxy. The position for SN 1945B is reported by NED at $\alpha(1950) = 13^h34^m02^s.8$ and $\delta(1950) = -29°39'43''$. Unfortunately, this is somewhat different from the position as calculated via offsets from the galaxy center from NED. If I use a position for the galaxy center from Gallouët, Heidmann, & Dampierre (1975), the positions (NED and via offsets) match up exactly. I adopt an uncertainty in SN position of 10″ since NED reports it at 150″.

Details of the analysis of the radio maps has been reported by Cowan & Branch (1985) and CRB. No detection was reported of SN 1945B at any of the epochs or wavelengths (see Table 5.1).

SN 1950B Discovered by Haro in March, this SN is of an unknown type but it is strongly suspected to be an SN II. It resides in NGC 5236 whose position is of

some debate (see SN 1945B in the same galaxy). SN 1950B has a NED position at $\alpha(1950) = 13^h34^m03^s.7$ and $\delta(1950) = -29°36'39''$. This position is different from the position calculated using offsets from the galaxy center by about $0^s.5$ in α and $3''$ in δ, which is close to the difference between the NED galaxy position and the one quoted by CRB. I adopt the NED uncertainty ($2''$) as representative of the SN positional uncertainty since the radio position from CRB is likely to be more certain than $10''$.

The analysis of the radio maps for this SN have been discussed in Cowan & Branch (1985) and CRB and summarized in Chapter 1.

This SN was revealed as a radio source at all wavelengths and epochs (see Table 5.1).

SN 1951H This SN was discovered by Humason in the spiral galaxy NGC 5457 (M 101) and classified as an SN II. Although discovered in Feb. 1951, it is guessed that the optical maximum had actually occurred in October 1950 (Sandage & Tammann 1974). Its position according to NED is at $\alpha(1950) = 14^h02^m07^s.2$ and $\delta(1950) = +54°36'21''$, but this is somewhat inconsistent with the position ($\alpha(1950) = 14^h02^m06^s.6$ and $\delta(1950) = +54°36'03''$) as determined by offsets from the NED position for the galaxy center and with the position given by the Sternberg Astronomical Institute Supernova Catalog [$\alpha(1950) = 14^h02^m09^s.4$ and $\delta(1950) = +54°36'02''$]. While NED reports the uncertainty in SN position at $150'' \times 150''$, it is certainly less than that (see footnote on SN 1909A) but it is not certain how much the uncertainty is. I adopt a positional uncertainty of $10''$ but acknowledge that it may be more than this.

I re-reduced the radio observations of this SN (with the permission of W. M. Goss)

recently and found the noise level to be at 0.0145 mJy / beam^{-1}. A radio map of the region near the site of SN 1951H is in Figure B.3. I confirm the original observations from Goss, Sramek, & Cowan (1992) that no signal from this SN is detected at this age. Goss et al. (1992) report 20 cm observations of SN 1951H by Skillman also with no detection. Brown & Marscher (1978) also report 8.085 GHz observations of SN 1951H with an upper limit of 4 mJy.

A map of the eastern region of M 101 (also containing the site of SN 1951H) can be seen in Figure B.4. Prominent features include emission regions from the H II regions NGC 5461 & 5462. Superposition of the radio map with Hα maps found in Israel, Goss, & Allen (1975) reveals that sources κ, η, ϕ, and χ in NGC 5461 lie over Hα emission regions. The same positional coincidence is found for γ, ϵ, δ, β and α in NGC 5462. All of these are probable H II regions. The positions of these sources can be compared to H II regions observed by Hodge et al. (1990). I find that π, η, ϕ, γ, ϵ and α have peak positions that are within the uncertainties for the H II regions. In addition, λ, κ, χ, δ, β and θ have peak positions within twice the uncertainties of a particular H II region. The Hodge et al. (1990) data indicate that these sources *may* be H II regions.

Both comparisons indicate that κ, η, ϕ, χ, π, γ, ϵ, δ, β and α are all probable H II regions.

Comparison with SNRs in M 101 from Matonick & Fesen (1997) shows no SNRs coincident with positions of any of the sources in the eastern region of M 101.

I report no detection of 20 cm radio emission from the site of SN 1951H with a 3σ upper limit of 0.044 mJy beam^{-1}.

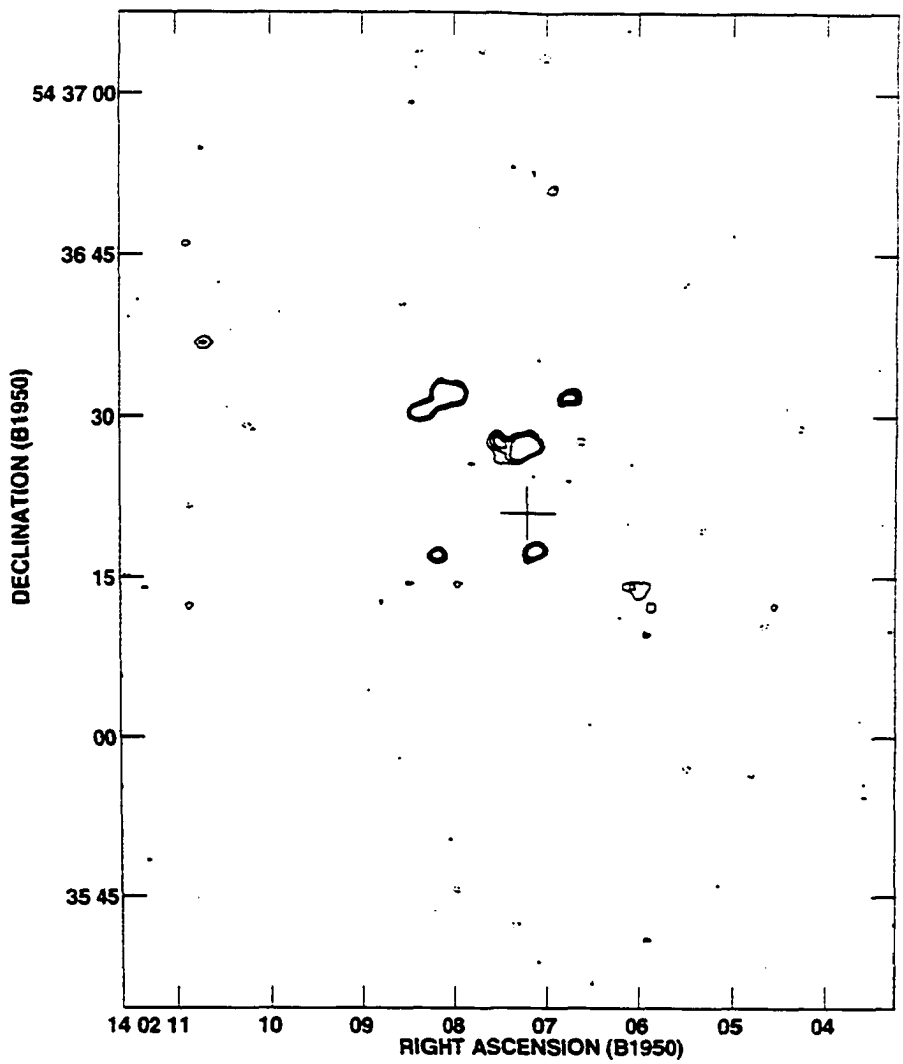

Figure B.3: A (20 cm) contour map of the region immediately surrounding the site of SN 1951H. The (NED) SN position is denoted by a cross whose bars are 5″ from one side to the other. The contour levels are −0.044, 0.058, and 0.073 mJy beam^{-1} and and the rms noise level is 0.15 mJy beam^{-1}.

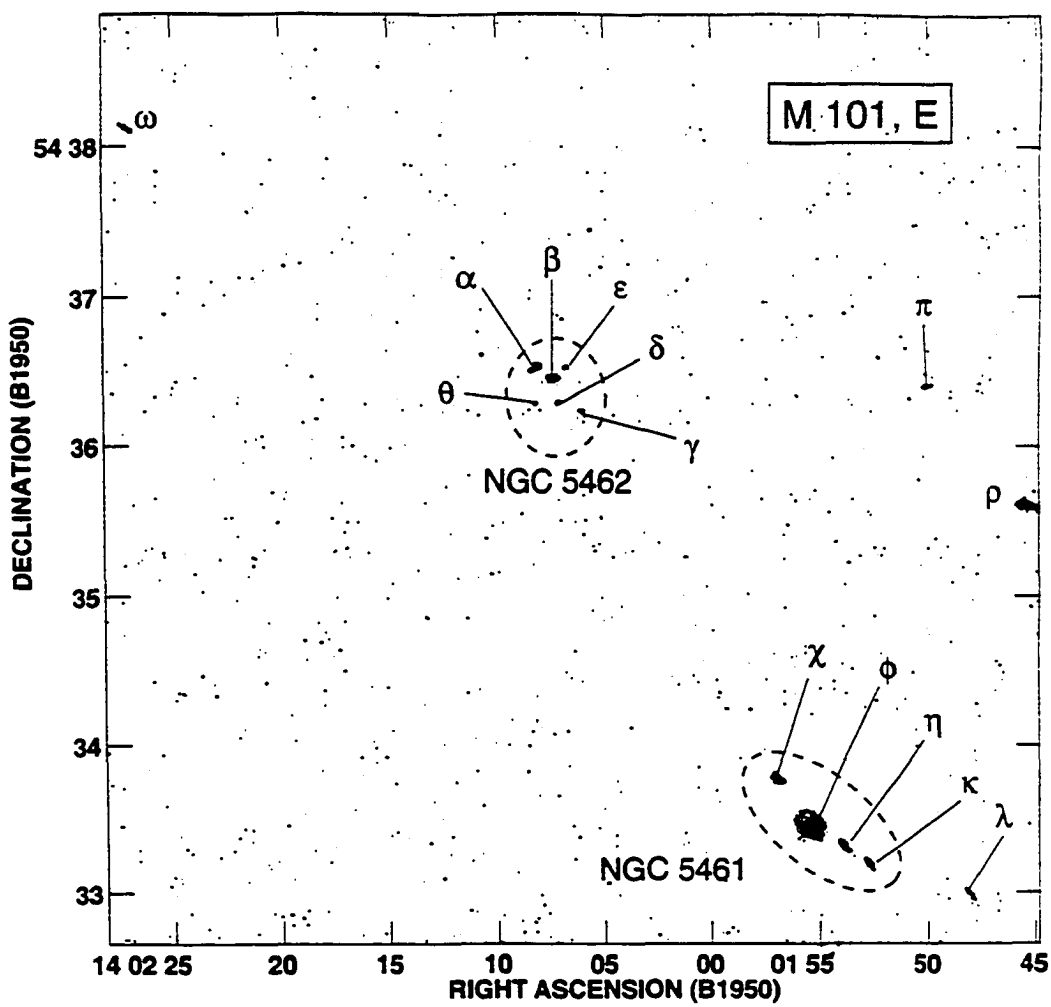

Figure B.4: A contour map of part of the field of view for the eastern region of NGC 5457 (M 101) at 20 cm, labeled as in Table B.1. Clearly visible are the (circled) emission regions associated with NGC 5461 and NGC 5462. The contour levels are at 0.043, 0.064, 0.086, 0.13, 0.21, 0.43, 0.64 and 0.85 mJy beam^{-1} and the rms noise is 0.015 mJy beam^{-1}.

SN 1954A SN 1954A is classified as a Type Ib SN residing in NGC 4214, a nearby irregular that may have interacted via a merger or collision with another small system or gas cloud(s) (Hartmann, Geller, Huchra 1986). Discovered by Wild it was observed at maximum light on April 19 with a position at $\alpha_{1950} = 12^h13^m15\overset{s}{.}2$ and $\delta_{1950} = +36°32'54''$. I adopt the uncertainty in the galaxy center as representative of the uncertainty in SN position, $2'' \times 2''$, since the SN uncertainty according to NED ($150'' \times 150''$) is not representative of the actual uncertainty in SN position (see SN 1909A).

A radio map of the region near the SN site is in Figure B.5. While no radio source is visible near the SN position at a level greater than 3σ, there are more than 8 regions in the field of view clearly showing radio emission. A map of these sources can be seen in Figure B.6. One of these sources, labeled η in the map, seems to be a complex of at least 6 smaller sources. Using an Hα map of the galaxy provided by Van Dyk (1997) and superposing the radio map with it, I can attempt to identify probable H II regions. Sources α, β, γ, ϵ and η have excellent positional coincidences with Hα emitting regions and are all probably H II regions. Hartmann et al. (1986) list positions of H II regions, and their source H59 lies $3''$ from the peak position of source ρ. This source is likely to be an H II region. In addition, the Hartmann et al. (1986) source H48 lies $3''$ from the strongest source in the η complex. H54 & H55 lie close ($5\overset{''}{.}5$ and $2''$, respectively) to the peak positions of β and α to make their identification probable.

I report no detection of radio emission from the site of SN 1954A at 20 cm with an rms noise level of 0.0218 mJy and a 3σ upper limit of 0.0653 mJy.

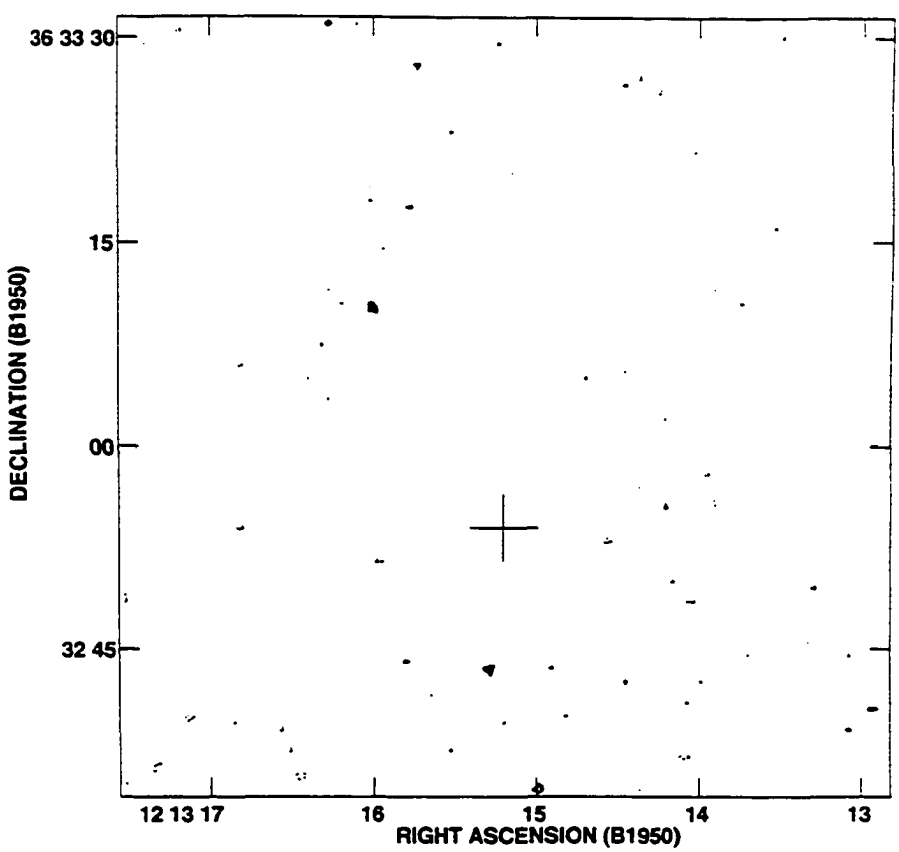

Figure B.5: A (20 cm) contour map of the region immediately surrounding the site of SN 1954A. The (NED) SN position is denoted by a cross whose bars are 5″ from one side to the other. The contour levels are −0.060, 0.066, 0.086, 0.11, 0.13, and 0.20 mJy beam^{-1} and the rms noise level is 0.022 mJy beam^{-1}.

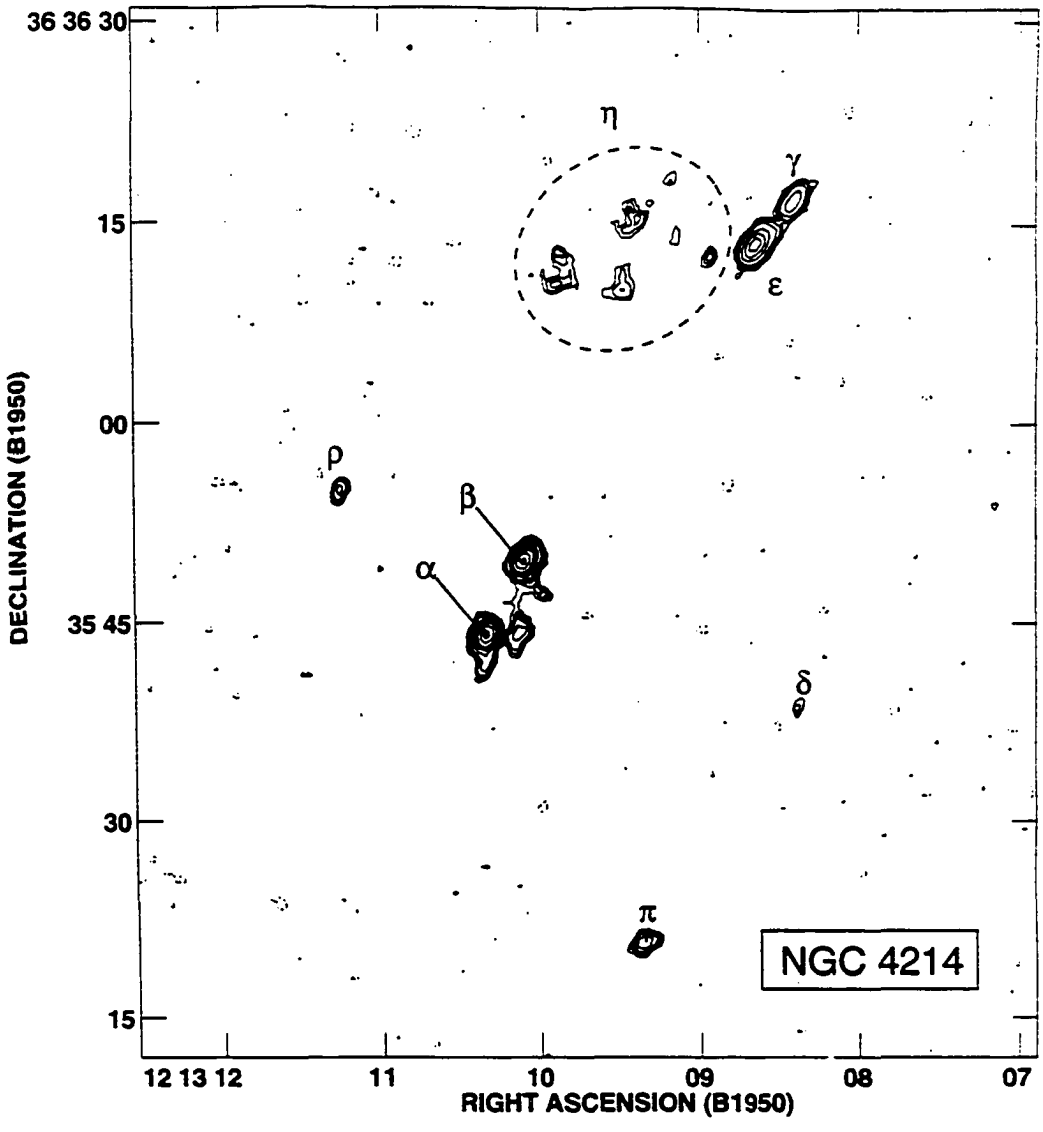

Figure B.6: A contour map of part of the field of view for NGC 4214 at 20 cm, labeled as in Table B.1. The sources that appear to be a part of a larger complex are circled and labeled η. Sources α, β, γ and η are all likely to be H II regions (see text). Contour levels are at -0.053, 0.066, 0.083, 0.099, 0.13, 0.20, 0.27, 0.33, 0.47, 0.60 and 0.66 mJy beam^{-1} and the rms noise is 0.022 mJy beam^{-1}.

SN 1954J Discovered by Zwicky in October 1954, SN 1954J is classified as a Zwicky Type V supernova, similar in type to the intermediate age SN 1961V. It resides in the spiral galaxy NGC 2403 and has a reported position according to NED at $\alpha_{1950} = 07^h32^m08^s, \delta_{1950} = +65°44'.4$ with a rather large uncertainty ($150'' \times 150''$) The Asiago Supernova Catalogue lists the position of the supernova (via offsets) at $\alpha_{1950} = 07^h32^m05^s.8, \delta_{1950} = +65°44'40''$ and does not report an uncertainty for the position.

I can derive my own estimate for the SN position. By examining a photograph of NGC 2403 in the Atlas of Galaxies (NASA) that contains the SN clearly visible in it, I compare the distances from the supernova, in the NASA photograph, to visible H II regions in the same photograph. These H II regions can be matched to H II regions whose positions are known from observations made by Sivan, Petit, Compte & Maucherat (1990). By using the scale in each map to measure the distance from each H II region, I can make my own estimate of the supernova position. Performing this procedure relative to 3 different H II regions I get positions that are consistent with each other to within $0^s.5$ and $10''$. The average location is $\alpha(1950) = 07^h32^m06^s.3, \delta(1950) = +65°44'33''.7$.

All three SN positions (NED, Asiago, Eck) are within $25''$ of each other.

One final method to estimate the uncertainty of SN 1954J is to use the published (NED) uncertainty of the galaxy center ($10'' \times 10''$). The uncertainty for the SN must be comparable to the uncertainty of the galaxy center if I use the Asiago offsets to locate the SN. A map of the region near the SN site is in Figure B.7. Some ringing is visible in the map at the 4σ level.

Although the distance to NGC 2403 is reported by Tully (1988) to be 4.2 Mpc.

Cepheid observations in this galaxy (see Table 5.2) place the distance at 3.18 Mpc. While reported to be a supernova event, there is very little evidence to show that the outburst associated with SN 1954J was due to a supernova explosion. The only data available from the outburst is a light curve from Tammann & Sandage (1968) which yields $M_{B,max} = -11$, using the Cepheid distance modulus. It is even suggested by Tammann & Sandage that the outburst is an η Car type object (SN 1961V is also believed to be similar to η Car (Goodrich et al 1989)).

Turner & Ho (1994) report 6 cm radio observations of NGC 2403, including 7 sources whose positions lie within 1″ to 5″ of a corresponding source found in this 20 cm map. However, spectral index calculations were not possible since none of the mutually observed sources had the same beamsize and none were unresolved. Examination of integrated fluxes reveals that source β is consistent with thermal emission.

A map of H II regions from Sivan et al. (1990) superimposed onto our radio map reveals that β lies directly over a group of H II regions (including No. 293 in Sivan et al. 1990). Source β is likely a group of H II regions. The same positional coincidence with a radio source and H II region is found for sources γ, δ, ϵ, ρ, θ, ω, η, χ and ξ. They are likely H II regions as well. I find that the luminosities of these sources is comparable to H II regions identified in CRB.

Comparison with reported SNRs in NGC 2403 by Matonick et al. (1997) reveals that source μ has a peak position very close to that of SNRs No. 6 & 7. At a distance of 3.2 Mpc to NGC 2403 (see Table 5.2), μ is about 50 pc from both SNRs No. 6 & 7. Since SNR No. 7 has a reported diameter of 60 pc, it is very possible that μ is identified with this SNR. More radio observations are recommended to confirm this

identification.

With an rms noise of 0.117 mJy, I detect 15 sources, with peak fluxes greater than 5σ, whose positions and fluxes are listed in Table B.1. A map of the galaxy can be seen in Figure B.8.

9 sources in the radio map lie within the large NED uncertainty for this SN—sources ρ, β, γ, π, δ, θ, μ, ϵ, and ω. Of these, only π and μ remain unidentified. None of the sources lie between the 3 positions (NED, Asiago, Eck) for SN 1954J or within 10″ of the NED SN position. I then conclude that *none* of the sources are from the outburst of SN 1954J. Using a 3σ detection threshold, I measure the upper limit for detection to be 0.351 mJy at 31 years past outburst.

Brown & Marscher (1978) report a 3σ upper limit of 4 mJy at 11 cm (2.695 GHz) from the site of this SN at 18 years past outburst.

SN 1957D This SN also resides in NGC 5236 and was discovered by Gates in December, 1957. See the sections on SNe 1945B and 1950B for a discussion of the position for the galaxy center. This SN is of an unknown type but is suspected to be an SN II (e.g., CRB). Its NED position is at $13^{h}34^{m}14\overset{s}{.}4$ and $\delta_{1950} = -29°34'24\overset{''}{.}3$. As for SN 1950B, the position calculated via offsets is off by almost exactly the difference between galaxy centers found from Cowan & Branch (1985) and the NED position. I adopt the NED uncertainty (2″) since there is a radio position from CRB (see the section on SN 1950B).

The analysis of the radio maps for this SN have been discussed in Cowan & Branch (1985) and CRB (where the detections at all epochs and wavelengths are described) and summarized in Chapter 1.

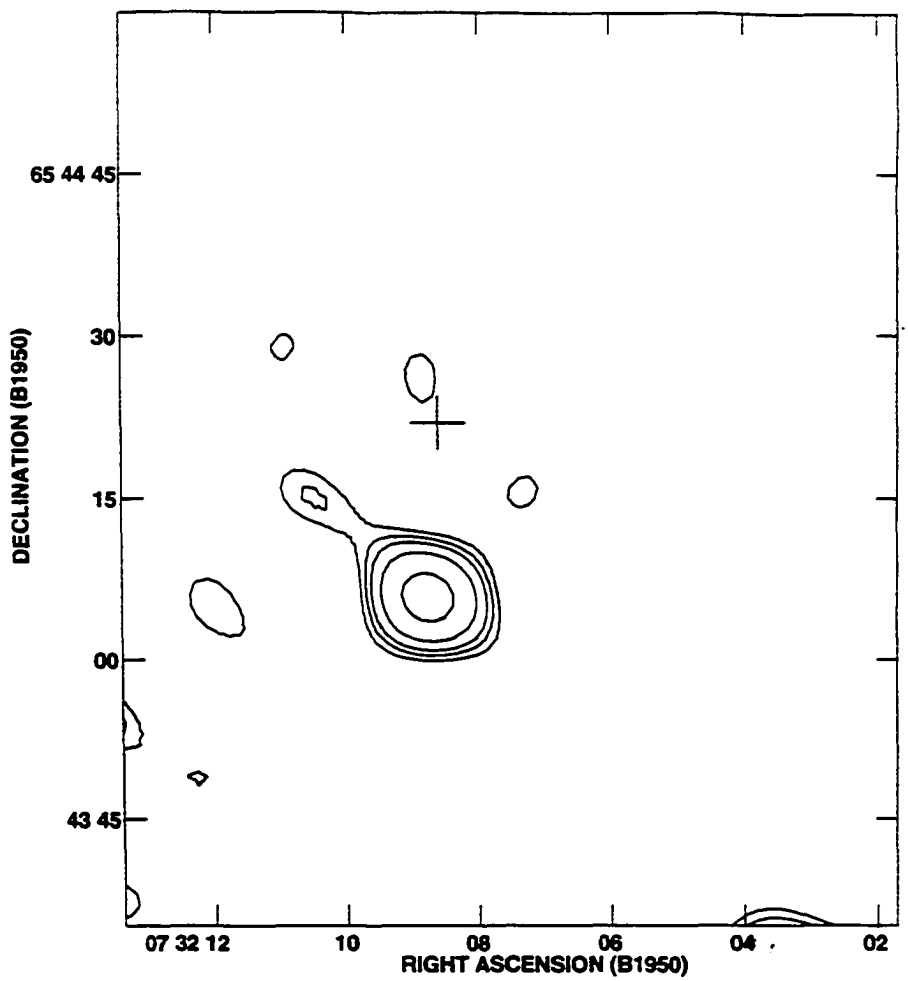

Figure B.7: A (20 cm) contour map of the region immediately surrounding the site of SN 1954J. The (NED) SN position is denoted by a cross whose bars are 5″ from one side to the other. Source γ is visible in the center of the map. The contour levels are -0.47, 0.47, 0.59, 0.70, 0.94, 1.4, 1.9, and 2.3 mJy beam^{-1} and the rms noise level is 0.12 mJy beam^{-1}.

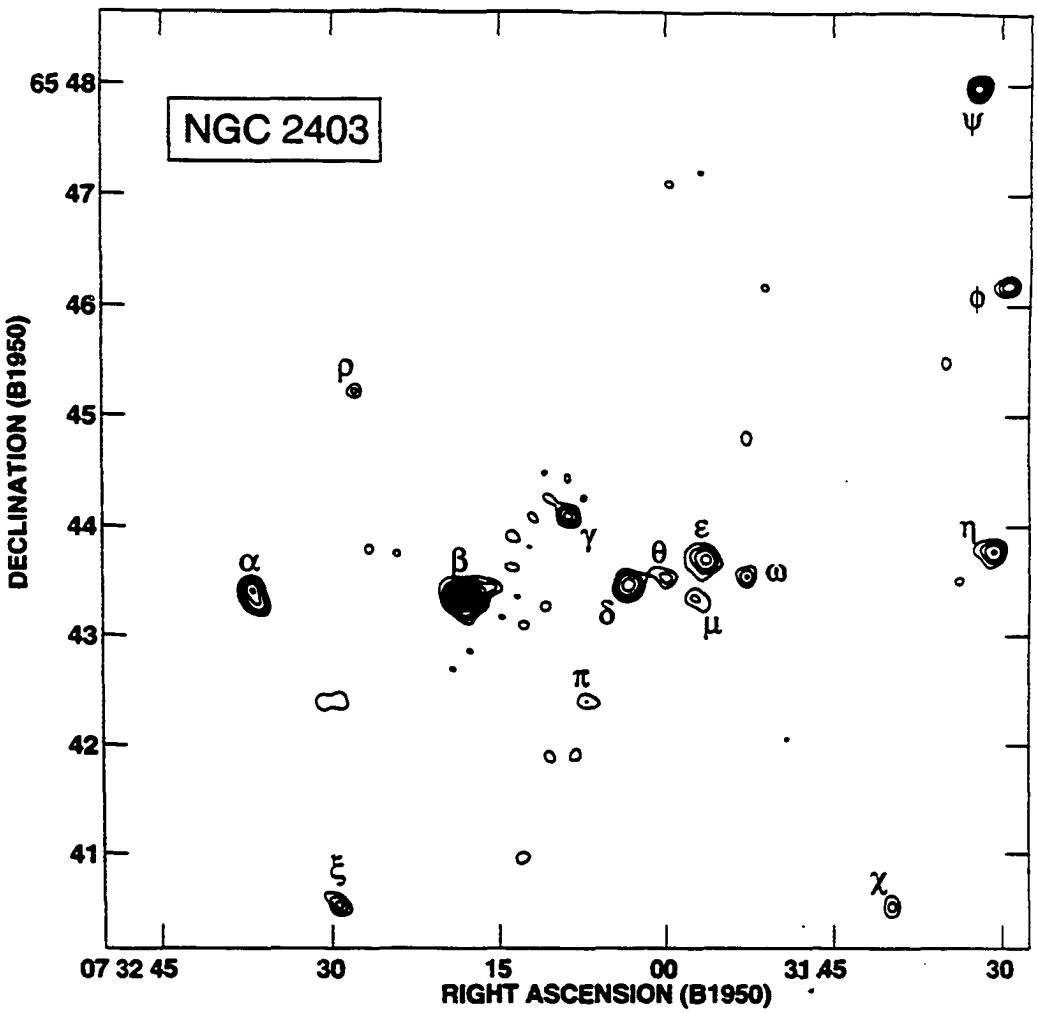

Figure B.8: A contour map of the field of view for the 15 sources in NGC 2403 at 20 cm, labeled as in Table B.1. Sources β, γ, δ, ϵ, ρ, θ, ω, η, χ and ξ are probably H II regions (see text). Contour levels are at 0.47, 0.70, 0.94, 1.4, 1.9, 2.3, 2.8, 3.3, 3.7, 4.2, and 4.6 mJy beam^{-1} and the rms noise is 0.12 mJy beam^{-1}.

SN 1959D This SN Type II-L was discovered by Humason in the spiral NGC 7331. SN 1959D was at maximum light on 2 July 1959 and has a position $\alpha_{1950} = 22^h34^m44^s.39$ and $\delta_{1950} = +34°09'33''.10$ according to NED with a positional uncertainty of $< 1'' \times < 1''$.

Maps of the region near the SN site are in Figures B.9, B.10, and B.11. The SN site was observed three times, twice at 20 cm (in C and A array) and once at 6 cm (in B array) enabling calculation of the spectral index for the sources in the map. A search of the region surrounding the SN site reveals no source with a flux greater than 3σ at each wavelength.

The structure of the radio emission region is very interesting—a ring-like extended structure surrounding a central source. It is suspected that this galaxy harbors a black hole as the central source observed here. These complex structures have been discussed by Cowan et al. (1994b) and I leave further discussion of the radio emission regions to Stockdale et al. (1998)

Brown & Marscher (1978) report 3σ upper limits to detection of radio emission from the site of SN 1959D of 6 and 8 mJy at 2.695 and 8.085 GHz, respectively.

I report no detection of radio emission from the site of SN 1959D at 3 epochs and 2 wavelengths. The 3σ detection thresholds to be used as upper limits are as follows: 0.0581 and 0.0791 mJy at 20 cm, and 0.0417 mJy at 6 cm.

SN 1961V Discovered by P. Wild in December 1961, this SN was originally classified as a Zwicky Type V and is classified nowadays as a Type II peculiar. It resides in the Sc galaxy NGC 1058 and has a position at $\alpha_{1950} = 02^h40^m29^s.679, \delta_{1950} = +37°08'01''.77$ with an uncertainty of less than $1'' \times 1''$ according to NED. Similar to

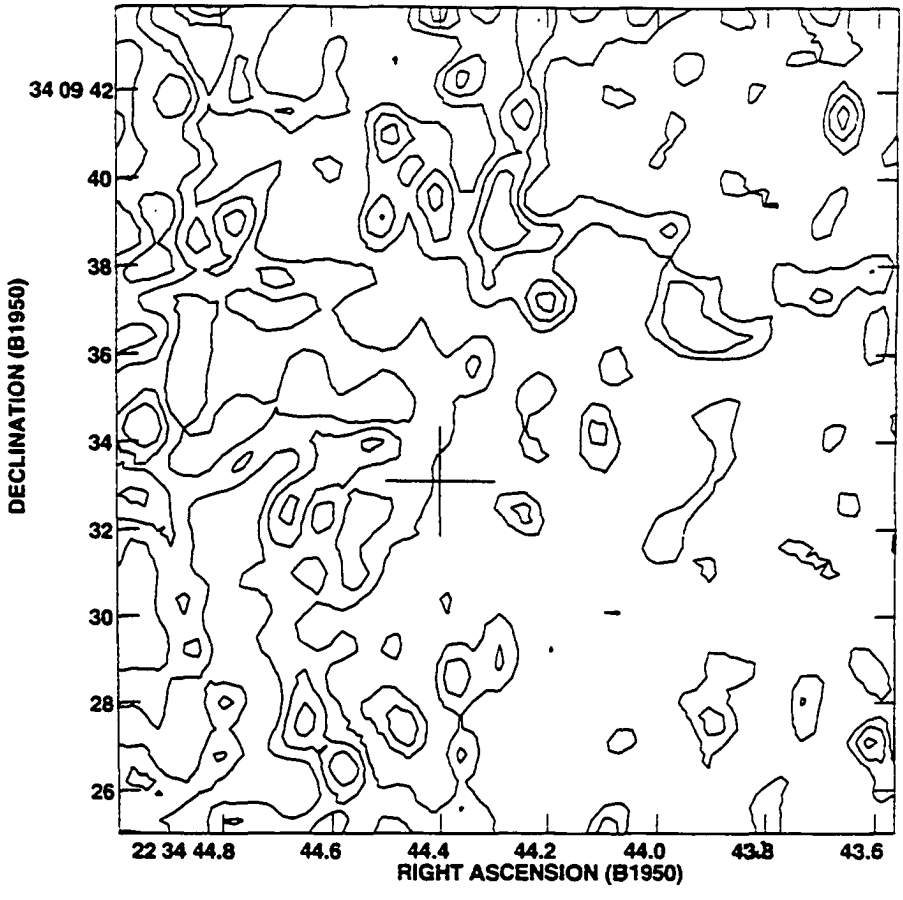

Figure B.9: A (20 cm) contour map of the region immediately surrounding the site of SN 1959D at the first epoch. The (NED) SN position is denoted by a cross whose bars are 2″.5 from one side to the other. The contour levels are −0.059, 0.078, and 0.097 mJy beam^{-1} and the rms noise level is 0.019 mJy beam^{-1}.

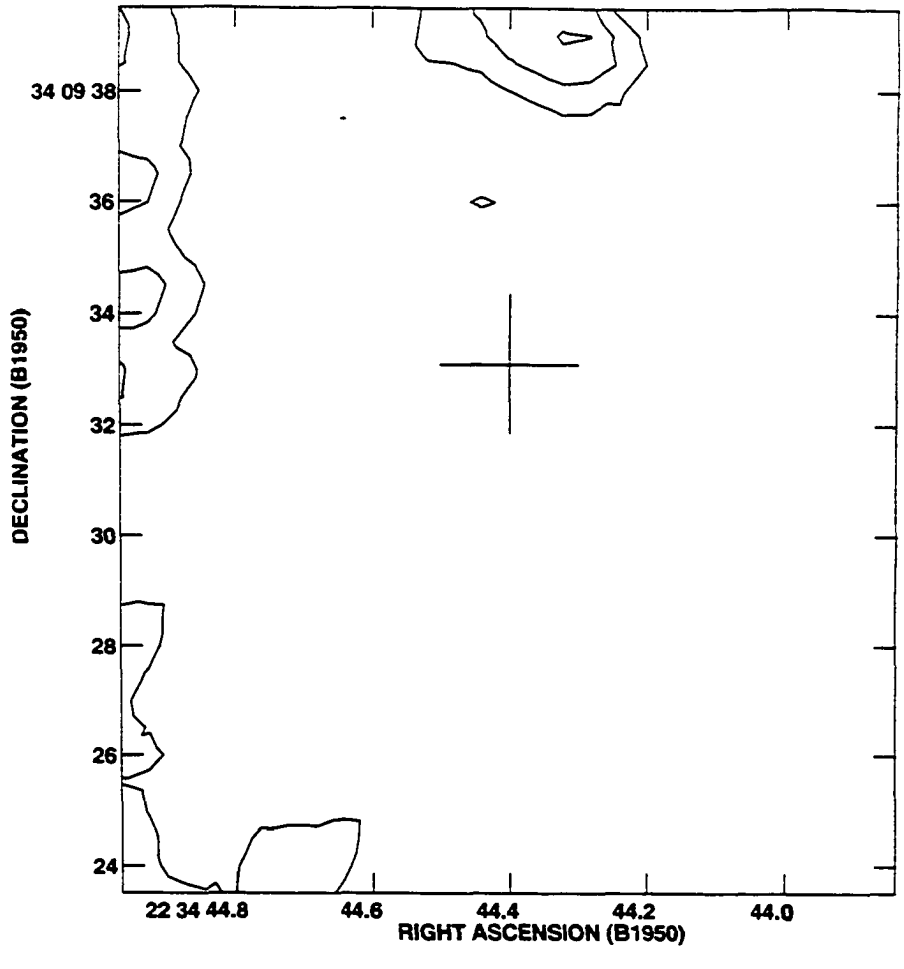

Figure B.10: A (20 cm) contour map of the region immediately surrounding the site of SN 1959D at the second epoch. The (NED) SN position is denoted by a cross whose bars are 2.″5 from one side to the other. The contour levels are −0.077, 0.077, 0.10, 0.15, and 0.18 mJy beam^{-1} and the rms noise level is 0.026 mJy beam^{-1}.

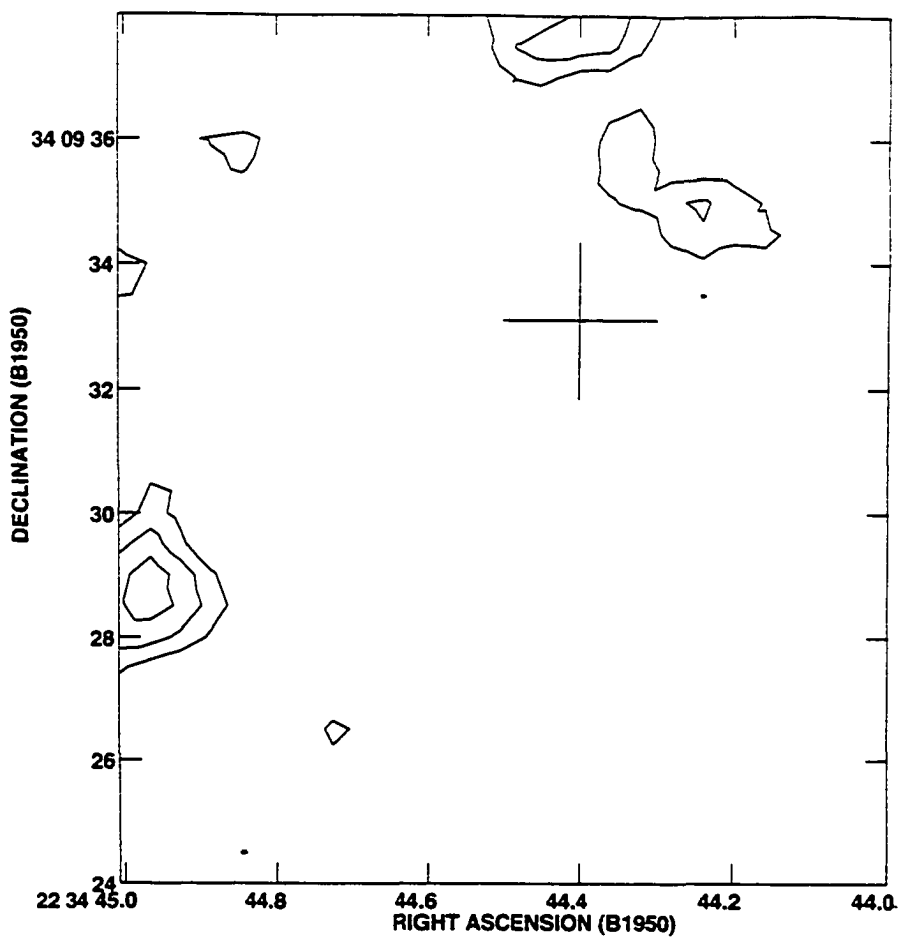

Figure B.11: A (6 cm) contour map of the region immediately surrounding the site of SN 1959D. The (NED) SN position is denoted by a cross whose bars are 2.″5 from one side to the other. The contour levels are −0.042, 0.042, 0.056, 0.071, 0.085, and 0.99 mJy beam^{-1} and the rms noise level is 0.014 mJy beam^{-1}.

the other Zwicky Type V supernova in this paper (SN 1954J), it is suspected that SN 1961V is not the outburst associated with the death of a star. Indeed, recent optical images of the site for this outburst show an object coincident with the SN position. This implies the object survived the explosion that produced the outburst in 1961 (Filippenko et al. 1995). Various mechanisms have been proposed to explain the explosion associated with SN 1961V, including the explosion of a very massive star (Utrobin 1984) and the object being a luminous blue variable analogous to η Carinae (Goodrich et al. 1989). The evidence seems to support the luminous blue variable explanation over the others. SN 1954J, the other Zwicky Type V SN, is also suspected to be an η Carinae analog. One may speculate that the Zwicky Type V SN is representative of η Carinae type of star undergoing a large eruption, but the small sample size limits the validity of this hypothesis. More observations of SNe of this type and comparison to models of luminous blue variables are needed to determine more about this type of outburst.

This object has been well studied in the radio (Cowan, Henry, & Branch 1988, Cowan & Branch 1985, Cowan et al. 1991) where the original observations have been reported. I will use the original observations here to add to the pool of radio SN data. To summarize: Observations were made of NGC 1058 at 20 cm in 1985 and at 6 cm in 1988. Both observations resulted in detections and a spectral index calculated to be -0.60 ± 0.08, indicating non-thermal radio emission. Hα observations made at Kitt Peak showed emission from the region near the position of the SN, indicative of an H II region at or associated with the SN site. Photometry in other bands indicate the H II regions are normal with respect to other optically bright H II regions that do not emit in the radio. Another radio source lies a little more than 2″ to the west

and also has an associated H II region. The radio spectral index for this source is also non-thermal, implying this source may be an SNR whose explosion was not observed optically.

There are two other sources in the field of view for the 6 cm map. Source α lies to the extreme east of the map and has a peak flux of 0.19 mJy per beam. The Hα map does not extend out to this area so no optical ID can be attempted with the data here. No optical observations of this area could be found in the literature to confirm or discount the possibility of identification as an H II region. Given its distance from the galaxy center ($> 4'$), this source is unlikely to be an H II region and may be a background source. Source β has a peak flux per beam of 0.091 mJy and is similarly located on the northern edge of the map some distance from the galactic center. However, β has a position within the Hα map field of view and is not found to lie over any Hα emission region. Source β is therefore unlikely to be an H II region.

Brown & Marscher (1978) report 2.695 and 8.085 GHz observations at an age of about 13 yrs for the SN site that result in upper limits to the radio emission of 3 and 6 mJy, respectively.

I report detections of the emission from the astrometrically determined site of SN 1961V at an age of about 23 yrs past outburst. The emission levels are at 0.27 ± 0.02 and 0.13 ± 0.01 at 20 and 6 cm, respectively. It is unclear at this time whether this radio emission is a result of the decline in radio emission from the initial outburst or of the rise in radio emission possibly associated with a young SNR or another outburst. Further monitoring of the radio emission from this outburst is needed to determine whether the radio emission is increasing or decreasing with time.

SN 1966B SN 1966B, independently reported first by V. Yakimov and then by H. Gates in January 1966, is identified as a Type II-L supernova and had a peak blue magnitude of 14.9 . Its parent galaxy, NGC 4688, is a spiral galaxy whose center has a variety of positions (varying within a range of about 6^s in RA and more than 30″ in decl.). This complicates determination of the position for the SN usually done by using offsets from the galaxy center. I will adopt the most recent positional data on the SN position at $\alpha(1950) = 12^h45^m12^s.1, \delta(1950) = 04°35'58''$ according to NED who report the uncertainty in this position to be 150″ × 150″ (see footnote in section SN 1909A). I find that the uncertainty in the position for the galaxy center, according to NED, is 10″ which I adopt as our uncertainty in the SN position. Very similarly, Van Dyk (1992) adopts a representative uncertainty of 10″ for most of the supernovae (based on center of galaxy uncertainties) in his paper on the associations of SNe with H II regions, including SN 1966B.

A search of the VLA database revealed no other obvious attempts to observe NGC 4688 or SN 1966B in the radio at the VLA. A map of the field of view near the SN site can be sen in Figure B.12. A search of the radio map near the NED SN position reveals only one feature barely having a 3σ signal, but its position is 19″ from the SN site. I report no detection of radio emission from the site of SN 1966B.

There is one very prominent extended feature visible in the map with a peak flux of 1.2 mJy. Unfortunately, a map of the positions of H II regions in NGC 4688 is unavailable to help identify the unknown source in the radio map. By examining the DSS R-band image of the galaxy, I can match up the galaxy center in the radio map with the galaxy center in the DSS map. After scaling the maps appropriately, I find that the extended source lies over no emission regions in the R-band DSS map.

The rms noise measurement is made at 0.053 mJy so the 3σ upper limit to detection of SN 1966B is 0.159 mJy.

SN 1968L This SN is classified as an SN II-P discovered by Bennett in NGC 5236 with a maximum light in July, 1968. Its position according to NED is close to the center of the galaxy at $13^h34^m11\overset{s}{.}3$ and $\delta_{1950} = -29°36'42\overset{''}{.}6$, which is consistent with the position calculated via offsets from the NED galaxy center. However, this position is right over the large radio emission region that makes up the center of NGC 5236, so detection would be difficult. The upper limits are at the usual 3σ level, but the SN could be as radio bright as the central regions (see Cowan & Branch 1985, CRB) and not be visible if it has been a radio emitter at all observations. Turner & Ho (1994) mention the possibility of detection of a source close to the SN position, but it is very uncertain because of the confusing underlying emission from the radio bright central regions.

The analysis of the radio maps for this SN have been discussed in Cowan & Branch 1985 and CRB and summarized in Chapter 1.

No detection of radio emission from this SN has been reported at all epochs and wavelengths.

SN 1969L SN 1969L is a Type II-P SN discovered by Rosino in December residing in the Sc galaxy NGC 1058, the same parent galaxy as SN 1961V. Its position is given by NED at $\alpha_{1950} = 02^h40^m38\overset{s}{.}6$ and $\delta_{1950} = +37°05'58''$ with a reported uncertainty of $150'' \times 150''$. I can adopt the uncertainty in galaxy center, $1\overset{''}{.}5 \times 1\overset{''}{.}3$, as being representative of the SN uncertainty (see SN 1909A). But, if I calculate the SN

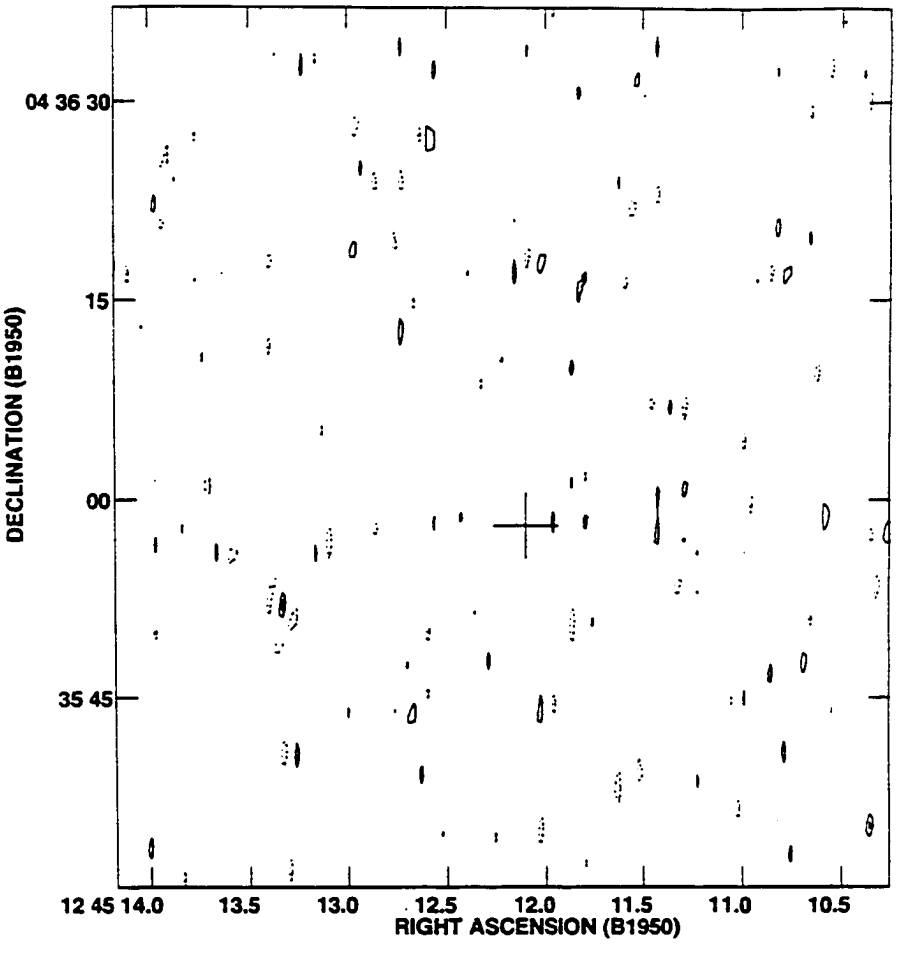

Figure B.12: A (20 cm) contour map of the region immediately surrounding the site of SN 1966B. The (NED) SN position is denoted by a cross whose bars are 5″ from one side to the other. The contour levels are −0.11, 0.16, 0.21, 0.26, and 0.28 mJy beam^{-1} and the rms noise level is 0.053 mJy beam^{-1}.

position based on offsets (e.g., from Asiago) from the galaxy center, I get a slightly different SN position than that reported by NED. The position from offsets is $\alpha_{1950} = 02^h40^m39^s.0$ and $\delta_{1950} = +37°05'55''$. The difference in positions is about $6''$ which I adopt as the uncertainty in SN positions.

A map of the region near the SN site at the second epoch is in Figure B.13. The features in the radio map of the galaxy have been described in the section on SN 1961V. Again, as in that section, the initial results of the observation have been published by Branch & Cowan (1985) and Cowan et al. (1988), but I include them here to add to the database.

Brown & Marscher (1978) observed NGC 1058 in 1973 and 1974 at two frequencies, 2.695 and 8.085, respectively. They report upper limits to detection of 3 and 6 mJy at each frequency, respectively.

I report no detection of radio emission from the site of SN 1969L at two frequencies, 20 and 6 cm. The 20 cm upper limit I quote, from Cowan & Branch (1985) since the map of the entire field of view was unavailable, at a 3σ level of 0.09 mJy. At 6 cm, I may obtain an independent measurement of the noise to obtain a 3σ upper limit of 0.042 mJy.

SN 1970G The first SN to be observed in the radio, SN 1907G is a Type II-L sharing the same parent galaxy as SN 1909A, NGC 5457 (M 101). Discovered by Lovas, the maximum light occurred around 30 July 1970. Its position is well established at $\alpha_{1950} = 14^h01^m14^s.4$ and $\delta_{1950} = +54°28'55''.8$ with an uncertainty of $2''.5 \times 2''.5$ according to NED. Unfortunately it lies very close to the H II region, NGC 5455, which made early measurements difficult shortly after explosion.

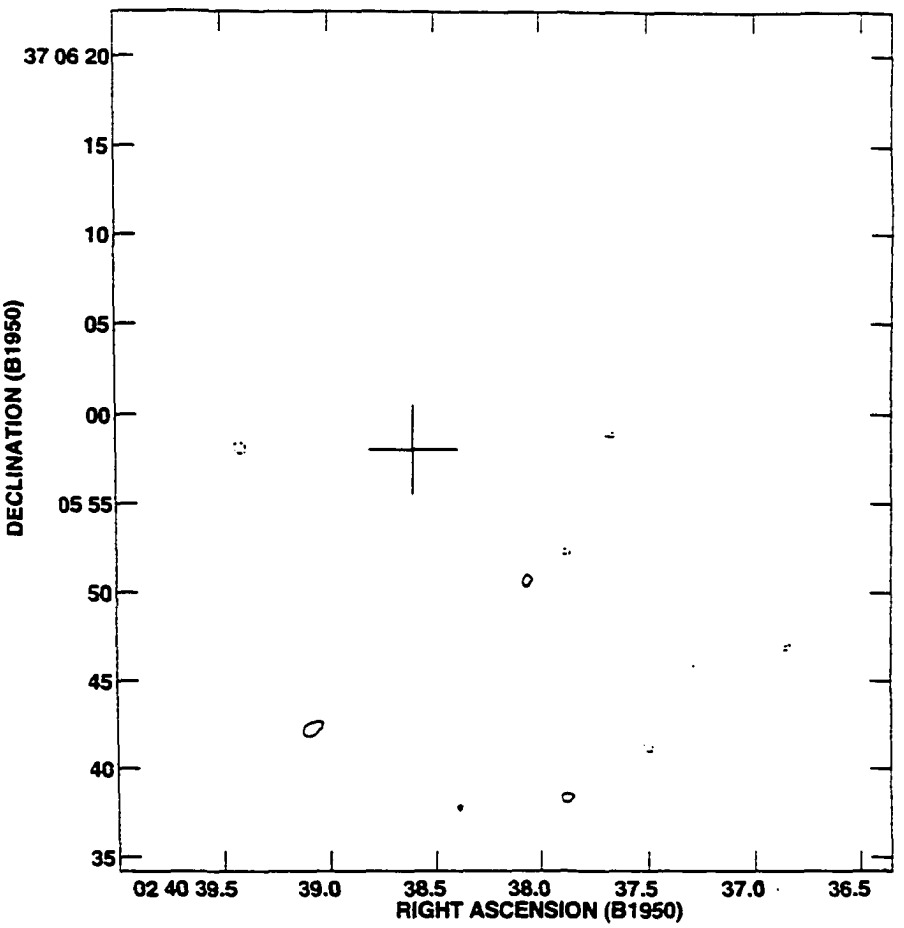

Figure B.13: A (6 cm) contour map of the region immediately surrounding the site of SN 1969L at the second epoch. The (NED) SN position is denoted by a cross whose bars are 5″ from one side to the other. The contour levels are −0.042, 0.042, 0.057, 0.071, and 0.084 mJy beam^{-1}, and the rms noise level is 0.014 mJy beam^{-1}.

Results and analysis of the radio detection of SN 1970G in these maps have already been published (Cowan et al. 1991) and I leave the details to that paper. To summarize: NGC 5455 (an H II region) is clearly visible in both maps. Just to the northwest of NGC 5455 lies an emission region whose position is about 1″ from the position of SN 1970G. The 20 cm peak flux is 0.211 ± 0.021 mJy and the 3.6 cm peak flux is 0.0758 ± 0.013 mJy. These scaled array observations enable calculation of a spectral index at -0.59 ± 0.11, indicative of non-thermal emission characteristic of synchrotron radiation, believed to originate in RSNe and/or SNRs.

A map of the (southern) region surrounding NGC 5455 and containing many of the sources can be seen in Figure B.14. SN 1970G is visible as a prominence pointing to the northwest from α. Source α has a flat spectral index and an excellent positional coincidence with NGC 5455, a known H II region. Sources δ and ω have spectral indices between 0.0 and 0.1 indicating they are likely H II regions as well. If I compare the positions of these sources with those of H II regions found by Hodge et al. (1990), positional coincidences (within the uncertainties) are found for ψ, ρ, θ, ϵ and δ. These are also probable H II regions. Comparison of the positions of SNRs in M 101 reported by Matonick & Fesen (1997) with these sources reveals no positional coincidences.

Brown & Marscher (1978) report an upper limit to the detection of radio emission from the site of SN 1970G of 4 mJy at 8.085 GHz.

I report detection of radio emission at two frequencies, 1.490 and 8.415 GHz, from SN 1970G at a level of 0.211 ± 0.021 and 0.0758 ± 0.013 mJy respectively. They imply a spectral index of -0.59 ± 0.11, indicative of non-thermal emission consistent with emission from RSNe and/or SNRs.

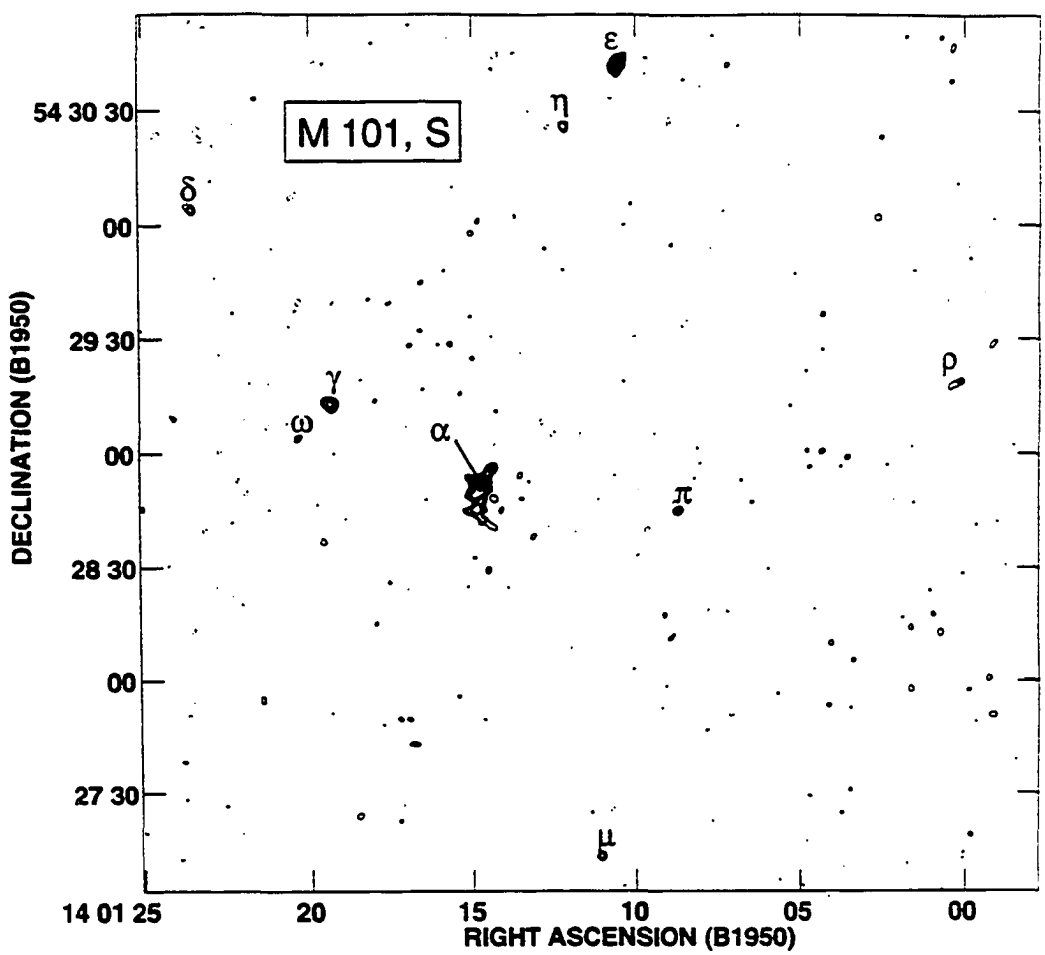

Figure B.14: A contour map of part of the field of view for the southern region of NGC 5457 (M 101) at 20 cm, labeled as in Table B.1. Emission from SN 1970G (source β) is visible just to the northwest of α, but not labeled. Sources α, δ and ω are probably H II regions from their flat spectral indices (see Table B.1). Contour levels are at -0.065, 0.065, 0.093, 0.14, 0.19, 0.37, 0.56, 0.74 and 0.92 mJy beam^{-1} and the rms noise is 0.021 mJy beam^{-1}.

SN 1972E Discovered by Kowal with a maximum light in May, this SN I resides in the same galaxy as SN 1895B, NGC 5253. It has a NED position at $\alpha(1950) = 13^h37^m02^s.4$ and $\delta(1950) = -31°25'04''$. I adopt an uncertainty in position of 10″ (see discussion of SN 1895B).

Details of the observations and data reduction can be found in Cowan & Branch (1982) and Branch & Cowan (1985). Since a radio map was unavailable for independent analysis, I quote the rms noise levels and upper limits from those papers.

I report no detection of radio emission from SN 1972E with 3σ upper limits at 20 cm of 0.9 and 0.15 mJy for the 1981 and 1983 observations, respectively.

SN 1973R In December 1973, Rosino discovered SN 1973R in the spiral galaxy NGC 3627, a member of the Leo Triplet—a group of galaxies suspected to have interacted with one another at some time. The SN is classified as a Type II-P and has a position according to NED at $\alpha(1950) = 11^h17^m35^s.0$ and $\delta(1950) = +13°16'13''$ with a reported uncertainty of 150″ × 150″. I ignore this uncertainty as due to the systematic way NED reports its data (see SN 1909A) and adopt the uncertainty for the galactic center, 10″, as representative of the SN uncertainty.

A map of the area surrounding the SN site is in Figure B.15. The nearest source in this radio map is more than 50″ from the SN position, so I can only report an upper limit to the radio detection of this SN.

There are 3 fairly strong (mJy) sources in the radio map of the galaxy that merit investigation. The strongest of these has a peak flux of 7.14 mJy/beam and is just barely resolved. The position of peak flux for this source, designated α, lies just within the uncertainties for the position of the galaxy center. Noticing that P. Alexander

had observed NGC 3627 at the VLA, I can superpose the coordinates of the radio map onto the coordinates in their CO and H I map of the galaxy (Zhang, Wright & Alexander 1993). I find that source α lies right on top of the CO peak in the center of the galaxy. This suggests that this position (of source α) may be the true (dynamical) center for the galaxy. Source α is offset from the NED center by $8\farcs6$, less than the reported uncertainty for the galaxy center.

In an attempt to observe SN 1989B in the same galaxy in early 1989, a source was observed whose position is consistent with α. The observation was made at 6 cm GHz and the peak flux measured is 3.1 mJy, indicative of non-thermal emission when compared to the 20 cm peak flux.

Prior observations of NGC 3627 were found in Hummel et al. (1987) (1.49 GHz), Crane (1977) (2.7 & 8.1 GHz), Zhang, Wright, & Alexander (1993) (CO and H I) and Hodge (1974) (optical H II). Source α has a non-thermal spectral index and a position within the uncertainty ($10''$) for the galactic center. It lies directly over the CO peak in the center of the galaxy from Zhang et al. (1993) and is probably associated with the galactic center. Hummel et al. observe a source $< 0\farcs5$ from α with an integrated flux over the inner $2''$ of 15 ± 2 mJy. I measure the integrated flux over approximately the same region to be 12.5 ± 0.1 mJy.

Hα observations taken on the 18-inch telescope at University of Oklahoma by W. Romanishin (1997) reveal an emission region lying over β.

Hodge (1974) reports observations of H II regions expressed as offsets and plots them relative to the galactic center. If I superpose α with the position for the galactic center on the plot, I find that β lies directly over a couple of H II regions (No. 12 & 13 in Hodge) indicating that β is probably an H II region. Source γ has no counterpart

in Hodge (1974).

Source ϵ has a position that is coincident with the position of an H II region (No. 47) reported by Hodge (1974). This coincidence assumes that the center of the galaxy is at α. Examination of the fluxes at two wavelengths indicates that the emission from ϵ is non-thermal. This probably indicates that there is an SNR nearby or possibly associated with the H II region. If I again assume that α is the center of the galaxy, it is found that π lies 4″ from the position of an H II region (No. 50), so it is not clear whether this is emission from an H II region or not.

Brown & Marscher (1978) observed NGC 3627 in search of radio emission from SN 1973R about 9 months after the discovery date. They report 3σ upper limits at 2.695 (11 cm) and 8.085 (3.6 cm) GHz of 5 and 6 mJy, respectively.

I report no detection for SN 1973R with an rms noise level of 0.0934 mJy at 20 cm and a 3σ upper limit of 0.28 mJy.

SN 1980D SN 1980D was independently discovered by Wild and Kimeridze in March 1980 and was classified as a Type II-P supernova residing in the spiral galaxy NGC 3733. Its position is very well established, $\alpha(1950) = 11^{h}32^{m}13^{s}.40$, $\delta(1950) = +55°09'30''.00$ according to NED, with an uncertainty of less than an arc-second and a distance of 22.1 Mpc to NGC 3733 (Tully 1988).

A map of the field of view near the SN site is seen in Figure B.16. There does not appear to be many attempts to observe SN 1980D or NGC 3733 in the radio, and our observation may have been the only one to look at this galaxy at the VLA. The observation yields an rms noise level of 0.0312 mJy and no sources were visible in the field of view. Using 3σ as a benchmark for detection, I calculate the upper limit to

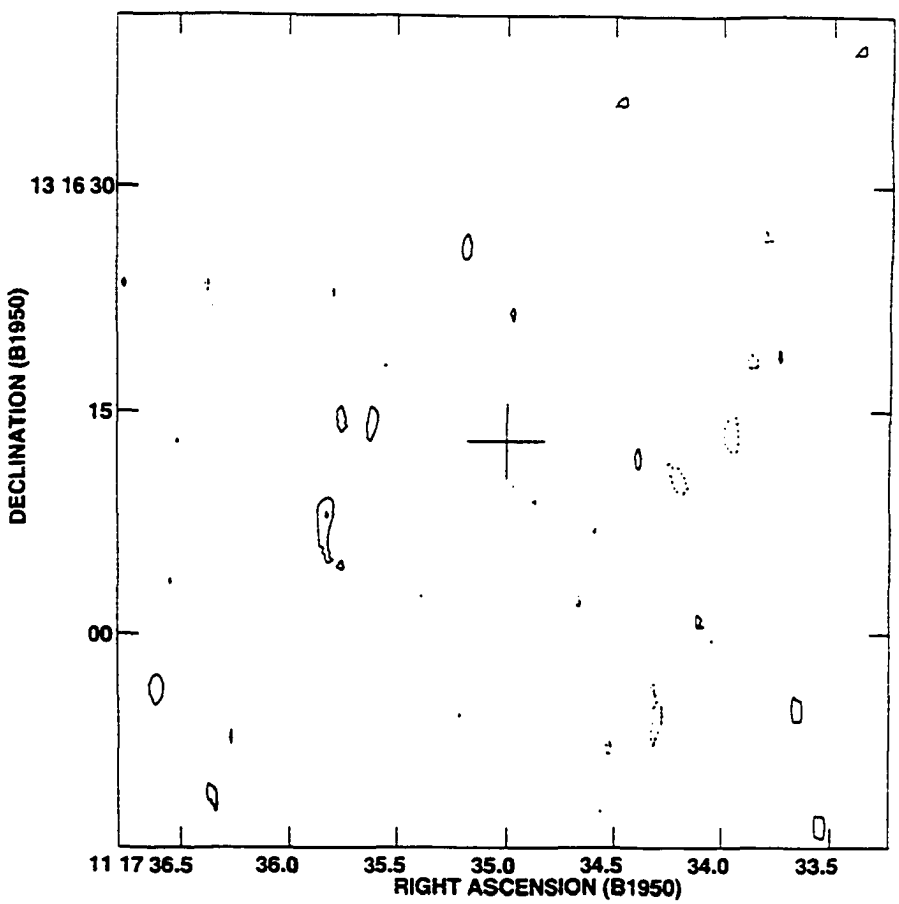

Figure B.15: A (20 cm) contour map of the region immediately surrounding the site of SN 1973R. The (NED) SN position is denoted by a cross whose bars are 5″ from one side to the other. The contour levels are −0.28, 0.28, 0.37, 0.46, 0.56, and 0.71 mJy beam^{-1}, and the rms noise level is 0.093 mJy beam^{-1}.

be 0.0936 mJy.

SN 1983K SN 1983K is an SN Type II-P discovered by Wischnjewski in NGC 4699 observed to be at maximum light on 23 June 1983. It has a well determined position according to NED at $\alpha_{1950} = 12^h46^m36^s.400$ and $\delta_{1950} = -08°21'21''.00$ with an uncertainty of less than an arc-second. NGC 4699 is also host to SN 1948A but the field of view was not large enough to include both. Further, the slow initial rise time of the light curve for SN 1983K can be interpreted as being due to a large circumstellar shell (Phillips et al. 1990), possibly indicative of radio emission.

A contour map of the region near the SN site is in Figure B.17. There were no sources visible in the radio map around the SN site to a radius of about 1′. Previous observation of NGC 4699 have revealed a radio source close to the optical center of the galaxy (e.g., Condon 1987) but unfortunately outside of the field of view.

I report no detection of radio emission from SN 1983K with an rms noise level at 0.017 mJy implying a 3σ upper limit of 0.052 mJy at a frequency of 4.835 GHz (6 cm) and an age of about 4 years.

SN 1983N Discovered by Evans in NGC 5236, the same galaxy as SNe 1923A, 1945B, 1950B, 1957D and 1968L, this SN is classified as an SN Ib with a maximum light in July, 1983. The NED position is at $13^h34^m02^s.0$ and $\delta_{1950} = -29°38'45''.0$ with an uncertainty of 2″. This SN has been detected by others at several different epochs (Sramek, Panagia, & Weiler 1984, Weiler et al. 1986), but at post-peak times.

The analysis of the radio maps for this SN have been discussed in Cowan & Branch (1985) and CRB and summarized in Chapter 1.

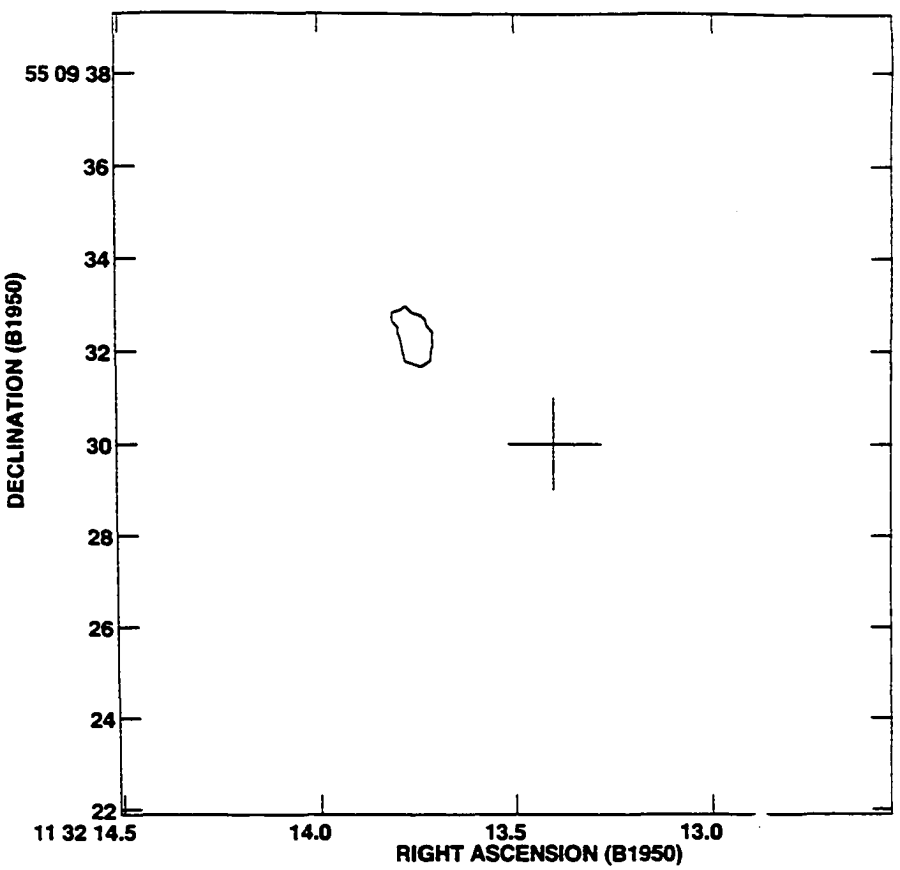

Figure B.16: A (20 cm) contour map of the region immediately surrounding the site of SN 1980D. The (NED) SN position is denoted by a cross whose bars are 2″ from one side to the other. The contour levels are −0.092, 0.092, 0.11, and 0.13 mJy beam^{-1}, and the rms noise level is 0.031 mJy beam^{-1}.

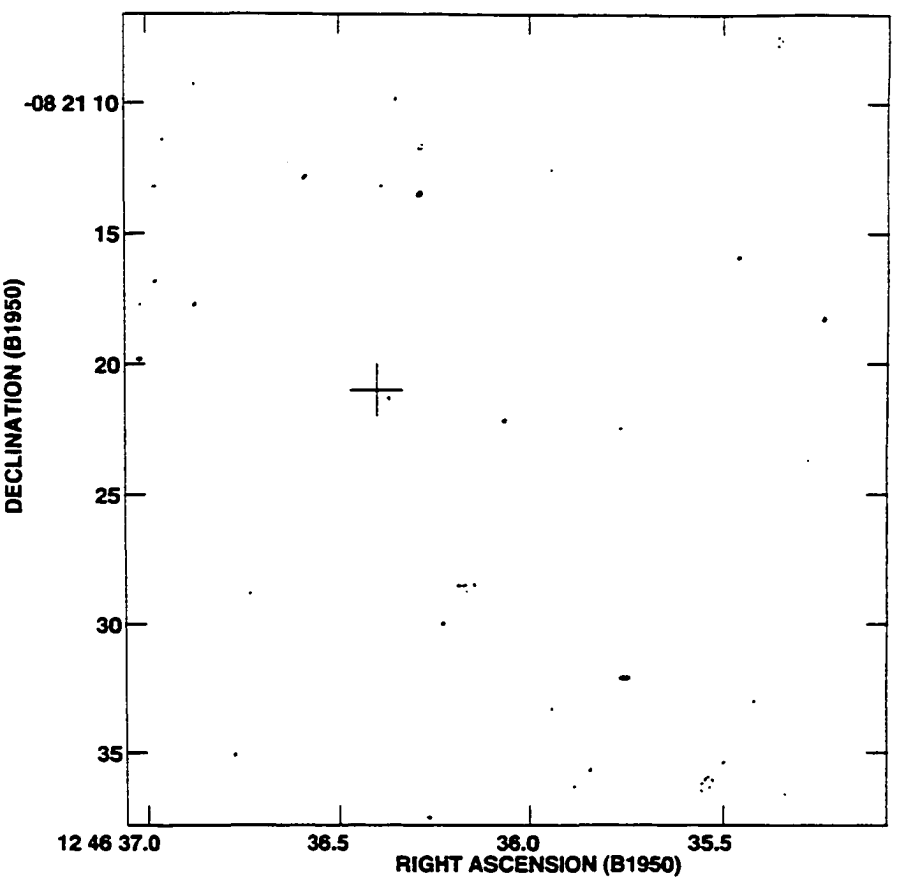

Figure B.17: A (6 cm) contour map of the region immediately surrounding the site of SN 1983K. The (NED) SN position is denoted by a cross whose bars are 2″ from one side to the other. The contour levels are −0.051, 0.051, 0.055, and 0.049 mJy beam^{-1}, and the rms noise level is 0.017 mJy beam^{-1}.

Detections were reported by Cowan & Branch (1985) and CRB at the first epoch at both wavelengths, but only upper limits at the second epoch (see Table 5.1).

SNe 1984E and 1986E Details on these SNe and the analysis of the radio maps are found in Chapter 2.

SN 1986G Details on this SNe and the analysis of the radio maps are found in Chapter 2.

SN 1989B SN 1989B was discovered by Evans in late Jan 1989 and shares the same parent galaxy as SN 1973R, NGC 3627. This galaxy is a member of the Leo Triplet—three galaxies believed to have interacted with each other (Zhang et al 1993). SN 1989B is a Type Ia and has a position given by NED at $\alpha(1950) = 11^h17^m37^s.40$ and $\delta(1950) = 13°16'45''.00$ and an uncertainty of less than $1'' \times 1''$.

Since the SN was a Type Ia, this SN was observed at the VLA as close to maximum light as possible at the shortest possible wavelength. The observations were made three days before maximum light, at 6 cm and 3.6 cm and a map of the area surrounding the SN sites are seen in Figures B.18 and B.19. As noted in section on SN 1973R, the source designated α in that map is observed here at 6 cm with a peak flux of 3.1 mJy. This is indicative of a non-thermal source when compared with the 20 cm peak flux of 7.1 mJy. Recall that source α lies within the uncertainty for the position of the galaxy center. Because the field of view shrinks with wavelength for a given array and because the pointing center was centered on the SN position, not the galaxy center, α remained outside the field of view at 3.6 cm.

The only other source in the fields of view was visible only at 6 cm and had a

peak flux of 0.42 mJy. It was not visible at 20 cm because of the increased noise level at that wavelength.

Our observations result in non-detections and 3σ upper limits of 0.107 and 0.0891 mJy at 6 and 3.6 cm, respectively.

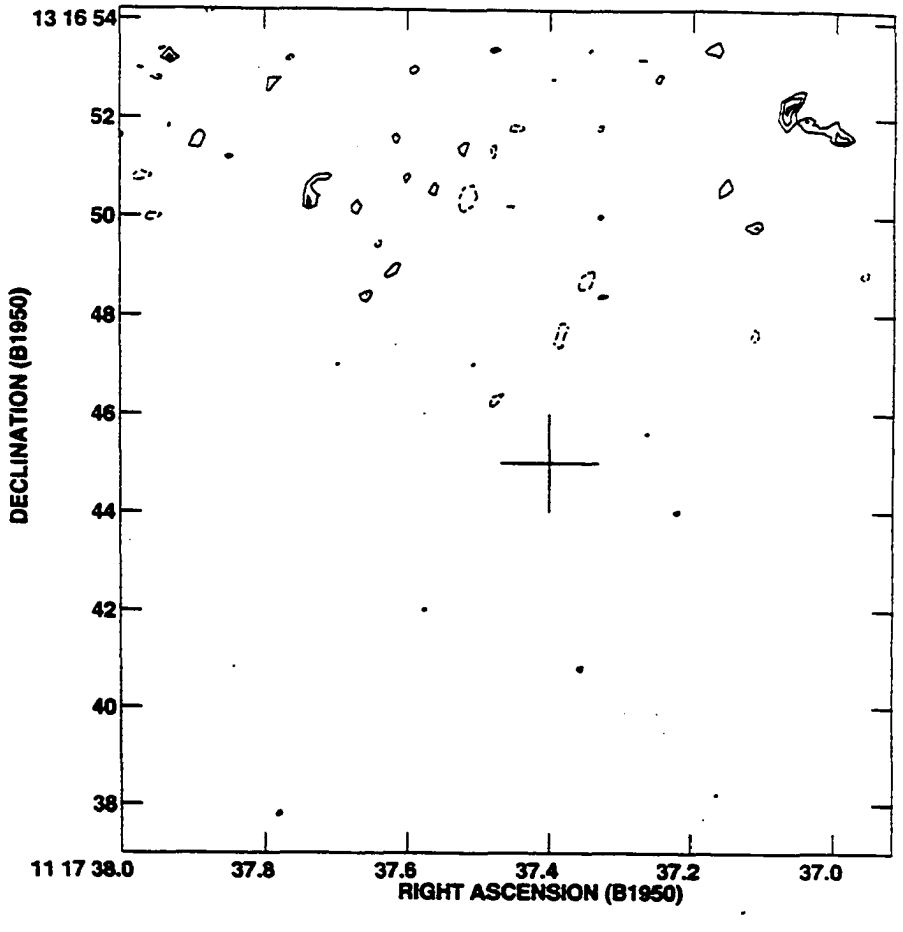

Figure B.18: A (6 cm) contour map of the region immediately surrounding the site of SN 1989B. The (NED) SN position is denoted by a cross whose bars are 2″ from one side to the other. The contour levels are −0.11, 0.11, 0.15, 0.18, 0.22, and 0.31 mJy beam^{-1}. Due to what I believe to be CLEANing in approximately the bottom portion of the map and not in the top portion, the noise levels are slightly different in each region. In the bottom half of the map (containing the SN site), the rms noise level is 0.011 mJy beam^{-1}. In the top half the rms noise is 0.045 mJy beam^{-1}.

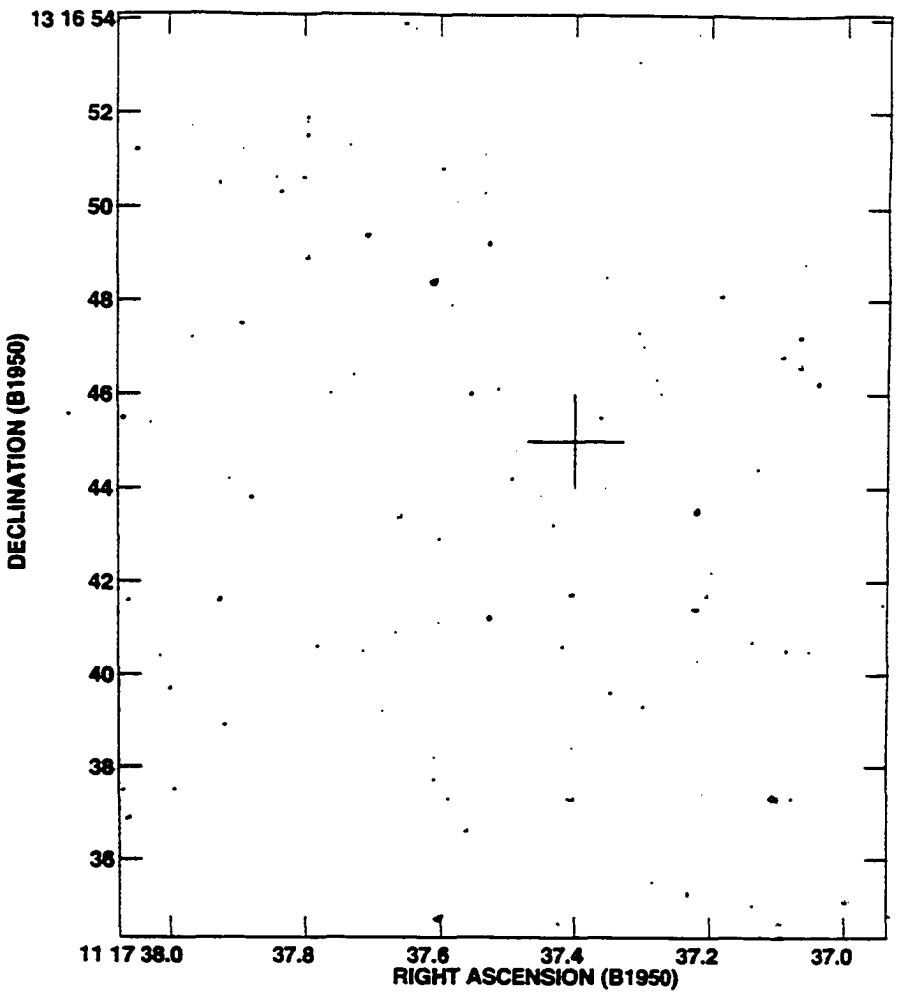

Figure B.19: A (3.6 cm) contour map of the region immediately surrounding the site of SN 1989B. The (NED) SN position is denoted by a cross whose bars are 2″ from one side to the other. The contour levels are −0.089, 0.12, 0.15, 0.18 and 0.21 mJy beam^{-1}, and the rms noise level is 0.030 mJy beam^{-1}.

Galaxy Name	Galaxy Type	Position of Peak[a] α_{1950}	δ_{1950}	Peak Flux (mJy beam^{-1}) 20 cm	6 cm	3.6 cm	Classification?	Notes
NGC 1058	Sc	β:02^{h}40^{m}31^s.4	+37°09′03″.0	···	0.10 ± 0.01	···		1
		α:02^{h}40^{m}45^s.9	+37°07′21″.7	···	0.25 ± 0.01	···		
NGC 2403	Scd	ϕ:07^{h}31^{m}29^s.4	+65°46′10″.9	1.2 ± 0.1	···	···		
		η:07^{h}31^{m}30^s.7	+65°43′46″.1	1.3 ± 0.1	···	···	H II	2
		ψ:07^{h}31^{m}32^s.1	+65°47′58″.8	2.3 ± 0.1	···	···		
		χ:07^{h}31^{m}39^s.9	+65°40′30″.6	0.75 ± 0.1	···	···	H II	
		ω:07^{h}31^{m}52^s.7	+65°43′32″.3	0.87 ± 0.1	···	···	H II	2
		ϵ:07^{h}31^{m}56^s.4	+65°43′41″.9	1.4 ± 0.1	···	···	H II	2
		μ:07^{h}31^{m}57^s.0	+65°43′19″.5	0.62 ± 0.1	···	···	SNR?	
		θ:07^{h}32^{m}00^s.1	+65°43′32″.6	0.72 ± 0.1	···	···	H II	2
		δ:07^{h}32^{m}03^s.4	+65°43′28″.1	1.6 ± 0.1	···	···	H II	2
		π:07^{h}32^{m}07^s.1	+65°42′24″.5	0.61 ± 0.1	···	···		
		γ:07^{h}32^{m}08^s.7	+65°44′05″.7	1.5 ± 0.1	···	···	H II	2
		β:07^{h}32^{m}18^s.1	+65°43′21″.5	4.4 ± 0.1	···	···	H II	2
		ρ:07^{h}32^{m}28^s.0	+65°45′13″.2	0.78 ± 0.1	···	···	H II	
		ξ:07^{h}32^{m}29^s.6	+65°40′32″.7	0.92 ± 0.1	···	···	H II	
		α:07^{h}32^{m}36^s.9	+65°43′22″.1	1.9 ± 0.1	···	···		
NGC 3169	Sa pec	C:10^{h}11^{m}39^s.4	+03°42′52″.5	3.4 ± 0.02	···	···	GC	3
		α:10^{h}11^{m}41^s.7	+03°41′37″.2	0.67 ± 0.02	···	···		
NGC 3627	SAB(s)b	γ:11^{h}17^{m}36^s.5	+13°14′03″.3	2.1 ± 0.07	···	···		4
		π:11^{h}17^{m}36^s.7	+13°17′01″.8	···	···	0.17 ± 0.03		5
		ϵ:11^{h}17^{m}36^s.9	+13°16′52″.0	···	0.47 ± 0.04	0.25 ± 0.03		6
		α:11^{h}17^{m}38^s.5	+13°15′55″.7	8.1 ± 0.07	3.2 ± 0.04	···	GC	7
		β:11^{h}17^{m}40^s.1	+13°15′09″.8	1.3 ± 0.07	···	···	H II	8
NGC 4214	Im	δ:12^{h}13^{m}08^s.3	+36°35′39″.0	0.13 ± 0.03	···	···		9
		γ:12^{h}13^{m}08^s.4	+36°36′16″.8	0.32 ± 0.03	···	···	H II	
		ϵ:12^{h}13^{m}08^s.6	+36°36′13″.4	0.59 ± 0.02	···	···		
		π:12^{h}13^{m}09^s.3	+36°35′20″.7	0.34 ± 0.03	···	···		
		η:12^{h}13^{m}09^s.9	+36°36′12″.5	0.09 ± 0.02	···	···	H II	10
		β:12^{h}13^{m}10^s.1	+36°35′49″.6	0.80 ± 0.03	···	···	H II	
		α:12^{h}13^{m}10^s.3	+36°35′44″.0	0.82 ± 0.02	···	···	H II	
		ρ:12^{h}13^{m}11^s.3	+36°35′55″.0	0.20 ± 0.03	···	···		
		ω:12^{h}13^{m}19^s.1	+36°35′27″.2	0.32 ± 0.03	···	···		
		θ:12^{h}13^{m}20^s.5	+36°35′24″.8	0.16 ± 0.03	···	···		
		ξ:12^{h}13^{m}26^s.5	+36°35′09″.5	0.43 ± 0.02	···	···		
NGC 4302	Sc	δ:12^{h}19^{m}01^s.3	+14°53′51″.3	···	0.44 ± 0.02	···		11
		β:12^{h}19^{m}09^s.8	+14°54′51″.2	1.1 ± 0.07	2.0 ± 0.03	···		12
		γ:12^{h}19^{m}14^s.0	+14°53′35″.2	0.84 ± 0.07	2.2 ± 0.02	···		13
NGC 4688	SBcd	α:12^{h}45^{m}11^s.7	+04°35′27″.5	0.96 ± 0.07	···	···		14
NGC 5128	S0 pec	C:13^{h}22^{m}31^s.7	−42°44′59″.5	···	5660	^{2cm}131	GC	15

Table B.1: Summary of observational data on non-SN radio sources

Galaxy Name	Galaxy Type	Position of Peak[a] α_{1950}	δ_{1950}	Peak Flux (mJy beam^{-1}) 20 cm	6 cm	3.6 cm	Classification	Notes
NGC 5457, S	Scd	ψ:14^{h}00^{m}42^s.9	+54°30′39″.9	···	···	0.07 ± 0.01	H II	22
		θ:14^{h}00^{m}44^s.0	+54°30′33″.6	···	···	0.06 ± 0.01	H II	22
		ρ:14^{h}01^{m}00^s.2	+54°29′18″.6	0.11 ± 0.02	···	···	H II	16, 22
		π:14^{h}01^{m}08^s.7	+54°28′44″.9	0.18 ± 0.02	···	0.06 ± 0.01		
		ϵ:14^{h}01^{m}10^s.5	+54°30′42″.0	1.1 ± 0.02	···	0.39 ± 0.01	H II	22
		μ:14^{h}01^{m}11^s.0	+54°27′13″.2	0.10 ± 0.02	···	···		16
		η:14^{h}01^{m}12^s.2	+54°30′25″.8	0.14 ± 0.02	···	···		16
		α:14^{h}01^{m}14^s.7	+54°28′52″.1	0.69 ± 0.02	···	0.72 ± 0.01	H II	17
		γ:14^{h}01^{m}19^s.4	+54°29′12″.9	0.51 ± 0.02	···	0.19 ± 0.01		
		ω:14^{h}01^{m}20^s.3	+54°29′03″.9	0.10 ± 0.01	···	0.09 ± 0.01	H II	18
		δ:14^{h}01^{m}23^s.5	+54°30′04″.2	0.14 ± 0.02	···	0.11 ± 0.01	H II	19, 22
NGC 5457, E	Scd	ρ:14^{h}01^{m}45^s.6	+54°35′36″.3	0.18 ± 0.02	···	···		
		λ:14^{h}01^{m}48^s.1	+54°32′59″.9	0.094 ± 0.02	···	···		
		π:14^{h}01^{m}50^s.1	+54°36′23″.9	0.12 ± 0.02	···	···	H II	23
		κ:14^{h}01^{m}52^s.7	+54°33′11″.9	0.12 ± 0.01	···	···	H II	24
		η:14^{h}01^{m}53^s.8	+54°33′19″.2	0.17 ± 0.02	···	···	H II	23, 24
		ϕ:14^{h}01^{m}55^s.4	+54°33′26″.6	0.78 ± 0.01	···	···	H II	23, 24
		χ:14^{h}01^{m}57^s.0	+54°33′46″.5	0.10 ± 0.01	···	···	H II	24
		γ:14^{h}02^{m}06^s.1	+54°36′14″.0	0.057 ± 0.02	···	···	H II	23, 24
		ϵ:14^{h}02^{m}06^s.8	+54°36′31″.6	0.11 ± 0.02	···	···	H II	23, 24
		δ:14^{h}02^{m}07^s.1	+54°36′17″.2	0.13 ± 0.02	···	···	H II	24
		β:14^{h}02^{m}07^s.2	+54°36′27″.3	0.20 ± 0.02	···	···	H II	24
		α:14^{h}02^{m}08^s.1	+54°36′32″.0	0.18 ± 0.01	···	···	H II	23, 24
		θ:14^{h}02^{m}08^s.2	+54°36′17″.2	0.10 ± 0.02	···	···		
		ω:14^{h}02^{m}26^s.9	+54°38′06″.3	0.15 ± 0.01	···	···		
IC 4182	Sm	α:13^{h}03^{m}12^s.9	+37°51′59″.5	0.48 ± 0.02	···	···		20
		β:13^{h}03^{m}12^s.4	+37°51′53″.9	1.4 ± 0.03	···	···		21

a. The sources are designated according to the label on each map.

Notes

1) Comparison of the 20 cm map with an Hα image of the galaxy reveals no source coincident with source β.
2) The position of each of these sources is within 1″ – 5″ of a corresponding source found by Turner & Ho (1994).
3) This emission region is associated with the central regions of NGC 3169.
4) This source is relatively far from the center of NGC 3627.
5) This source is only visible at 3.6 cm due to the reduced noise at that wavelength. It has a position within 4″ of an H II region listed by Hodge (1974) (see Appendix B).
6) This source is not visible at 20 cm because of reduced noise level at 6 and 3.6 cm. The reduced flux at 3.6 cm relative to 6 cm is indicative of non-thermal emission, but this source is coincident with an H II region from Hodge (1974) (see Appendix B).
7) The non-thermal spectral index for this source and the coincidence with the central regions of NGC 3627 indicate this region may be associated with the dynamic center for the galaxy.
8) The amorphous shape of this extended emission region and its positional coincidence over several Hodge (1974) H II regions indicate this source is probably one or more H II regions.
9) Source δ has a peak flux of only 4.5σ.
10) Source η seems to be a complex composed of several distinguishable smaller sources. The flux and position listed is for the strongest source.
11) This source was not visible at 20 cm due to increased noise at that wavelength.
12) The spectral index for this source, +0.6, is very similar to those of background radio galaxies and/or quasars found in Donnelly, Partridge, & Windhorst (1987).

Table B.1:—Continued

13) The spectral index for this source, +0.4, is also similar to background radio galaxies and/or quasars in Donnelly et al. (1987).
14) This source is also extended and has an amorphous shape. Perhaps it is actually several sources.
15) The source detected here is resolved at both wavelengths. The integrated fluxes are 6060 and 380 mJy at 6 and 2 cm respectively. The resulting scaled array spectral index is -2.5
16) These sources did not have a signal above 4σ at 3.6 cm.
17) This source is coincident with the position of NGC 5455, an HII region. While α is 3.″6 outside of the uncertainty ($\pm 10''$) of a source (No. 416) reported to be associated with NGC 5455 in Hodge et al. (1990), our source has an extended structure (see Figure 8) which makes the identification likely.
18) The flat spectral index ($\alpha_{3.6}^{20} = -0.052$) indicates probable identification as an HII region.
19) The flat spectral index for this source ($\alpha_{3.6}^{20} = +0.026$) indicates thermal emission characteristic of HII regions.
20) This source was observed by the FIRST survey at the VLA at 21.4 cm and is somewhat amorphous. The flux reported by FIRST is about 2.5 times larger than our peak flux.
21) Also observed in the FIRST survey, this source is extended and has a jet-like shape that points towards/away from source α. The peak flux observed by us is very similar to that reported by FIRST.
22) This source has a position that is within the uncertainties for an H II region found by Hodge et al. (1990). We list our source and the corresponding H II region identification in Hodge et al. (1990): ψ - No. 141, ρ - No. 217, θ - No. 158, ϵ - No. 365, δ - No. 592.
23) These sources have positions within the uncertainties for H II regions found by Hodge et al. (1990).
24) Superposition of the radio map of NGC 5461 & 5462 with Hα maps in Israel, Goss, & Allen (1975) has these sources lying over Hα emission regions.

Table B.1:—Continued

IMAGE EVALUATION TEST TARGET (QA-3)

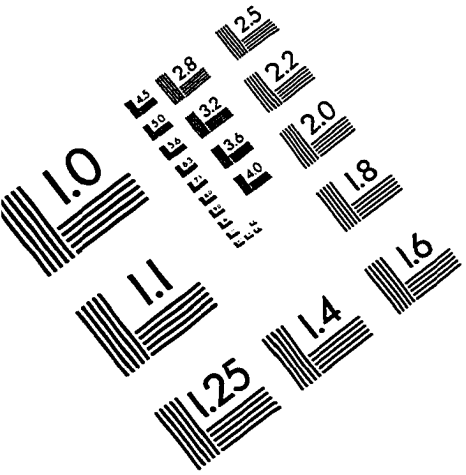

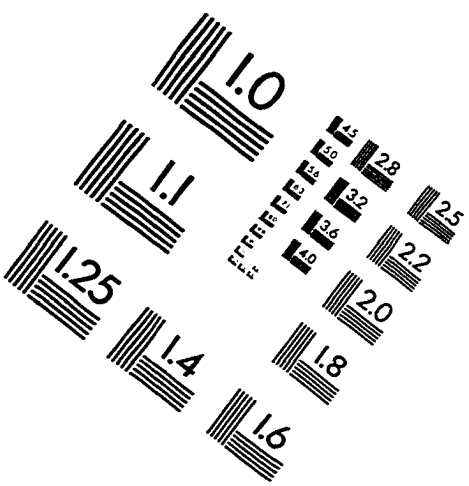

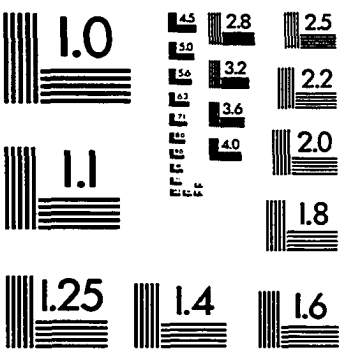

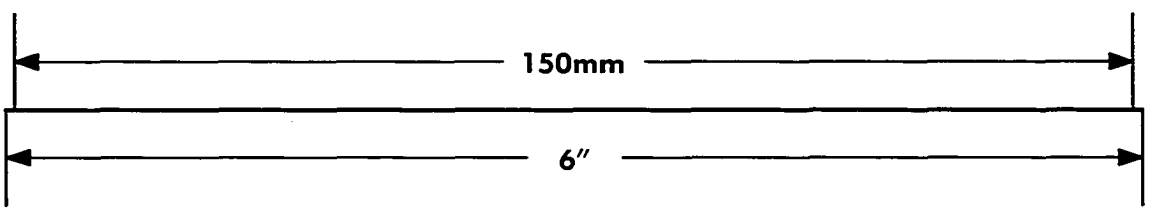

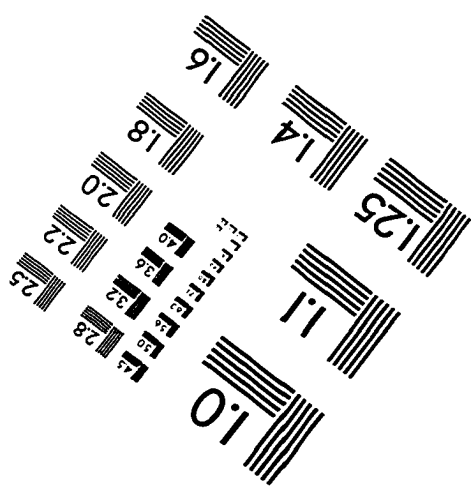

APPLIED IMAGE, Inc
1653 East Main Street
Rochester, NY 14609 USA
Phone: 716/482-0300
Fax: 716/288-5989

© 1993, Applied Image, Inc., All Rights Reserved

